Microstructures and Mechanical Properties of Al 6061 /Al2O3-TiB2 Hybrid Nano-Composite layer Produced via Friction Stir Processing Using Optimized Process Parameters

Vahid Mohammadzadeh Khojastehnezhad

Submitted to the
Institute of Graduate Studies and Research
in partial fulfillment of the requirements for the degree of

Doctor of Philosophy
in
Mechanical Engineering

Eastern Mediterranean University
January 2019
Gazimağusa, North Cyprus

Approval of the Institute of Graduate Studies and Research

Assoc. Prof. Dr. Ali Hakan Ulusoy
Acting Director

I certify that this thesis satisfies all the requirements as a thesis for the degree of Doctor of Philosophy in Mechanical Engineering.

Assoc. Prof. Dr. Hasan Hacışevki
Chair, Department of Mechanical Engineering

We certify that we have read this thesis and that in our opinion it is fully adequate in scope and quality as a thesis for the degree of Doctor of Philosophy in Mechanical Engineering.

Asst. Prof. Dr. Mohammed Bsher A. Asmael
Co-Supervisor

Assoc. Prof. Dr. Neriman Özada
Supervisor

Examining Committee

1. Prof. Dr. Ali Oral
2. Assoc. Prof. Dr. Hasan Hacışevki
3. Assoc. Prof. Dr. Neriman Özada
4. Assoc. Prof. Dr. Qasim Zeeshan
5. Asst. Prof. Dr. Tülin Akçaoglu
6. Asst. Prof. Dr. Mohammed Bsher A. Asmael
7. Asst. Prof. Dr. Murat Özdenefe

ABSTRACT

Aluminum and its alloys have been used effectively in the aerospace and automotive industries because of their useful properties, such as high strength-to-weight ratio, low density, high thermal conductivity, and corrosion resistance. However, low outer part features, such as hardness and wear resistance, are some of the disadvantages for usage in those industries. Aaluminum matrix composites (AMCs) been manufactured by incorporating ceramic particles as reinforcement in the metal matrix has been used to enhance surface characteristics. In addition, Metal-matrix composite materials are finding a variety of applications in sectors of engineering fields due to their crucial properties. Hybrid composite materials are advanced composite materials reinforced with more than one element so as to produce a uniquely combined effect. This permits a more high degree of flexibility in the design of the material. The necessity for light-weight and high-performance materials increases by the day due to an increase in its usage professional fields such as automotive, aerospace, deep-ocean, nuclear-energy-generation, structural applications, etc., that has consequently brought about the invention of hybrid materials in terms of composites.

This thesis concentrates on the fabrication of Al6061/ Al_2O_3-Tib_2 hybrid metal matrix composite using friction stir processing. Al6061 and Al_2O_3-Tib_2 nano powder were utilized as the fundamental material and reinforcement particles, respectively. The influence of a number of FSP passes and tool pin profiles were studied on the distribution of Al_2O_3-Tib_2 particles in aluminum matrix, microstructure, hardness, and wear properties of specimens. Also relation between process parameters

(rotational speed, feed rate, number of passes) and hardness behavior of the composite layer was studied using mathematical models such as artificial neural network (ANN) and response surface methodology (RSM).

Friction stir processing was conducted using different tool pin profiles, different rotation and traverse speeds, and a number of passes. Microstructural characterization done using optical microscopy, (SEM) and (TEM). Wear resistance analysis and hardness (H) were obtained. It was presented that fine grains formed in the stir zone due to the dynamic re crystallization. It was confirmed that refinement of these particles can increase the effective pining of the grain boundaries and reduce grain growth.

The outcomes showed that increase in the number of passes led to a more uniform dispersion of composite particles thereby decreasing the particles clustering. Additionally, an increase in the number of FSP passes was found to reduce the matrix grain size (minimum grain size 0.7 μm) of the outer surface hybrid composite. With an increasing number of FSP passes, the hardness of the composite layer increases significantly as result of the pinning effect and the presence of hard Al_2O_3-Tib2 particles. The peak hardness for the composite layer was 175 HV while that the hardness of received AL6061 was 110 HV. Also, at higher number of passes, the outer surface hybrid composite wear rate increased.

In addition, the distribution of Al_2O_3-Tib2 particles in the specimens produced using square and triangular tool pin profiles was more aligned due to their tool geometry, which resulted in a better stirring of the material and good material flow.

A greater reduction of particle clustering was noted consequently, and thus the mechanical properties were improved. Moreover, the samples made utilizing square and triangular pin profiles showcased more grain refinement (minimum grain size 1.1 μm) than the other samples. More uniform structure, less clustering, and finer grains produced by square and triangular pin profiles caused a higher hardness (maximum hardness 160 HV) and wear resistance.

The artificial neural networks and response surface methodology have been effectively utilized to predict the hardness behavior of the friction stir processed Al6061/Al_2O_3-Tib_2 nano composite. ANN was found a better tool to model the hardness performance of the FSPed composite layer. The trained ANN proved acceptable results when compared with the experimental results. Similarly, Response surface methodology could be employed to model the hardness of the processed composite layer. The error of both model was less than 1.5% which was satisfactory.

Keywords: Friction stir processing, hybrid composite layer, Al_2O_3-Tib_2, number of passes, tool pin profile, rotational speed and feed rate

ÖZ

Alüminyum ve alaşımları, havacılık ve otomotiv sanayisinde, yüksek güç / ağırlık oranı, düşük yoğunluk, yüksek ısı iletkenliği ve korozyon direnci gibi faydalı özelliklerinden dolayı etkin bir şekilde kullanılmıştır. Bununla birlikte, sertlik ve aşınma direnci gibi düşük dış kısım özellikleri, bu endüstrilerde kullanım için dezavantajlardan bazılarıdır. Alüminyum kompozitler (AMK), metal matrikse takviye olarak seramik partiküllerin katılmasıyla üretilmiş ve yüzey özelliklerini arttırmak için kullanılmıştır. Ek olarak, Metal-matris kompozit malzemeleri, önemli özelliklerinden dolayı mühendislik sektörlerde çeşitli uygulamalar bulmaktadır. Hibrit kompozit malzemeler, benzersiz bir şekilde birleştirilmiş bir etki üretmek için birden fazla elemanla takviye edilmiş ileri kompozit malzemelerdir. Bu, malzemenin tasarımında daha yüksek derecede esneklik sağlar. Hafif ve yüksek performanslı malzemelere duyulan gereksinim, otomotiv, havacılık, derin okyanus gibi kullanım alanlarındaki artış nedeniyle gün geçtikçe artmaktadır.

Bu çalışma, Al6061 / Al_2O_3 - TiB_2 hibrit metal matris kompozitin sürtünme karıştırma işlemi kullanılarak imal edilmesine odaklanmaktadır. Al6061 / Al_2O_3 - TiB_2 hibrit metal matris kompozit ve onun üretim tekniği bu çalışmanın yeniliği sayılır. Al6061 ve Al_2O_3 – TiB_2 Nano tozu sırasıyla temel malzeme ve takviye partikülleri olarak kullanılmıştır. sürtünme karıştırma işlemi diğer komposit üretme teknolojilerile kıyaslandığı zaman çok daha iyi bir performans ortaya koymaktadır. Bir dizi FSP geçişinin ve takım pimi profillerinin etkisi, Al_2O_3 / TiB_2 partiküllerinin alüminyum matriks, mikro yapı, sertlik ve numunelerin aşınma özelliklerinde

dağılımı üzerinde çalışılmıştır. Ayrıca yapay sinir ağı (ANN) ve yanıt yüzey metodolojisi (RSM) gibi matematiksel modeller kullanılarak proses parametreleri (dönme hızı, ilerleme hızı, geçiş sayısı) ve kompozit katmanının sertlik davranışı arasındaki ilişki incelenmiştir.

Sürtünme karıştırma işlemi, farklı takım pimi profilleri, farklı dönme ve travers hızları ve birkaç geçiş kullanılarak gerçekleştirildi. Optik mikroskopi, taramalı elektron mikroskobu (SEM) ve TEM kullanılarak mikroyapısal karakterizasyon incelenmiştir. Aşınma direnci analizi ve sertliği (H) elde edildi. Dinamik yeniden kristalleşme nedeniyle karıştırma bölgesinde ince tanelerin oluştuğu gösterilmiştir. Bu parçacıkların rafine edilmesinin, tahıl sınırlarının etkili bir şekilde çivilenmesini artıracağı ve tane büyümesini azalttığı doğrulandı.

Sonuçlar, geçiş sayısındaki artışın kompozit partiküllerin daha homojen bir dağılımına yol açtığını ve böylece partikül kümelenmesini azalttığını göstermiştir. Buna ek olarak, FSP geçiş sayısında bir artışın dış yüzey hibrid kompozitinin matris tanecik boyutunu (minimum minimum tane büyüklüğü 0.7 μm) düşürdüğnü göstermiştir. Sabitleme etkisinin ve sabit Al_2O_3 / TiB_2 partiküllerinin varlığının bir sonucu olarak geçiş sayısı arttıkça maksimum sertliğin 175 HV kadar arttığı da gözlenmiştir. Ayrıca, daha yüksek sayıda geçişte, dış yüzey hibrid kompozit aşınma direnci artmıştır.

Ek olarak, Al_2O_3 – TiB_2 partiküllerinin kare ve üçgen takım pimi profilleri kullanılarak üretilen numunelerdeki dağılımı, takım geometrileri nedeniyle daha iyi hizalandı, bu da malzemenin daha iyi bir şekilde karıştırılmasıyla sonuçlandı.

Sonuç olarak daha büyük bir partikül kümelenmesi azalması kaydedildi ve böylece mekanik özellikler geliştirildi. Ayrıca, kare ve üçgen pim profilleri kullanılarak yapılan numuneler diğer numunelere göre daha fazla tane inceltme (minimum tane büyüklüğü 1.1 μm) sergilemiştir. Kare ve üçgen pim profillerinin ürettiği daha düzgün yapı, daha az kümelenme ve daha ince taneler, numunelerin daha yüksek sertlik (maksimum sertlik 160 HV) ve aşınma direncine neden olmuştur.

Yapay sinir ağları ve tepki yüzeyi metodolojisi, işlenmiş Al6061 / Al_2O_3-TiB_2 nano kompozitin sertlik davranışının öngörülmesinde etkili bir şekilde kullanılmıştır. ANN, kompozit katmanının sertlik performansını modellemek için daha iyi bir araçtır. Eğitimli ANN, deneysel değerleri karşılaştırırken kabul edilebilir sonuçlar verir. Benzer şekilde, işlenmiş kompozit katmanın sertliğini modellemek için Tepki yüzey metodolojisi kullanılabilir. Her iki modelde de hata oranı 1.5 % den daha azdır ve tatmin edicidir.

Anahtar Kelimeler: Sürtünme karıştırma işlemi, hibrit kompozit katman, Al_2O_3-Tib_2, geçiş sayısı, takım pimi profili, dönme hızı ve ilerleme hızı

To my family

ACKNOWLEDGMNETS

I would like to express my gratitude to my supervisor Assoc. Prof. Dr. Neriman Özada for her continues support and encouragement. I am grateful to my co-supervisor Asst. Prof. Dr. Mohammed Bsher A. Asmael who helped us at every stage of thesis writing and defense.

TABLE OF CONTENTS

LIST OF TABLES

LIST OF FIGURES

Chapter 1

INTRODUCTION

1.1 Overview

Friction stir processing (FSP) is a solid state material processing technique based on the principles of friction stir welding (FSW) developed by The Welding Institute in 1991 [1]. In FSW a rotating tool with a specially designed pin and shoulder treads along the weld seam; the high rotating speed of the tool together with the frictional forces between the work piece and the shoulder encourages the joining by frictional heating, softening and severe plastic deformation. The process is shown schematically in Figure 1-1, and 1-2. Severe plastic deformation and stirring action imposed by the tool during the process has brought about many interesting applications for friction stir processing [2,3], some examples are infrastructural modification and homogenization of cast alloys and powder metallurgy fabricated parts and production and homogenization of metal matrix composites [4-10].

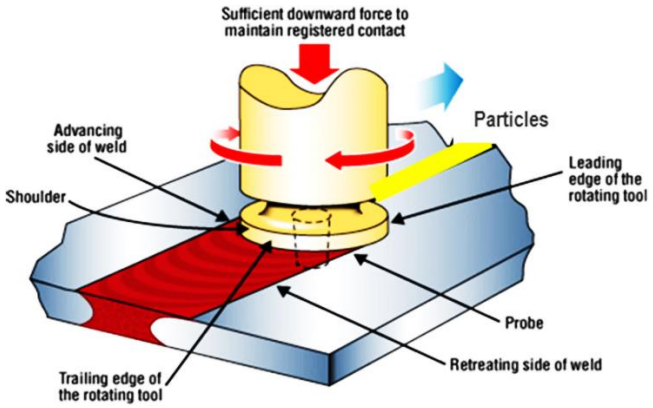

Figure 1. (a) Schematic of the Friction Stir Process

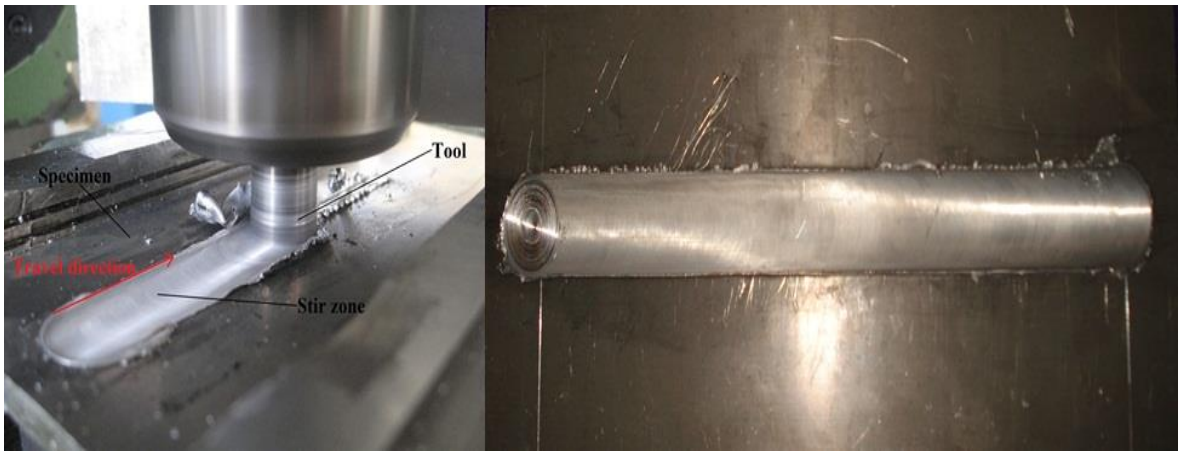

Figure 1. (b) Friction Stir Processing

The potential of FSP technique in fabricating silicon carbide (SiC) reinforced surface composite layer on aluminum (Al) 5083 alloy was explored in the last decade by Mishra et al. (2003)[11]. Since then, a variety of surface composites based on magnesium, copper, titanium and steel have been developed. However, comprehensive coverage of surface composites prepared by FSP is very limited. The present study is concentrated on nano, in-situ and hybrid surface composites fabricated by FSP. In this thesis, recent advancement of FSP in fabricating surface composites are expatiated on.This is followed by discussion on the effect of process parameters of FSP such as the number of FSP passes, tool geometry on microstructure and resultant mechanical properties. The obstacles faced and the future direction of FSP is summarized.

Although FSP is a novel processing method, it has had tremendous applications in different industries due to its significant benefits in comparison with the other metalworking techniques. These advantages include: 1) few processing steps with relatively simple equipment, 2) good control of material properties by optimizing the process parameters (such as tool geometry, rotation speed, traverse speed, downward force, cooling rate), 3) controlled selective modification of microstructure, 4)

sustainable environmental friendliness and energy efficiency. Furthermore, Generated temperature in this processs is at a lower point than the metal melting point. Formation of the joint without any melting drastically reduces the faults that occur in the fusion welding [11].

The stirred material undergoes severe plastic deformation during friction stir processing. The material flow concerned with stirring and severe plastic deformation can be utilized for huge alloy modification by the combination of second elements, the mixing followed by the precipitation of second phases, distribution of fine particles of second element, increased density of defects, and so forth. The stirred area becomes a metal matrix composite with an upgraded hardness and wear resistance successively [11, 12].

The Formation of a defect free weld directly depends on the material flow during FSW. On the other hand in FSP, material flow determines the development of infrastructural characteristic and in the unique case of composite fabrication by FSP material, flow in the stir zone governs the particle distribution. Thus, the study of the material flow has been done using many different study techniques in recent years. This particular aspect remains the subject of many studies although it is not entirely understood yet [13, 14].

1.2 Problem statement

Aluminum and its alloys have multipurpose applications in automobile and aerospace industries due to their unique properties such as low density, and high strength to weight ratio, high thermal conductivity, and a good corrosion resistance. However, poor surface-dependent properties are of major concern for prolonged use

[15, 16]. presently, aluminum matrix composites (AMCs), which is the outcome of the incorporation of hard ceramic particles into aluminum alloys, have been widely used to improve the mechanical behavior of the aluminum alloys. A clear interface with no porosity or reaction products, as well as homogeneous distribution of the particles, is needed to obtain enhanced properties.

To develop a new hybrid nano composite material, based on FSP, to overcome the limitations of the applications of aluminum 6xxx, 7xxx due to weak hardness and wear resistance which can be a disadvantage in Marine and aircraft production, especially in their body structures. In addition, effect of composite particles and its properties in metal matrix composites is still unclear. However material flow during process has significant effect on properties of FSP composite layer. Material flow of the processed material with reinforcement particles showed that the distribution of particles was affected by the stirring action of the probe as well as the extrusion of the plasticized material as a result of the movement of the tool. Process parameters, particularly number of passes and tool geometry, rotational speed, feed rate showed a dominant influence on the dispersion of reinforcement particles [17-20].

Efforts have been implemented to fabricate hybrid metal matrix using Friction stir processing. Production of composites using friction stir processing requires uniform distribution of reinforcement particles with the metal matrix. Titanium diboride (Tib_2) outputs a number of advantages over local ceramic reinforcements such as silicon carbide (SiC) or alumina (Al_2O_3). But fabrication of composite reinforced with TiB_2 has various challenges. Tib_2 (titanium–boron) particles can be utilized as reinforcement particles for aluminum alloys due to their high melting point, high hardness, good wear resistance, and high thermal conductivity. However, sintering of

the Tib_2 particles must be engaged at high temperature or high-pressure conditions, which causes grain growth that results in weak mechanical properties [21, 22]. Therefore, using Tib_2 as reinforcement particles for aluminum matrix has its constraints. The combination of Tib_2 and Al_2O_3 particles is a viable solution to resolve this issue. Al_2O_3-Tib_2 particles have good hardness and stiffness and do not react with aluminum to form an alloying product at the interface of the reinforcement particles and the matrix. The good hardness and wear resistance properties and low sintering temperature of the Al_2O_3-Tib_2 composite particles make them a competent candidate for aluminum alloys [23-25].

1.3 Research contribution and objectives

The study of the conceptualization of the microstructure and mechanical properties of Al 6061 before and after friction stir processing and then produce Al 6061 matrix composites reinforced with Al_2O_3-Tib_2 nano composite particles using friction stir processing is the first major aim of this thesis study. New fabrication of Al6061/Al_2O_3-Tib_2 hybrid metal matrix composite using friction stir processing are among the novelties of this dissertation. This new approach is founded on details of material flow dictated by different tool geometries, multiple FSP passes and different rotational speed and feed rates apply the effect of process parameters to achieve uniform distribution of the secondary particles. The main objectives of this dissertation are as follows:

To investigate the effect of different process parameters on microstructure characterization of the Al6061/ Al_2O_3-Tib_2 composite layer.

To inspect the effect of different process parameters on mechanical properties of the Al6061/ Al_2O_3-Tib_2 composite layer.

To correlate the effect of distribution of the reinforcement particles at different FSP parameters on microstructure characterization and properties of the Al6061/ Al_2O_3-Tib_2 composite layer.

To model hardness behavior of the Al6061/ Al_2O_3-Tib_2 composite layer using artificial neural network (ANN) and response surface methodology (RSM).

1.4 Research methodology

The proposed methodology of this thesis contains three phase namely problem identification, research and development and results and comparison.

1.5 Structure of this thesis

The rest of this research is organized as follows:

Chapter 2 is the literature review of the research which also proposes the aim and contribution to science. Chapter 3 is the methodology of the research which includes setup of the experiment aligns with introduction of base material, tools design and generation, FSP parameters setup, as well as procedures of conducting hardness test, wear test and metallographic studies. Chapter 4 shows the results of the mechanical tests and metallographic studies. Also, this chapter analysis the results and describes the correlation between them. Chapter 5 is the numerical investigation of mechanical properties of the composite layer. Chapter 6 is conclusion.

The results of this thesis are published in two journal papers as bellow:

Khojastehnezhad, V. M., Pourasl, H. H., & Vatankhah Barenji, R. (2017). Effect of tool pin profile on the micro structure and mechanical properties of friction stir processed Al6061/ Al_2O_3-Tib_2 surface hybrid composite layer. Proceedings of the

Institution of Mechanical Engineers, **Part L: Journal of Materials: Design and Applications, 1464420717715048.**

Vatankhah Barenji, R., M Khojastehnezhad, V., H Pourasl, H., & Rabiezadeh, A. (2016). Wear properties of Al– Al_2O_3-Tib_2 surface hybrid composite layer prepared by friction stir process. **Journal of Composite Materials, 50(11), 1457-1466**.

Khojastehnezhad, V. M., & Pourasl, H. H. (2018). Microstructural characterization and mechanical properties of aluminum 6061-T6 plates welded with copper insert plate (Al/Cu/Al) using friction stir welding. Transactions of Nonferrous Metals Society of China, 28(3), 415-426.

Pourasl, H. H., Barenji, R. V., & Khojastehnezhad, V. M. (2017). Elucidating the effect of electrical discharge machining parameters on the surface roughness of AISI D6 tool steel using response surface method.

Barenji, R. V., Pourasl, H. H., & Khojastehnezhad, V. M. (2016). Electrical discharge machining of the AISI D6 tool steel: Prediction and modeling of the material removal rate and tool wear ratio. Precision Engineering, 45, 435-444.

Chapter 2

LITERATURE REVIEW

2.1 Aluminum and Its Alloys

The world's most vast metal and the third most common element is Aluminum which is composed of 8% of the earth's crust. The natural versatility of aluminum makes it the most widely used metal following steel.

Aluminum metal was first produced around 170 years ago, although aluminum compounds have been in use acres of years before. Vast majority of the world's demand for aluminum has grown to around 29 million tons per year in the 100 years since the first industrial measures of aluminum were produced. About 22 million tons of aluminum is produced newly and 7 million tons of aluminum scraps are recycled. The use of recycled aluminum is economically and environmentally beneficial. To produce a tone of new aluminum, 14,000 KWh is required. Conversely, it takes only 5% of this to remelt and recycle one tone of the used aluminum. There are no distinctions in quality between the fresh and recycled aluminum alloys.

Pure aluminum is soft, ductile, and corrosion resistant and has a high electrical conductivity. It is mostly used for foil and conductor cables, but as an alloy with other elements it is necessary to make available higher strengths which are needed

for other applications. Aluminum ranks among the lightest engineering metals, having strength to weight ratio advantage over steel [26].

By making use of varying combinations of the beneficial properties of aluminium which include strength, lightness, corrosion resistance, recyclability and formability, it is being implemented in an ever-increasing number of applications. This variety of products ranges from structural materials through to thin packaging foils.

An aluminum alloy is a chemical composition in which other elements are combined with pure aluminum in order to improve its characteristic properties, primarily to increase its strength. These other elements are composed of iron, silicon, copper, magnesium, manganese and zinc at levels that when merged together may make up as much as 15 percent composition of the alloy by weight. Alloys are given a four-digit number, in which the first digit indicates a general class, or series, described by its main alloying elements [26].

Aluminum alloys can be classified into a number of groups based on the specific material characteristics that includes its ability to respond to thermal and mechanical treatment and the basic alloying element added to the aluminum alloy. When we take into account the numbering / identification system used for aluminum alloys, the above characteristics are identified. The wrought and cast aluminums have different systems of identification. The wrought system is a 4-digit system and the castings having a 3-digit and 1-decimal place system. Wrought Alloy Designation System - We shall first take into attention the 4-digit wrought aluminum alloy identification system. The first digit (Xxxx) shows the major alloying element, which has been added to the aluminum alloy and is often used to describe the aluminum alloy series,

i.e., 1000 series, 2000 series, 3000 series, up to 8000 series (see Table 1). The second single digit (xXxx), if different from 0, indicates a modification of the specific alloy, and the third and fourth digits (xxXX) are arbitrary numbers given to pinpoint a specific alloy in the series. Example: In alloy 5183, the number 5 indicates that it is of the magnesium alloy series, the 1 indicates that it is the 1st adjustment to the original alloy 5083, and the 83 identifies it in the 5xxx series. The only exception to this alloy numbering system is with regards to the 1xxx series aluminum alloys (pure aluminums) in which case, the last 2 digits provide the lowest aluminum percentage above 99%, i.e., Alloy 13(50) (99.50% minimum aluminum) [26].

Table 1: Wrought Aluminum Alloy Designations System

Alloy Series	**Principle Alloying Element**
1xxx	99% Minimum Aluminum
2xxx	Copper
3xxx	Manganese
4xxx	Silicon
5xxx	Magnesium
6xxx	Magnesium and Silicon
7xxx	Zinc
8xxx	Other elements

The 6xxx series are versatile, heat treatable, highly formable, weldable and have reasonably high strength coupled with excellent corrosion resistance. Alloys in this series are made up of silicon and magnesium in order to form magnesium silicide within the alloy. Extrusion products from the 6xxx series are the first choice for architectural and structural applications. Alloy 6061 is the most widely used alloy in this series and is often used in truck and marine frames.

2.1.1 AL 6061

Aluminum alloy 6061 been a medium to high strength heat-treatable alloy has a strength that exceeds 6005A. It has very fine corrosion resistance and very good weldability although it possesses reduced strength in the weld zone. It has and average fatigue strength. It also has good cold formability in the temper T4, but limited formability in T6 temper. It is not suitable for very complex cross sections.

2.1.2 Applications

Alloy 6061 is typically used for heavy duty structures as:

1. Rail coaches
2. Truck frames
3. Ship building
4. Bridges and Military bridges
5. Aerospace applications including helicopter rotor skins
6. Tube
7. Pylons and Towers
8. Transport
9. Boilermaking
10. Motorboats
11. Rivets

2.1.3 Properties of AL 6061

Table 2: Physical Property	**Value**
Density	2.70 g/cm³
Melting Point	650 °C
Thermal Expansion	23.4 x10^-6 /K
Modulus of Elasticity	70 GPa
Thermal Conductivity	166 W/m.K
Electrical Resistivity	0.040 x10^-6 Ω .m

Mechanical Property	**Value**
Proof Stress	240 Min MPa
Tensile Strength	260 Min MPa
Hardness Brinell	95 HB

2.2 Composites

A composite is a material composed of two or more materials that are synthetically made, distinct to one that develops naturally. A composite material, also, must include chemically different constituent phases which are determined by an intense interface. Although, most metallic alloys and many ceramics have multiple phases, they not fit this description because they occur due to natural phenomena. Numerous composite materials consist of just two phases; one is known as the matrix, which continuously encompass the other constituent, which is called the dispersed phase.

The properties of the component phases (i.e., volume fraction, shape, and size of particles, distribution, and orientation) define the properties of the composite [27].

Considering the type and the shape of reinforcement used in fabricating the final material, composites can be grouped in three main categories as shown in Figure 2 which consist of particle-reinforced, fiber-reinforced, and structural composites. Each group includes a minimum of two subsections. Equiaxed dispersed phase is the main characteristic of particle-reinforced composites (i.e., particle dimensions are nearly the same in all directions); whereas, the dispersed phase of fiber-reinforced composites, has the geometry of a fiber (i.e., a large length-to-diameter ratio). Structural composites are a combination of composites and homogeneous materials [27].

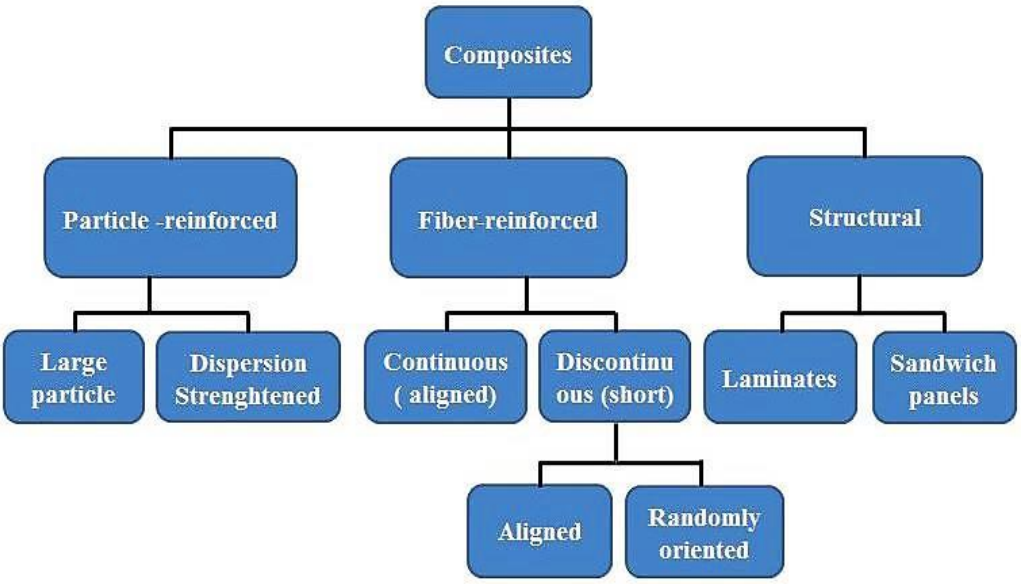

Figure 2. Schematic Classification for Various Composites

2.2.1 Particle reinforced composites

Particle-reinforced composites are made up of two sub- divisions that can be viewed as either large-particle or dispersion-strengthened composites. These two categories are differentiable by strengthening mechanism that is used to form the composite. When the particle–matrix relations cannot be related on the microscopic level, the term "large-particle" is used. The majority of composites in this category are composed of harder particulate phases than matrix material. The strengthening particles restrict movement of the matrix phase in the bounded area of each particle. Actually, a part of utilized stress is conveyed to the particles by matrix. Vibrant bonding at the matrix–particle interface ccompletes a crucial part in enhancing the mechanical behavior of composites. An example of large-particle composite is concrete, which is composed of cement (the matrix), and sand and gravel (the particulates) [27].

All three material types (metals, polymers, and ceramics) can be applied to develop large-particle composites. Cermets for instance are categorized as large particle ceramic–metal composites. The cemented carbide is the most common cermet which comprises of enormously stiff particles of a refractory carbide ceramic such as tungsten carbide (WC) or titanium carbide (TiC), surrounded in a matrix of a metal such as cobalt or nickel. Cutting tools for hardened steels are generally carved out of these types of composites [27].

Dispersion -strengthened composites include particles with diameters between 10 and 100 nm which is in contrast to large particle composite. The strengthening of the material due to addition of the particles occurs at atomic or molecular level as a result of particle–matrix interactions. The mechanism of strengthening is alike to that

of precipitation hardening. The small spread out particles hinders the movement of dislocations while the matrix condones the major portion of an applied load. Thus, restriction of plastic deformation results in an improved yield and tensile strength, as well as hardness. Efficient strengthening takes place when the particles are minute and uniformly spread out throughout the matrix. The effectiveness of dispersion strengthening is not as visible as with precipitation hardening; however, since the dispersed particles are generally not reactivated with the matrix phase in dispersion strengthened materials, the strengthening is held at higher temperatures and for longer time periods. For precipitation-hardened alloys, the improvement in strength may disappear upon heat treatment due to precipitate growth or dissolution of the precipitate phase in the matrix material.

The volume fraction of the two phases is affected by the total operation of a composite. Since in general, increasing the particulate content leads to enhancement of mechanical properties. The reliance of the elastic modulus on the volume fraction of the constituent phases for a two-phase composite has been expressed by two mathematical terms. These standards of mixture equations predicts that the elastic modulus should fall between an upper bound represented by [28]:

$$E_c(u) = E_m(V_m) + E_p(V_p)$$

Eq. (1)

And a lower bound represented by:

$$E_c(l) = \frac{E_m E_p}{E_p(V_m) + E_m(V_p)}$$

Eq. (2)

In these expressions, E and V denote the elastic modulus and volume fraction, respectively, whereas the subscripts c, m, and p represent composite, matrix, and particulate phases.

2.2.2 Metal Matrix Composites (MMCs)

Conventional monolithic materials have limitations in achieving good combination of strength, stiffness, toughness and density. To overcome these shortcomings and to meet the ever increasing demand of modern day technology, composites are most promising materials of recent interest. Figure 3 Shows the classification of Metal Matrix Composites [29].

Metal matrix composites (MMCs) contains significantly enhanced properties which includes high specific strength; specific modulus, damping capacity and good wear resistance compared to unreinforced alloys.

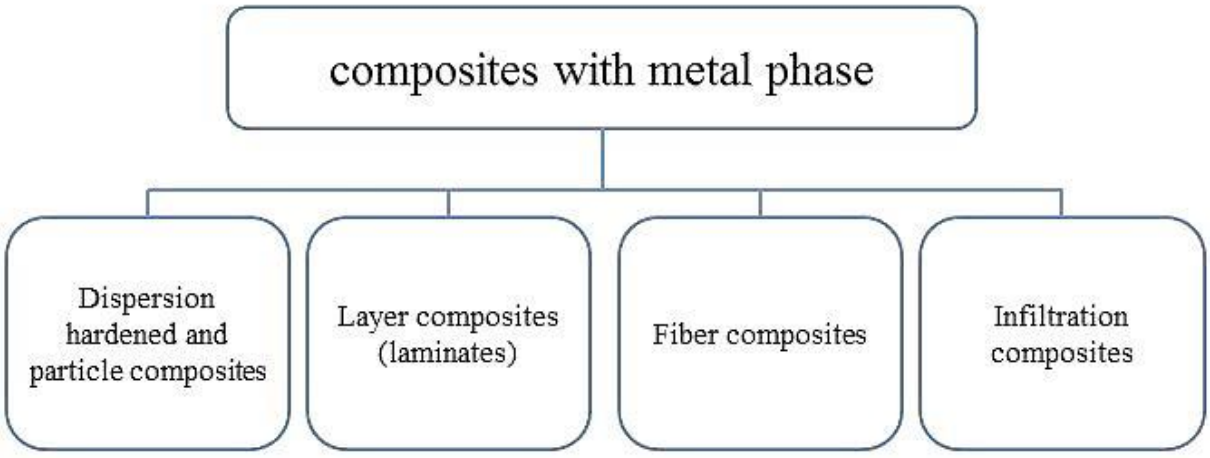

Figure 3. Classification of Metal Matrix Composite

A metal matrix composite (MMC) is a composite material with at least two constituent parts, one being a metal. The other material may be a different metal or another material, such as a ceramic or organic compound. When there is a minimum of three materials present, it is termed a hybrid composite [29].

MMCs are made by dispersing a reinforcing material into a metal matrix. The reinforcement surface can be coated to prevent a chemical reaction with the matrix. For example, carbon fibers are commonly used in aluminum matrix to synthesize composites.

2.2.3 Matrix

The reinforcement is embedded in to the matrix which is a monolithic material, and is completely continuous. This implies that there is a path through the matrix to any point in the material, unlike two materials intertwined together. The matrix is usually a lighter metal such as aluminum, magnesium, or titanium, and provides a concurrent support for the reinforcement.

2.2.4 Reinforcment

The reinforcement material is inserted into the matrix. It is used to modify physical assets such as wear resistance, friction coefficient, or thermal conductivity. The reinforcement can be either continuous, or discontinuous. Reinforcements for metal matrix composites have a manifold required profile, which is determined by production and processing and by the matrix system of the composite material. The following necessities are generally relevant:

- Low density
- Mechanical compatibility
- Chemical compatibility
- Thermal stability

- High Young's modulus
- High compression and tensile strength
- Good process ability
- Economic efficiency

2.3 Applications of Metal matrix composites (MMC)

• Tough cobalt matrix with hard tungsten carbide particles inside is usually used to form carbide drills.

• Metal matrix composites may perhaps be used to create some tank armors, probably steel reinforced with boron nitride. Boron nitride is an efficient reinforcement for steel because it is very stiff and it does not dissolve in molten steel.

• Honda and Toyota automobiles utilized the aluminum metal matrix composite cylinder liners in some of their engines,

• Specialized Bicycles incorporated the usage of aluminum MMC compounds for its high quality bicycle frames for several years. Griffen Bicycles also makes boron carbide-aluminum MMC bike frames, and Univega briefly did so as well.

• Some automotive disc brakes use MMC. Modern high-performance sport cars, such as those built by Porsche, use rotors made of carbon fiber within a silicon carbide matrix because of its high specific heat and thermal conductivity.

Material: AlMg1SiCu + 20 vol. % AL_2O_3P, Processing: extrusion from cast feed material. Development objective: high dynamic stability, low density, high fatigue strength, sufficient toughness.

Vented passenger car brake disk:

Material: G-AlSi12Mg + 20 vol. % SiCp, processing: sand or gravity die casting

Development aims: high wear resistance, low heat conductivity,

The Most Important MMC Systems

- Aluminum matrix
- Continuous fibers: boron, silicon carbide, alumina, graphite
- Discontinuous fibers: alumina, alumina-silica
- Whiskers: silicon carbide
- Particulates: silicon carbide, boron carbide
- Magnesium matrix
- Continuous fibers: graphite, alumina
- Whiskers: silicon carbide
- Particulates: titanium carbide
- Copper matrix

The Advantages of MMCs

- Higher temperature capability
- Fire resistance
- Higher transverse stiffness and strength
- No moisture absorption
- Higher electrical and thermal conductivities
- Better radiation resistance
- Fabric ability of whisker and particulate-reinforced MMCs with conventional metalworking equipment

THE DISADVANTAGES OF MMCs

- Higher cost of some material systems
- Relatively immature technology
- Complex fabrication methods for fiber-reinforced systems (except for casting)

Metal matrix composites present great potential and have attained a level of reliability that indicates an expansion of their use. To utilize their full potential however these composites need more attention and support.

The numbers of MMCs presently are in different levels of advancement: these are boron/aluminum, beryllium/titanium, and boron/titanium, graphite/aluminum, and super alloys reinforced with refractory metal. The boron/reinforced aluminum system is in most advanced stage of development and appropriate data for this system are enough for the design in structural application [29].

Metallic matrix composites (MMCs) reinforced with ceramic particles is a viable material for structural applications due to the excellent mixture of properties. MMCs synthesizes the properties of the metallic alloys (ductility and toughness) and the ceramic reinforcements (high strength and high modulus) leading to a superior profile of characteristics [30, 31]. The aluminum matrix composites (AMCs) identifies as a class of MMCs possessing properties like low density, high stiffness and strength, superior wear resistance, controlled co-efficient of thermal expansion, higher fatigue resistance and better stability at higher temperature. Due to this, these composites are used for the design of a wide range of parts for advanced applications [32]. It has been seen that the use of AMCs in engine applications can lower the total weight, fuel intake and pollution in the automobiles and aircraft's [33, 34]. AMCs reinforced with either silicon carbide (3.18 g/cm3) or alumina (3.9 g/cm3) particles are alluring materials for such applications [33-36]. These reinforcements are denser than those of aluminum alloys (2.7 g/cm3) and increases the weight of the composites depending on what the reinforcement contains. Moreover, the making of machining of developed composite becomes more enormous with the addition of

ceramic particles to the Al-alloy which increases the hardness of composite. Such challenges can be mitigated by the use of multiple reinforcements in the aluminum alloy. The ceramic reinforcements holds greater strength than any other type of reinforcement and because of this fact, they are used as a basic reinforcement for development of hybrid composites. However, the secondary reinforcements reduce the cost as these are readily available weights as they have lower density of the hybrid composites [8, 9]. The properties of the hybrid reinforcements (primary and secondary) can be combined to achieve optimization of material properties [37, 38].

2.4 Hybrid metal matrix composite

The use of a variety of ceramic particulates into a single matrix has led to the development of hybrid composites. Also, making use of a hybrid composite that has two or more types of particulates, the benefits of one kind of particulates could complement to what is lacking in the other [39].

Metal matrix composites

Conventional metal matrix composites are presently used in a way such that only one type of reinforcement is used.

Hybrid Metal Matrix Composites

Second generation composites, in which more than one type, shape and size of reinforcements are used to extract synergistic properties of the reinforcements and matrix chosen.

2.5 Mechanism of reinforcement in MMCs

The microstructure determines the characteristics of the metal matrix composite materials, constituents, and internal interfaces, which are affected by the processing history. The microstructure envelopes the structure of the matrix and the reinforced phase. The chemical composition, grain and/or sub-grain size, texture, precipitation behavior and lattice defects are of great usefulness to the matrix. The second phase is characterized by its volume percentage, its composition, size, distribution and orientation. Local varying internal tension affects it as a result of the different thermal expansion behavior of the two phases which is an additional influencing factor [40].

Strengthening Mechanisms

The high mechanical resistance of MMCs is the result of several strengthening mechanism contributions, namely: load transfer effect, Hall-Petch strengthening, Orowan strengthening.

Load Transfer Effect

The load transfer from the soft and compliant matrix to the stiff and rigid particles under an applied outside load adds to the strengthening of the foundation material. A modified Shear Lag model proposed by Nardone and Prewo [41] is usually used to predict the contribution in strengthening due to load transfer in particulate-reinforced composites [42, 43]:

$$\Delta\sigma_{LT} = v_p \sigma_m \left[\frac{(l+t)A}{4l}\right] \qquad \text{Eq. (3)}$$

Where V_p is the volume fraction of the particles, σ_m is the yield strength of the unreinforced matrix; l and t are the size of the particulate parallel and perpendicular to the loading direction, respectively. For the case of equiaxed particles Equation (1) reduces to [43]:

$$\Delta\sigma_{LT} = \frac{1}{2} v_p \sigma_m$$

Eq. (4)

Hall-Petch Strengthening: the grain size has a high influence on metal strength since the grain boundaries can obstruct the dislocation motion. This is due to the different positioning of adjacent grains and also to the high lattice disoriented characteristic of this area, which hinders the dislocations from moving in a continuous slip plane [44]. The Hall-Petch equation relates the strength with the average grain size (d) [44]:

$$\Delta\sigma_{H-P} = \frac{k_y}{\sqrt{d}}$$

Eq. (5)

Where K_y is the strengthening coefficient (characteristic constant of each material).

The particles play a basic role in final grain size seen in metal matrices of composites since they can relate with grain boundaries posing as pinning points, retarding or stopping their growth. The increase of v_p (volume fraction) and the decrease of d_p (particle diameter) lead to a finer structure, as theoretically modeled by the Zener equation. [43]:

$$d_m = \frac{4\alpha d_p}{3 v_p}$$

Eq. (6)

Where α is a proportional constant.

Orowan Strengthening

The so-called Orowan mechanism is contained in the interaction of nano-particles with dislocations. The non-shearable ceramic reinforcement particles pin the crossing dislocations and enhances dislocations bowing around the particles (Orowan loops) under outer load [44]. The Orowan effect can be expressed by the following expression.

$$\Delta\sigma_{OR} = \frac{0.13bG}{d_p\left(\sqrt[3]{\frac{1}{2}v_p} - 1\right)}\ln\left(\frac{d_p}{2b}\right) \qquad \text{Eq. (7)}$$

Where b is the Burger's vector and G is the matrix shear modulus.

There are several methods to produce metal-matrix composites. Some of these important techniques are explained below.

Solid-state Techniques

. Powder metallurgy

. Ball milling

. Diffusion bonding

. Friction stir processing

Liquid-state

. Stir casting

. Compo-casting

. Squeeze casting

. Ultrasonic assisted casting

2.6 Liquid-State Processes

Casting or liquid infiltration connotes infiltration into a fibrous or particulate reinforcement preform by a liquid metal. The poor wetting of ceramic reinforcement by the molten metal during liquid-phase infiltration leads many challenges during MMC fabrication. The reactions between the fiber and the molten metal, which considerably dismember the properties of the fiber, have a high probability of taking place when the infiltration of a fiber preform occurs. Applying fiber coatings before infiltration increases wetting and restrains inter facial reactions. In this case, however, the low side is that the fiber coatings must not be exposed to air before the infiltration due to the risk of surface oxidation of the coating [45].

Duralcan process is another liquid infiltration process in which ceramic particles and ingot-grade aluminum are combined and melted to form an MMC (Figure 4). The melted mixture is turned slightly above the melting temperature (600−700°C). Particles with sizes ranging between 8−12 μm is required for this technique. In foundry-grade MMCs, high Si aluminum alloys (eg, A356) are implemented, in order to avoid the development of the brittle compound Al4C3, which is formed from the inter facial reaction between Al and SiC. Al4C3 is extremely critical to mechanical properties, Specific to toughness and corrosion resistance. On the other hand, tows of fibers can be conveyed through a molten metal bath when the reinforcement is a fiber, where the single fibers are wetted by the liquid matrix scraped of its excess metal, and a composite wire is shaped. A pack of such wires can be consolidated by extrusion to produce a composite.

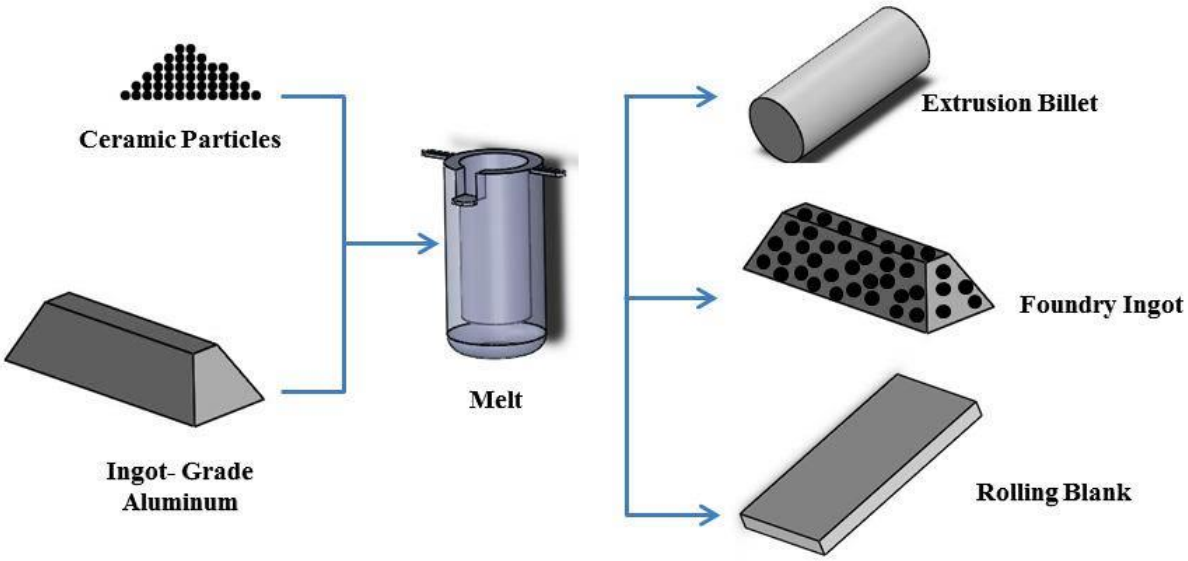

Figure 4. Casting process for particulate or short fiber MMCs [48]

The primex process (Lanxide) is known as another pressure-less liquid metal infiltration process for producing MMCs, which can be utilized with particular reactive metal alloys such as Al− Mg that infiltrate ceramic preforms (Figure 5). For an Al− Mg alloy, in a nitrogen-intense environment, the process occurs between 750−1000°C, and standard infiltration rates are less than 25 cm/h.

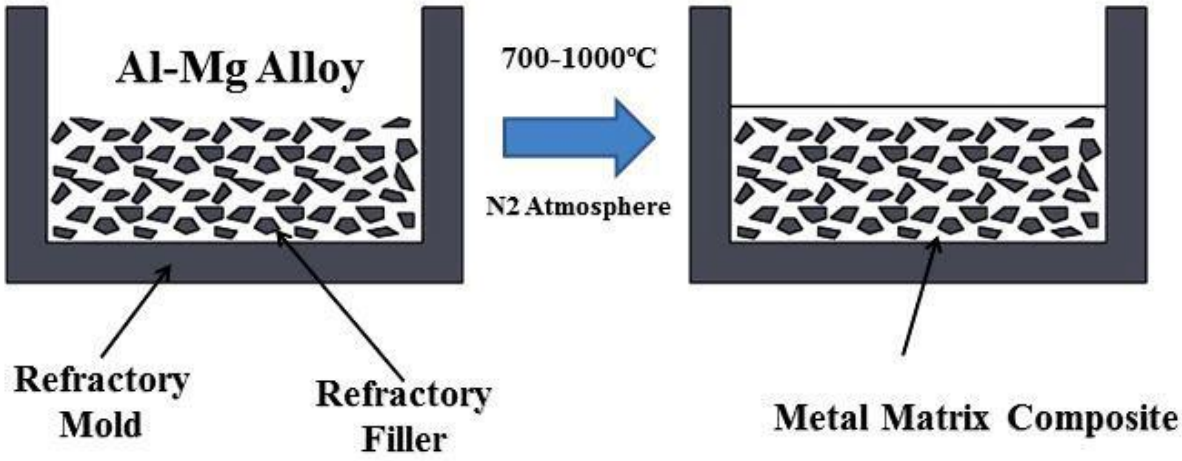

Figure 5. Reactive liquid metal infiltration process [48]

Squeeze casting or pressure infiltration refers to the liquid metal into a fibrous or particulate preform [46] (Figure 6). Upon the completion of solidification pressure is applied. The molten metal passes through miniature aperture in the fibrous preform as result of this pressure, so that a good wettability of the reinforcement by the molten metal is not needed. The processing period in this technique is quite short. Therefore, the reaction between the reinforcement and molten metal in the produced composite is reduced. Conventional casting defects such as porosity and shrinkage cavities are scarcely noticed in these types of composites [46, 47].

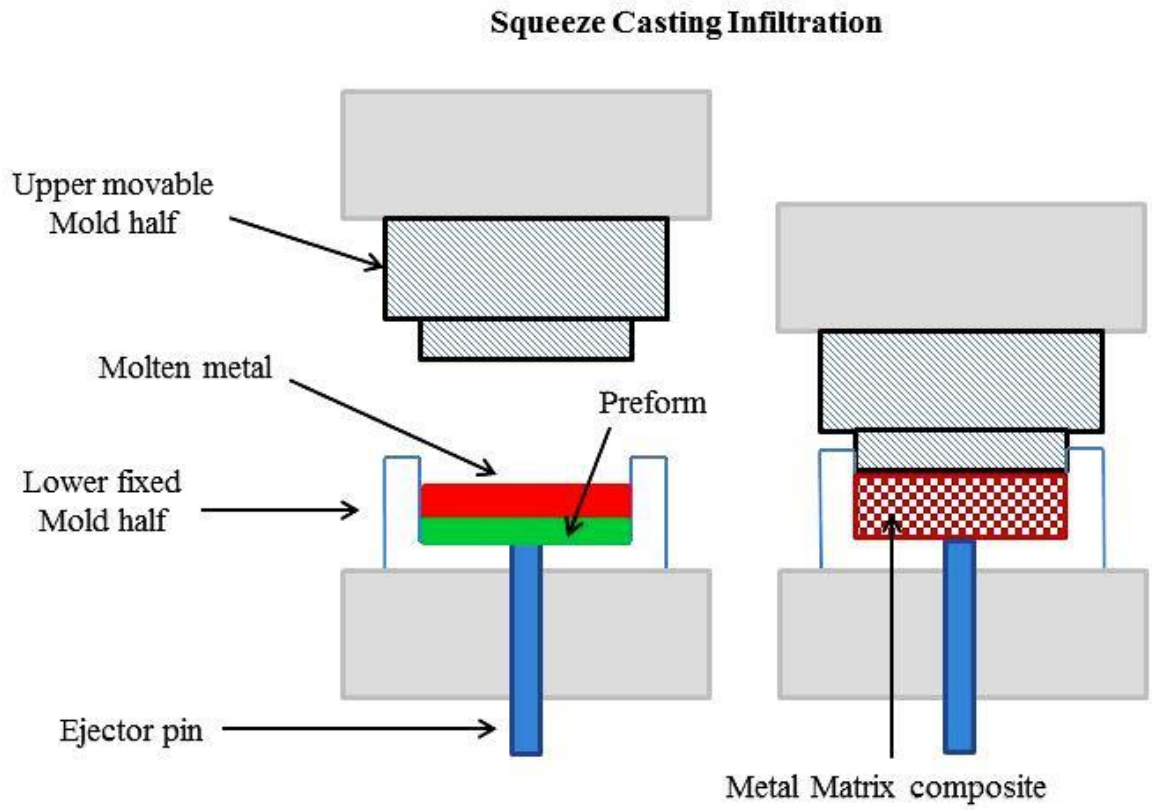

Figure 6. Squeeze casting or pressure infiltration process [48]

2.7 Solid-State Processes

The general solid-state processing method for merging similar or dissimilar metals is a diffusion bonding method. This is bonds created as a result of inter-diffusion of atoms between in-contact metallic surfaces at high temperature. As the major benefits, this technique is able to process a wide range of metal matrices and to control fiber orientation and volume fraction. However, long processing times, high processing temperatures and pressures (which leads to a costly process), and a restriction on producing complex profiles are the principle drawbacks of this method. In its present stage of development almost all forms of diffusion bonding processes is composed of application of pressure and elevated temperature simultaneously. In this method, matrix alloy foil and fiber arrays (composite wire) or monolayer laminate are compacted in a prearranged order (Figure 7). Vacuum hot pressing is a critical phase in the diffusion bonding processes for metal matrix composites. As an alternative of uni-axial pressing, hot iso-static pressing (HIP), may also be used in which the composite inside the container is consolidated via the gas pressure against a can. The HIP facilitates applying high pressures at high temperatures with inconsistent geometries [48, 49].

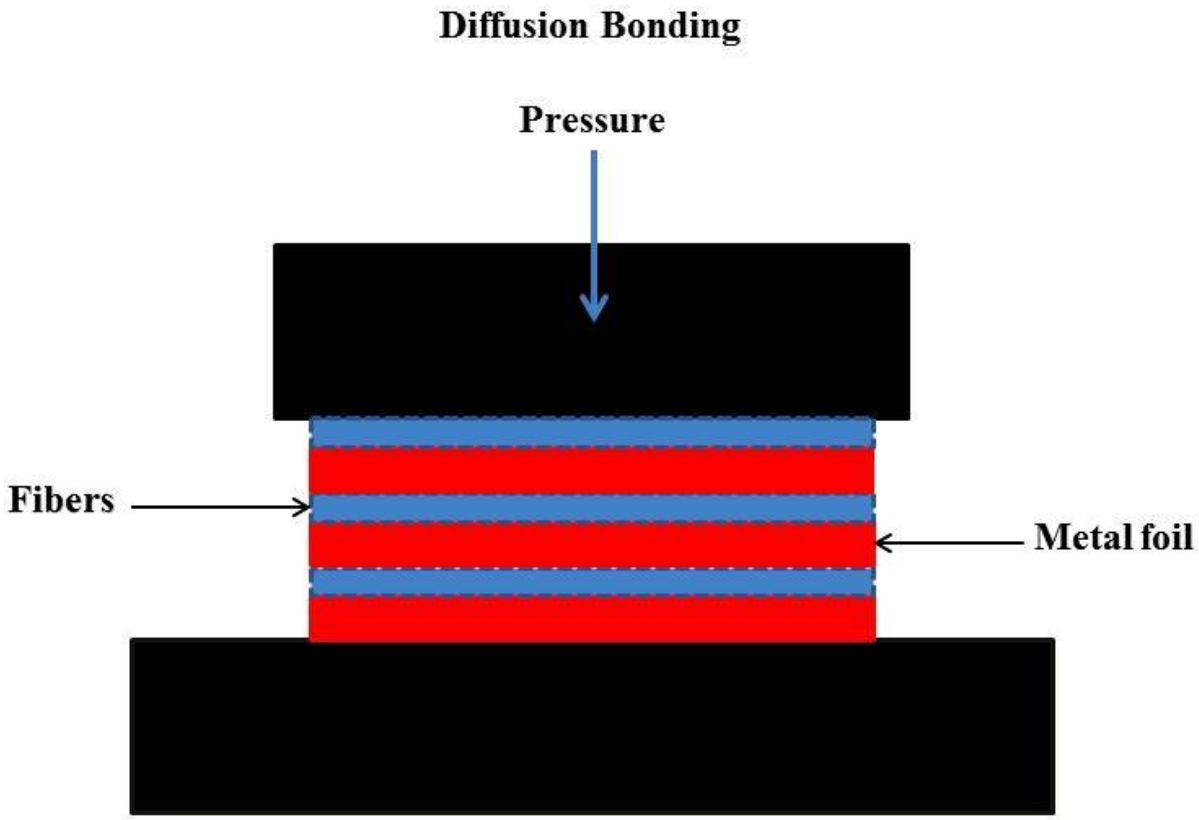

Figure 7. Diffusion bonding process [48]

Deformation processing is another solid state technique in which the composite material is deformed and/or densified. Mechanical processing (swaging, extrusion, drawing, or rolling) of a ductile two-phases metal−metal composite triggers the two phases to co-deform, leading to one of the phases to stretch out and become fibrous in nature within the other phase. The materials produced are sometimes denoted as in-situ composites. The characteristics of the preliminary materials dictates the properties of a deformation processed composite. The initial materials are normally a billet of a two-phase alloy that has been made by casting or powder metallurgy methods [50].

Another general practice to produce a laminated composite is roll bonding. The produced composite by this technique consists of unique sets of metals in layered

arrangement which is called sheet laminated metal-matrix composites [51]. The process of producing a laminated MMC using the Deformation processing is shown in the diagram schematic Figure 8.

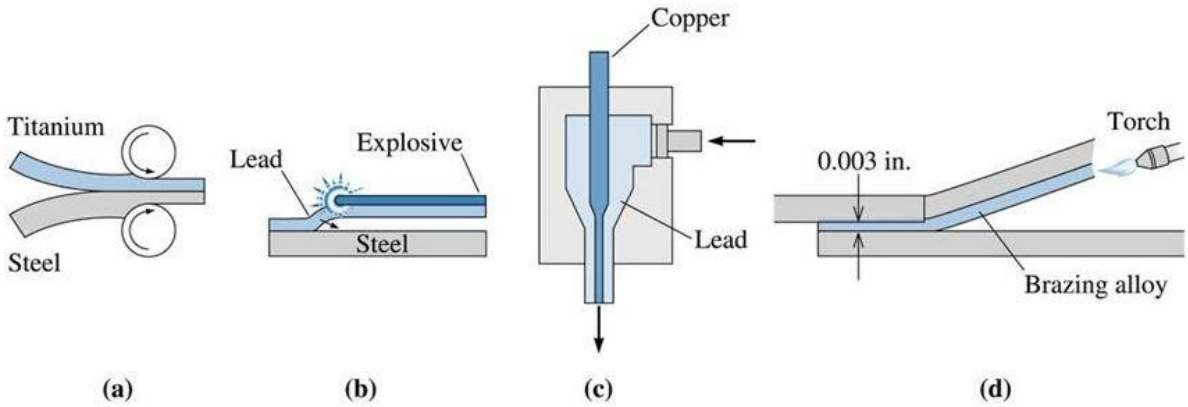

Figure 8. Deformation processing technique [51]

Powder processing techniques are utilized to make particulate or short fiber reinforced composites in association with deformation processing. Generally, this method includes cold pressing and sintering or hot pressing to manufacture primarily particle- or whisker-reinforced MMCs [52]. To create a uniform distribution, the matrix and the reinforcement powders are mixed together Figure 9. Cold pressing is applied accordingly to construct a so called green body which is about 80% dense and can be simply processed. To eradicate any absorbed dampness from the particle surfaces the cold pressed green body is preserved in a closed container and degassed. In order to attain a completely dense composite, the material is hot pressed either uniaxially or isostatically and extruded. The stiff particles or fibers trigger the matrix to be dismembered considerably. Furthermore, versatile re-crystallization at the particle/matrix interface during hot extrusion generates randomly oriented grains near the interface, and moderately textured grains far from the interface.

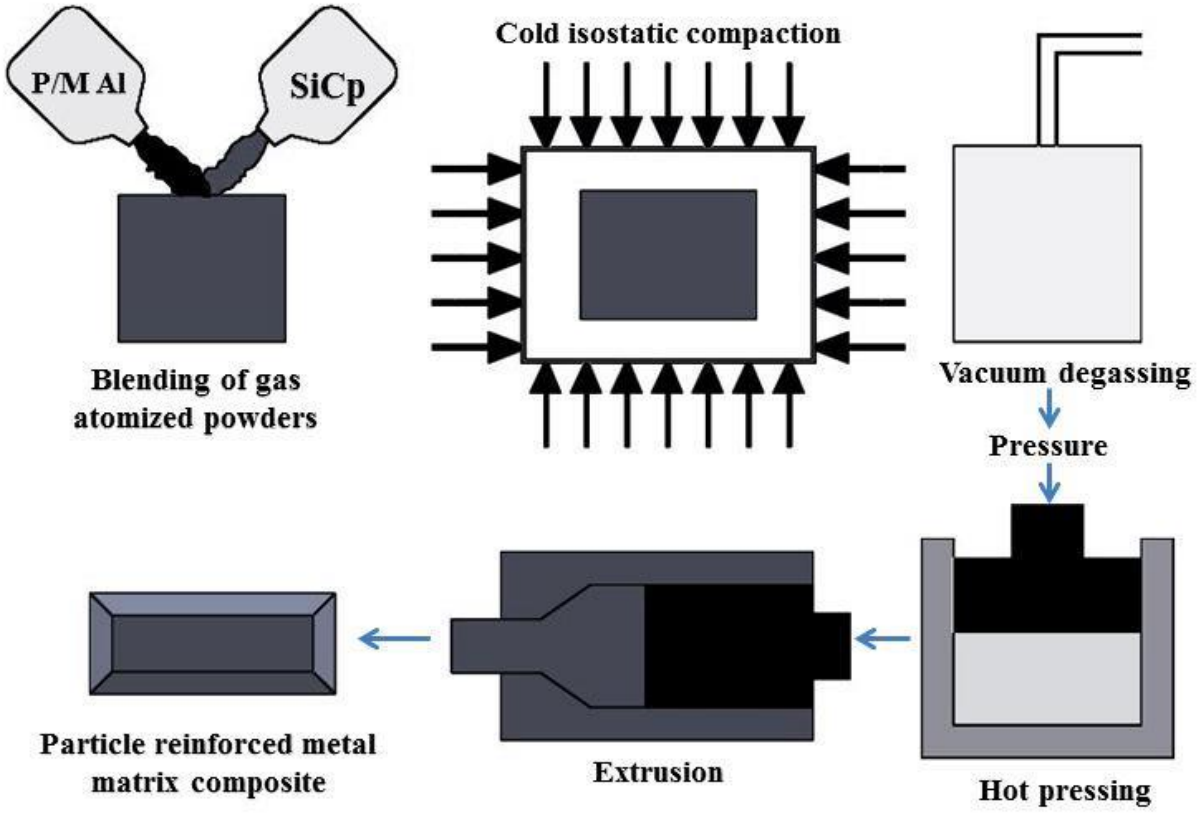

Figure 9. Powder processing, hot pressing, and extrusion process for fabricating particulate or short fiber reinforced MMCs [52]

A type of unique and economical deformation processing technique Sinter-forging [53]. In this method a powder mixture of reinforcement and matrix is cold compacted, sintered, and forged to total complete solid, see Figure 10. The major advantage of this technique is that forging is carried out to produce a near-net shape material, leading to a minimal machining operation and material waste. Tensile and fatigue properties of the low cost, sinter-forged composites are equal to those of materials made by extrusion.

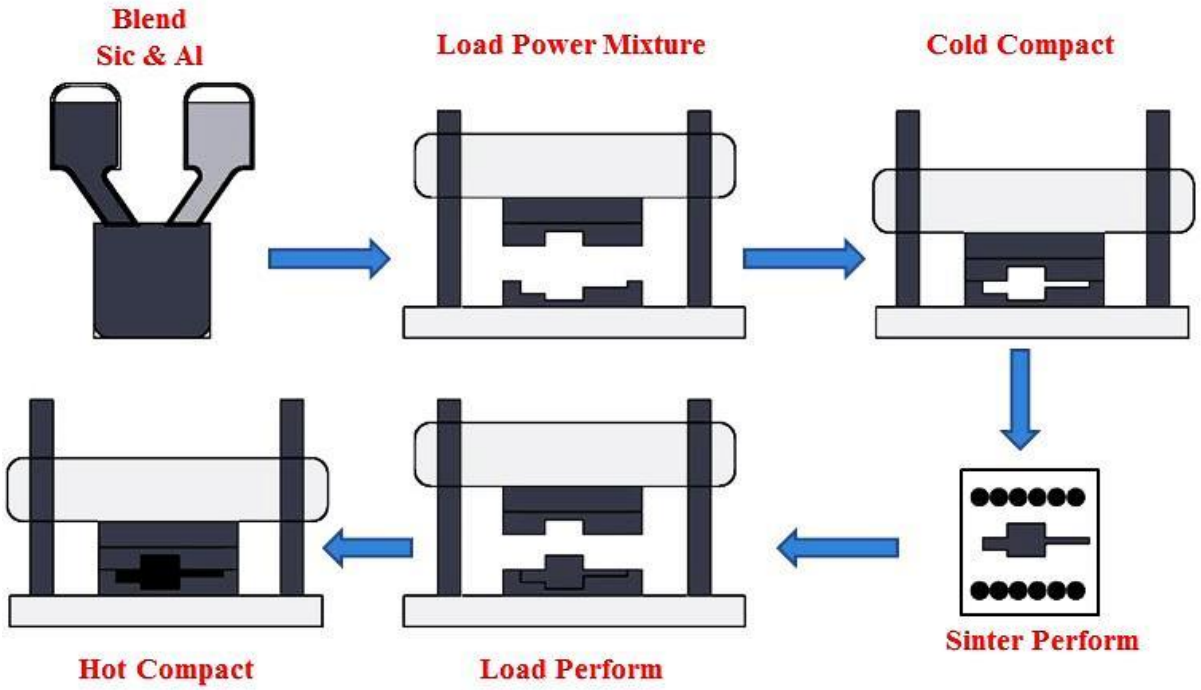

Figure 10. Sinter-forging technique for producing near-net shape, low cost MMCs

2.8 Friction Stir Processing, FSP

Friction stir processing (FSP) is a solid state processing technique that is founded on the laws of friction stir welding developed at The Welding Institute (TWI) in 1991 [1]. The primary concept of FSP is rather to the point. A no consumable spinning tool is placed in a single piece of material, and then traversed over the surface of material when the shoulder touches the work piece (Figure 11). The tool heats up the work piece and severely plastically deforms the material. The friction between the tool and work pieces and also the plastic deformation of the material conjures heat. The mixture of tool rotation and translation caused by localized heating softens the material around the pin and leads to the movement of material from the front to the back of the pin. At first, FSP was developed by Mishra et al., for microstructural modification [54, 55]. Accordingly, FSP has been used to produce surface composite on aluminum substrate [56], and the homogenization of powder metallurgy (PM)

aluminum alloys, metal matrix composites, and cast aluminum alloys. FSP has ascertained advantages in comparison to other metalwork methods. First, FSP is a direct solid-state processing technique that reaches microstructural modification, densification, and homogeneity simultaneously. Second, by optimizing the tool design, FSP parameters, and active cooling/heating the microstructure and mechanical properties of the processed zone can be precisely managed. Thirdly, while it is hard to attain an alternatively adapted processed depth using other metalworking procedures; the depth of the processed area can be optionally controlled by altering the length of the tool pin. Fourth, having a widespread use for the fabrication, processing, and synthesis of materials FSP is an adaptable technique. Fifth, FSP is a green and energy-efficient technique without toxic gas, radiation, and noise since the heat input during FSP comes from friction and plastic deformation. Sixth, FSP does not change the shape and size of the processed parts [57].

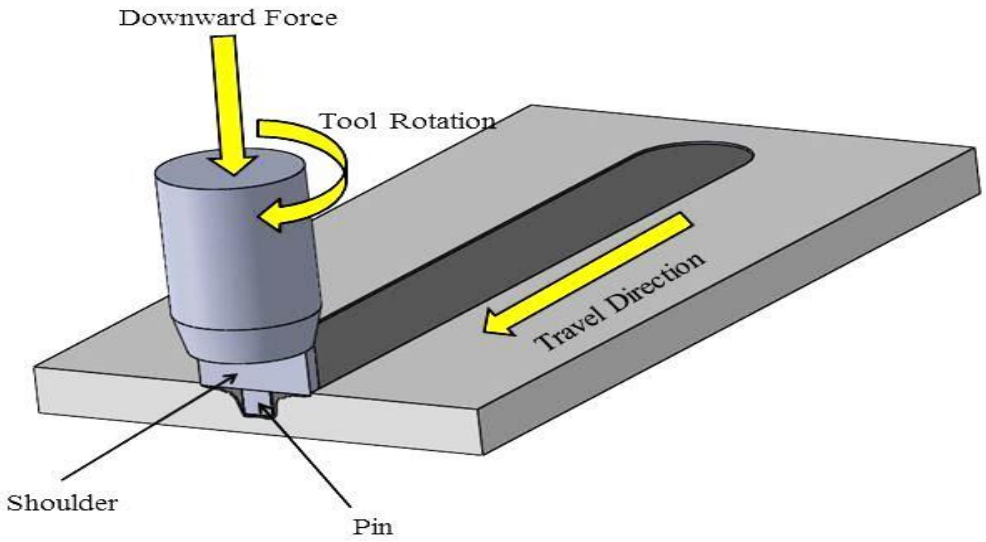

Figure 11. Schematic representation of FSP principle.

2.8.1 Fabrication MMCs using FSP

The size and volume fraction of reinforcing phases as well as the characteristics of matrix-reinforcement interface which control the mechanical properties of MMCs is a well documented case [58]. Powder metallurgy (P/M) method or molten metal processing has been the major way to fabricate particle-reinforced metal matrix composites. However, collecting a uniform spread of good reinforcement particles within the matrix is especially tasking through local casting or P/M processing. It is mainly due to the natural trend of fine particles to agglomeration when blending of the matrix and the reinforcement powders.

It has been elaborated clearly that FSP can be used to create aluminum matrix composites in-situ without alternative consolidation process. The usage of FSP to produce MMCs has the following advantages [59, 60]:

a. instigating sever plastic deformation to further mixing and refining of constituent phases in the material.
b. Generation of high temperature to ease the in-situ reaction to develop reinforcing particles.
c. Causing hot consolidation to establish fully dense solid

On the other hand, the availability of reinforcement particles in the metallic matrix leads to brittleness which generally is not desirable. Therefore, instead of bulk reinforcement, the use of the particles on the surfaces improves the wear properties, which is a surface reliant degradation mode, without sacrificing the bulk properties [61]. However, it is tasking to properly disperse ceramic particles on a metallic outer surface by general surface treatments. The existing processing techniques to produce

surface composites are founded based on liquid phase processing at elevated temperatures. However, it is hard to stop inter facial reaction between reinforcement and metal matrix and the growth of some harmful phases. In addition, to achieve precise solidified microstructure in surface layer, close surveying of processing parameter seems to be crucial. Apparently, processing of surface composite at minimal temperature, below the melting point, can hinder these issues [61, 62]. In such cases, FSP, as a solid state processing technique can be successfully utilized to produce surface composites.

Numerous processing methods such as thermomechanical treatment (TMT) , equal channel angular pressing (ECAP), torsion under compression, multi-axial alternative forging (MAF), and accumulative roll bonding (ARB) have been made use of in order to get the fine-grained materials for superplasticity. Contrasting these technique with the FSP there are certain advantages in FSP which can be noted. First, unlike other processing techniques which are relatively complicated and time-consuming, FSP is a partly direct processing method that generates a fine-grained microstructure. For example, TMT comprises solution treatment, over-aging, multiple-pass warm rolling with alternating reheating, and a recrystallization treatment. While at least 4 to 6 passes are needed to attain microstructural refinement by ECAP. Second, it is feasible to reach the superplastic forming of thick plates using FSP as it does not decrease the thickness of the processed plates. Whereas, to achieve the fine-grained microstructure to generate the superplastic plates less than 3 mm thick via TMT, a large rolling minimization is needed. Thirdly, it is a possibility to process locally through FSP and form local grain refinement in an area that will undergo super-

plastic deformation. While, microstructural refinement on a selective criterion the other hand is not promising through other processing methods.

2.8.2 Microstructure evolution during FSP

As a result of a considerable frictional heating and severe plastic deformation during FSP, dynamic recrystallization takes place in the stirred zone (SZ) metamorphosing in to a fine and equiaxed recrystallized grains of absolutely uniform size [63, 2]. Thus, the resultant grain microstructure in the SZ is determined by the factors impacting the nucleation and growth of the dynamic recrystallization. Among those factors, the FSP parameters, tool geometry, material chemistry, work piece temperature, vertical pressure, and active cooling significantly impact on the size of the recrystallized grains in the SZ [64]. Figure 12 shows the optical micrographs of FSP 7075Al-T651 [2].

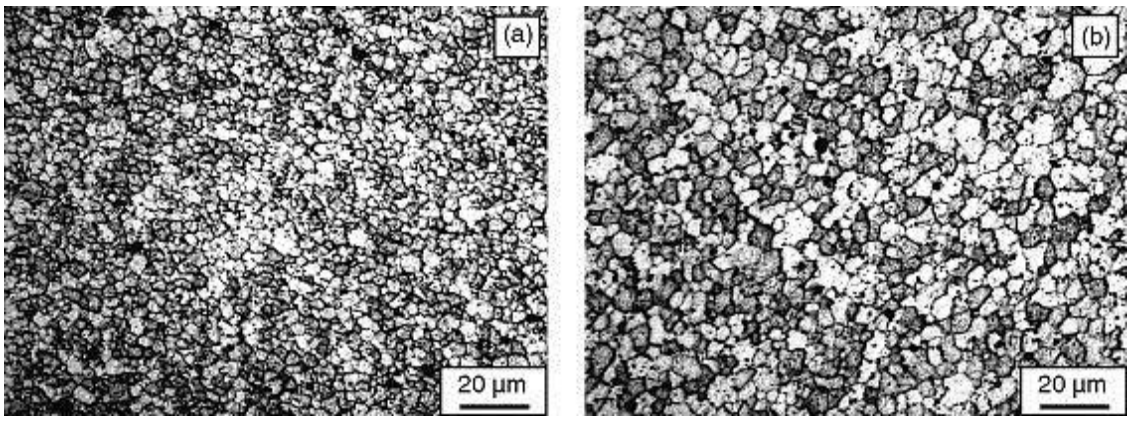

Figure 12. The optical micrographs of FSP 7075Al-T651

The heat and deformation formed during FSW outputs microstructurally distinct areas across the weld. The outermost parts of the weld were adjusted by the thermal field of the welding process which still did not have any deformation. This area is called the heat affected zone (HAZ) and is similar to heat-affected zones observed in welds prepared by more conventional fusion welding processes. Inward from the HAZ is founded in the thermo-mechanically affected zone (TMAZ), where the

material experienced plastic deformation as a result of the stirring process in contribution to the heat-induced microstructural changes. At the center of the weld, where the heat and deformation were the highest , aluminum alloys went through dynamic re crystallization inside an onion-shaped region known as the weld nugget, which in approximation is the size of the rotating pin of the tool [65, 66]. Figure. 13 shows the different regions of FSP specimen.

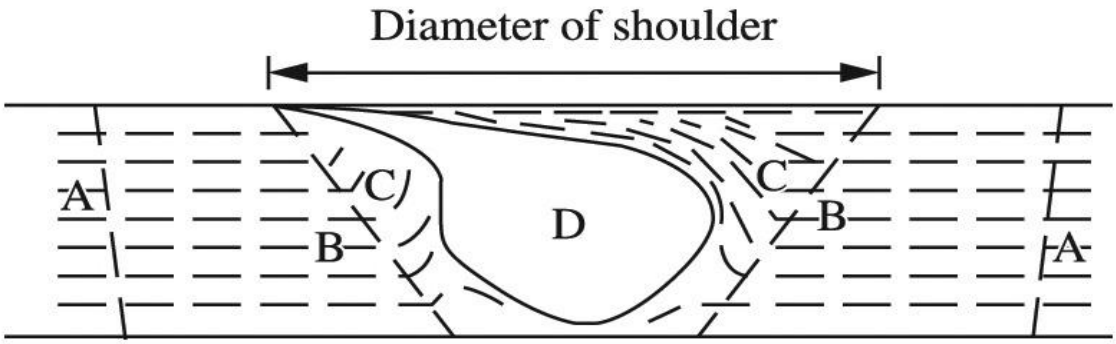

Figure. 13. Different regions of FSP specimen: (A) unaffected base metal, (B) heat affected zone (HAZ), (C) thermo-mechanically affected zone (TMAZ) and (D) friction stir processed (FSP) zone.

2.8.3 Mechanical Properties enhancement during FSP

It looks as if the mechanical properties of a metallic material can be custom-made through FSP, Since removing the FSP parameters, tool design, vertical pressure, and active cooling/heating influences the grain micro structure, . An increase in both yield strength (YS) and hardness have been reported to be as a result of continuous reduction in the grain size of aluminum and magnesium alloys by changing the FSP parameters [67, 68]. The variation pattern for YS and hardness fits in the Hall–Petch relationship. [69] The grain size reduction results in an increase in microhardness (HV) of FSP AZ31. Additionally, structural superplasticity takes place as a result of the microstructural refinement in the light alloys by means of FSP. It was reported that the microstructural refinement through FSP resulted in significantly improved

superplasticity, minimized flow stress, and a change to higher optimum strain rates and lower temperatures [70].

The effect of grain size on the superplasticity of FSP 7075Al alloys as a function of initial strain rate is described in Figure 14. The superplastic properties of various FSP alloys, with grain size and optimum strain rate and temperature are revised in Table 1. The application of the FSP resulted in the formation of considerable superplasticity in a number of aluminum and magnesium alloys, particularly, at high strain rates or low temperatures [71].

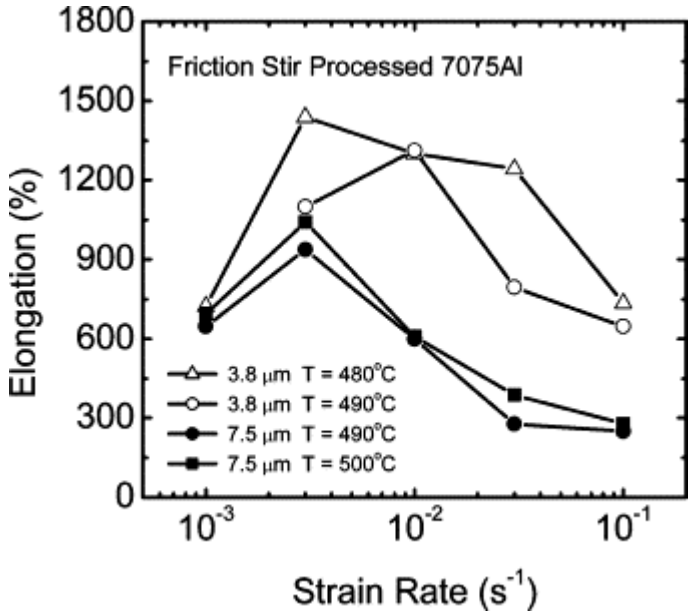

Figure. 14.Variation of elongation with initial strain rate at various test temperatures and grain size for FSP 7.5 μm-7075Al and as-rolled 7075Al.

2.8.4 Friction Stir Processing of Aluminum Matrix Composites

Friction stir processing reinforced aluminum alloys have also been studied [72-76]. Shafiei-Zarghani et al. [18] utilized friction stir processing (FSP) to incorporate nano-sized Al_2O_3 into AA6082 aluminum alloy to form particulate composite surface layer. The Al_2O_3 particles have an average size of about 50 nm. Perfect bonding between the surface composite and the aluminum alloy substrate was attained. Mechanical properties which included microhardness and wear resistance were tested. The outcomes shows that the increasing the number of FSP passes leads to more uniform distribution of nano-sized alumina particles. The microhardness of the surface is enhanced by three times in comparison with that of the as-received Al alloy. A significant enhancement in wear resistance in the nano-composite surfaced Al was noted in comparison to the as-received Al alloy. The wear rate is minimized to one third of that of the as-received Al alloy when friction stir processed composite layer was used.

A.Dolatkhah et all [77]. Researched effects of process parameters on micro structural and mechanical properties of Al5052/SiC metal matrix composite fabricated via friction stir processing. Surface composite layer was successfully formed on aluminum sheets. The best powder distribution (among our tested parameters) was attained with tool rotational and traverse speed of 1120 rev/min and 80 mm/min respectively. Further FSP passes and change of tool rotational direction between passes leads to significantly more homogeneous spread of SiC particles in MMC. Due to sever plastic deformation and dynamic recrystallization, FSP generates a fine equiaxed grain microstructure in stirred zone. Addition of SiC particles intensifies grain refinement. The most desired outcomes were gained with nano-sized SiC

powder. In this case FSP changed the initial microstructure with mean grain length of 243 μm to an ultrafine grained microstructure with a mean grain size of 0.9 μm. Addition of reinforcing SiC particles, greater number of FSP passes, shifting direction of tool rotation between passes and decrease of SiC particles size redound to hardness and wear resistance enhancement. Microhardness value was enhanced up to 55% and wear rate was reduced about 9.7 times when compared with 5052 aluminum.

TiC particles were made used to make discontinuously reinforced aluminum composite in addition to SiC and Al_2O_3 particles. Demarcation of the in situ formed reinforcement particles is a particularly big difficulty in Al based in situ composites. Friction stir processing was used to homogenize the particles distribution in Al–TiC in situ composites. It is shown that friction stir processing (FSP) can be used efficiently to homogenize the particle distribution in Al–TiC in situ composites. A single pass of FSP was sufficient to break the particle segregation from the grain boundaries and improve the distribution. Two passes of FSP resulted in complete homogenization and removal of casting defects. The grain size was also refined considerably after each FSP pass. The grain size after second pass was finer. The mechanical properties improved significantly after FSP due to improvement in the microstructure. Although the strength and hardness improved substantially the ductility was not compromised [78].

Three unique zones, i.e. the heat affected zone (HAZ), thermomechanically affected zone (TMAZ) and dynamically recrystallized nugget zone were revealed by macrostructure observations on friction stir processed Al_2O_3 particle reinforced aluminum composites. The microstructure transformation in HAZ is less noticeable.

However, particle fracture was found in this zone as shown by Cavaliere [61]. In the thermo mechanically affected zone (TMAZ), a deformation band was noted as shown in Figure 15(a). In the nugget zone, recrystallized microstructure and fractured particles are the major morphological features as illustrated by Figure 6(b). There exists variance in micro hardness of these zones. As shown in Figure 6(c), the microhardness for the material in the nugget zone is the highest because the grain size is the smallest in this zone.

Different zones formed by friction stir processing as revealed by morphology and microhardness profile (after Cavaliere [61]): (a) micrograph showing the deformation bands in TMAZ; (b) recrystallization in nugget zone; (c) microhardness profile in the FSP Al_2O_3/AA2618 composite.

Nanoscale reinforcements such as carbon nanotubes were used to create reinforced composite materials through FSP [79]. FSP could break down the CNT clusters and disperse the CNTs into the matrix, and the distribution homogenization of the CNTs increased with increasing FSP pass. The single dispersion of the CNTs was achieved in the 4-pass FSP CNT/2009Al composites with most of the CNTs being distributed along the grain boundaries. The CNTs in the composites were shortened compared to the as-received ones, but still remained larger than 400 nm. Al4C3 were detected to attach to the CNTs or be in the matrix near the CNTs. However, the layer structures of the CNTs were still retained. The grain size of the FSP CNT/2009Al composites was significantly refined compared with that of the FSP 2009Al. The mechanical strengths of the FSP CNT/2009Al composite, especially the YS, showed substantial improvements compared with the FSP 2009Al. Increasing the CNT concentration from 0 to 3 wt.% resulted in the increase in the YS. The UTS increased with

increasing the CNT concentration from 0 to 1 wt.%, however it decreased as the CNT concentration increased up to 3 wt.%. A YS equation based on the load transfer and grain refinement was proposed to predict the YS of the CNT/2009Al composites. The predicted results were in good agreement with the experimental results. This indicates that the YS increase of the CNT/2009Al composites is attributed to the load transfer from the matrix to the CNTs and the grain refinement.

Other types of micro- or nanoscale phases, such as in-situ formed particles including Al2Cu, and Al3Ti [80], NiTi [81], and AiFe [82] have been taken as the reinforcements for aluminum based composites and FSP has been used to modify the microstructures of these in-situ composites. Under high temperature processing conditions such as casting and powder metallurgical formation, considerable interfacial reactions lead to formation of a number of intermetallic phases, such as Al3Ti, Al3Ni, Ni3Ti, Ti2Ni, etc. depending on the compositions of the raw materials. The presence of these intermetallic phases, if they are physically or mechanically incompatible with the matrix alloys, they become the key sites for fracture initiation and failure. FSP could help to alleviate this problem.

The important factors that may be removed to attain uniform distribution of the secondary material are tool geometry and FSP process parameters. It is shown that applying different process parameters may affect particle distribution in different ways; by applying low axial force or low target depth, it has been seen that the particles will not distribute at all whereas with high axial force or high target depth, all the particles will be moved away from the pin surface. Hence, the best distribution can be provided by a moderate depth [17, 23]. Increasing travel speed may lead to lower heat input which could result in insufficient martial flow for

optimal particle distribution [83], and so repeated FSP passes may be required to improve distribution by introducing more stirring and mixing [18, 84, 85]. It is generally accepted that increasing the rotation speed and decreasing the travel speed improves particle distribution [83, 86]. This is attributed to the better stirring and mixing as a result of higher heat input. However, Azizieh et al. have reported the best particles distribution was enhanced with increase of rotation speed. The grain size of nanocomposite was effectively refined as compared with composite with micro-particles, sample without particles addition and initial state of matrix. In higher rotation speed, in spite of finer particles cluster, grain growth was occurred due to higher heat input and particles could not effectively retard the motion of grain boundary in this condition. [87]. On the other hand, one should consider that increasing the heat input results in larger grains in the final matrix microstructure which is detrimental to mechanical properties. Therefore optimum process parameters must be determined for each specific application [88].

Also researched was the effect of tool pin profile on particle distribution. Tool geometry is a crucial feature of FSP due to the major effect on heat generation, material flow and the resultant microstructure. Garcı´a-Bernal et al. [89] investigated the effect of FSP tool design on the microstructure and superplastic behavior of Al–Mg alloys. They showed that the tool with a larger shoulder region permitted more plastic deformation on the microstructure forming a better microstructure for high-temperature deformation. Faraji et al. [90] found that the particle size and grain size of the samples formed through a triangular tool were extensively smaller than that of a square tool in the fabrication of Al_2O_3-reinforced as-cast magnesium alloyAZ91 composite. Mahmoud et al. [91] showed that on the surface composite fabrication of

SiC-reinforced aluminum alloy, the square pin profile formed a more uniform distribution of SiC particles than the triangle and cylindrical pin profiles. Azizieh et al. [92] found that a threaded columnar pin profile generated composites without defects in the fabrication of Al_2O_3/AZ31 nano-composite compared with non-threaded and three-fluted columnar pin profiles due to better material flow.

Yu et al. [93] created a threedimensional transient computational fluid dynamics (CFD) standard to study the material flow and heat transfer throughout FSP with a threaded/ non-threaded pin in the AZ31B magnesium alloy. A comparison of the threaded and non-threaded models showed that the thread strongly affected the temperature distribution, material flow velocity and strain rate near the tool pin within the stir zone.

Arora et al. [94] reviewed composite fabrication using the FSP method and showed that FSP can be an effective and efficient process for refining the grain size of cast or wrought aluminium-based alloys. Mishra et al. [95] produced a surface composite of an Al5083 alloy with 0.7 mm SiC particles, and they noted hardness of the fabricated surface composite was 10% higher than the base metal (BM) as a result of SiC hard particles in processed material. Shafiei et al. [18] and Mahmoud et al. [96] incorporated Al_2O_3 and SiC particles into substrates such as Al, Cu, and Fe alloys, and they also observed an improvement in the abrasion and wear resistance of the base materials.

Moreover, Dolatkhah et al. [77] investigated the mechanical and microstructural properties of Al– SiC metal matrix composites fabricated by FSP. They found that a shift in tool rotational direction between FSP passes, increase in number of passes,

and decrease of SiC particles size will lead to an enhanced hardness and wear properties.

Lee et al. [97] investigated the microstructure and mechanical properties of an Al–Fe in situ nanocomposite produced by FSP. They also noted a uniform spread of the second phase particles (Al13Fe4) in the Al matrix. The fine dispersion of particles resulted in an aluminium matrix with ultrafine- grained structure. In addition, Qian et al. [98] synthesised Al–Al3Ni in situ composites using the FSP route, and they reported that the composite had enhanced hardness and tensile properties.

Rayes et al. [99] made an analysis on the influence of multi-pass friction stir processing on the microstructural and mechanical properties of aluminum alloy 6082. They found from tensile test results that there is a good cohesiveness between UTS and the hardness value as well as the particle size, where the UTS increases with increasing hardness and reducing the particle size.

Cui et al. [100] researched the effect of FSP parameters and in situ passes on the microstructure and the tensile properties of Al–Si–Mg casting. They came to a conclusion that for the multi-pass FSP, the two-pass FSP sample exhibited an obvious benefit in the microstructure modification and the tensile properties compared with the one-pass sample.

Sarkari Khorrami et al. [101] showed that the increase in FSP pass number did not have considerable effects on the stirring zone of the specimen subjected to FSP without reinforcement nanoparticles. In contrast, FSP with Sic nanoparticles can greatly affect the distribution of the nanoparticles and the microstructural evolution

and mechanical properties of the processed zone. A surface composite matrix using FSP was affected by the type of reinforced particles and methods of imputing these particles into the alloys during processing.

2.9 Prediction and optimization of process parameters

Estimation and Modeling of the mechanical features of engineering materials is an awfully significant factor of engineering investigation. The mathematical models based on regression analysis, have been utilized for modeling the features of engineering materials. Recently, significant consideration has been given to the improvement of statistical analysis techniques for exploring data collections [102-110]. ANN has been a principal computational method for modeling the features of engineering materials. Numerous researchers have fruitfully applied ANN to model features of engineering materials [112, 113]. Vignesh, R. V et al. [108] used ANN to model the mechanical properties of friction stir welded aluminum alloy AA1100 and Britto. A. S. F et al. [111] who applied ANN to model the shear and tensile strength of the diffusion bonded AA5083 and AA7075 aluminum. Esfe, M. H et al. [114] utilized ANN for Modeling and prediction of rheological behavior of Al_2O_3-MWCNT/5W50 hybrid nano-lubricant. Response surface method is a well-known mathematical model used widely to model engineering materials. Rostamiyan et al. [115] used RSM to model mechanical properties of epoxy/glass fiber/SiO2/clay hybrid laminate composite. Zhwan Dilshad IbrahimSktani et al. [116] applied RSM to find precise correlation between parameters and responses of ZTA ceramic. GurabvaiahPunugupati et al. [117] utilized RSM for Modeling and optimization of wear characteristics of gelcast fused silica ceramic composites.

From the comprehensive literature review in this chapter, it was shown that only a few studies have been carried out to fabricate hybrid nano composite. The main aim of this research, therefore, is to develop a new hybrid composite material, based on FSP, to overcome the limitations of al 6061.

Ref.	Parameters, tool	Material/ thickness	To find	Results
[118]	1000 rpm 40mm/min Various tools	LM25 12 mm Sic	wear behavior	Equiaxed recrystallized grains and homogeneously distributed find SiC particles. The increase in stir zone area increased the pin volume ratio. Therefore, the hardness decreased and consequently the wear rate increased.
[119]	1200 rpm 50 mm /min Different tools	6061 alloy 7mm ZrB2	Microstructural evolution and mechanical properties	The fine-grained Al matrix composites with homogenously dispersed ZrB2 nanoparticles were successfully fabricated by 4-pass FSP of in situ 0–2 vol% ZrB2/6061Al nanocomposites. As the ZrB2 content increased, the Zener pinning effect resulted in finer grain size and higher fraction of LAGBs; a simple shear texture component still remained but the peak intensity slightly decreased. Significantly enhanced mechanical properties can be attributed to grain refinement.
[120]	1600 rpm 40 mm/min square pin	2024 Alloy 3 mm Sic	High temperature characteristics	Embedding SiC particles enhanced the microhardness of FSPed samples up to 50% relative to the as-received condition. This improvement is attributed to the grain refinement and uniform distribution of both large and fragmented SiC particles at the SZ. Yield strength of the as-received samples improved about 2.5 folds, in relation with the refined microstructure after FSP.

[121]	220, 340 rpm 10, 20 mm /min cylindrical pin	magnesium Sic and Al_2O_3	Mechanical properties	The enhancement of FSP with the Mg MMC obviously increases the micro hardness of the given cast specimens. Mg grain refinement results have been obtained from the heterogeneous nucleation of the primary Mg phase, using conventional FSP through a single pass condition. The results of micro structural characterization have revealed uniform distribution of SiC and Al2O3 particles and Dispersed homogenously in NZ, ensured by EDS analysis.
[122]	1500-2100 rpm 25/100 mm/min threaded cylindrical pin	AA 6092 3.1 mm SiC	Microstructure mechanical properties	The rotational speed has a more significant effect on the generated peak temperature, while the traverse speed controls the exposure time and subsequent cooling rate. The microstructure of NZ exhibits an elliptical shape, and fine equiaxed grains resulted from the CDR process. Grain growth in the NZ occurs as a result of incomplete CDR or in particular when exposure time at high temperature is very long. The grain boundary in the NZ is a mixture of LAGBs and HAGBs, and it is fraction controlled by the traverse speed.
[123]	1000 rpm 14 mm/min cylindrical pin	AA5052 6 mm ZrSiO4	Corrosion behavior and mechanical properties	The four-pass composites exhibited the maximum tensile strength, the superior ductility and corrosion resistance was observed to occur for a three-pass composite specimen. It is believed that the superior performance of the zircon-reinforced composites is mostly due to the presence of well dispersed reinforcement particles and grain refinement of the Al matrix during FSP.
[124]	1400 rpm 40 mm/min cylindrical pin	5038 AL 5mm Ti	Microstructure mechanical properties	3-pass SFSP ensured Ti particles to be uniformly distributed in the SZ and the formation of defect-free Al/Ti interface, consisting of mutual diffusion of elements rather than harmful reaction products. During SFSP of 5083Al, the continuous dynamic recrystallization (CDRX) was mainly responsible for grain refining.
[125]	800 rpm 50 mm/min Cylindrical pin	Magnesium 5 mm ZrSiO4	Mechanical properties	A uniform distribution of ZrSiO4 and Al2O3 reinforcing particles was obtained in the SZ after four passes FSP and Mg–ZrSiO4–Al2O3 micro/nano composite was produced. Formation of the composites improved their mechanical properties including hardness and wear resistance.

[126]	1000, 1200 and 1400 rpm 100 mm/min. threaded cylindrical triangular	AA2024 6 mm	microstructure and mechanical Properties	The triangular pin profile provides better results when compared to Threaded cylindrical tool pin geometry. The feed rate of 110 mm/min showed the best results in terms of tensile properties during friction stir processing. The results of Vickers micro-hardness show the maximum hardness of 148 Hv in the stir nugget zone.
[127]	1000-1800 rpm 0.2-0.5 mm/s plain cylindrical	Al 5083 5mm Ni	Mechanical properties	Uniformly in 5083 Al. The fine (ball milled) particles were more uniformly distributed in the stir zone compared to the as-received coarse particles. FSP refined the grain size of the matrix from 25 μm to 3 μm by dynamic recrystallization process. The hardness and tensile properties of the composite improved significantly compared to the base alloy and more importantly a high ductility was also retained in the composite.
[128]	800 rpm 50 mm/min threaded cylindrical pin	AA5083 5 mm zirconia	wear properties	Wear rate of the fabricated materials significantly decreased after multi-pass friction stir processing. This could be explained by their higher hardness as well as load bearing effect of zirconia nanoparticles. Also, observation of worn surface of the 8-pass FSP'ed material suggested that abrasive wear has happened. Whereas, with regard to

[129]	1120 rpm 40 mm/min Cylindrical pin	Alloy 6061 6 mm TiB2	Tribological Properties	It is observed that increase in volume percentage of TiB2, microhardness increases up to 132 Hv and which is Higher than as received Aluminum alloy (104 Hv). It is found that high wear resistance exhibited at 4 volume percentage (vol. %) as compared with the 2 and 8 vol. %. It is observed that the worn debris formation is more at the 8 vol. %. Of Al-TiB2 surface nano composite.
[130]	1400 rpm 40 mm/min cylindrical pin	AA5083 5 mm Ti	Microstructure and mechanical properties	A relatively uniform distribution of Ti particles with excellent Al/Ti interface bonding without micropores and harmful reaction products was obtained in both FSPed AMCs, which indicates the suitability of the FSP processing parameters in air and water respectively. The FSPed AMCs exhibited considerable improvement in strength accompanied by an appreciable amount of ductility.
[131]	1075 rpm 30 mm/min Cylindrical pin	Al–Mg 5mm Titanium dioxide	Microstructure and texture development	The addition of TiO2 nanoparticles accelerated grain refinement of the aluminum matrix during FSP. The microstructural refinement became more intensive as the volume fraction of reinforcing particles was increased. Onion ring pattern was also seen at high TiO2 Concentrations.

[132]	1250 (r/min) 16 (mm/min) Cylindrical pin	Al6061 alloy 6 mm Al_2O_3/TiB_2	Wear properties	Increasing the number of FSP passes cause a more uniform dispersion of Al2O3/TiB2 particles. A good dispersion of Al2O3/TiB2 particles is obtained for the SHC produced by four FSP passes. The FSP with Al2O3/TiB2 particles more effectively reduce the grain size of the Al6061 matrix, the finest grain size is obtained as 0.7 mm by four FSP passes. The hardness of the SHC increases significantly with increasing number of FSP passes. The mechanism of wear is a combination of abrasive and adhesive.
[133]	1500 r/min 25 mm/min Different tools	Al6061 5 mm Al_2O_3/TiB_2	Mechanical properties	Grain refinement occurs in the processed samples, and more grain refinement is obtained for samples produced using SQ and TR pin tool profile due to the pulsating action in the SZ of these samples. The distribution of reinforcement particles (Al2O3–TiB2) in specimens generated by the SQ and TR tool pin profiles is more uniform than those of the other pin profiles. It is due to the tool geometry, such as sharp edges and corners, which produce better stirring of the material and good material flow.

Chapter 3

METEDOLOGY

3.1 Introduction

This chapter reports the specifics of the experimental work completed in this study. The preparation of used tool and the hybrid nano-composite and description of friction stir processing steps will be provided in the figure (1).

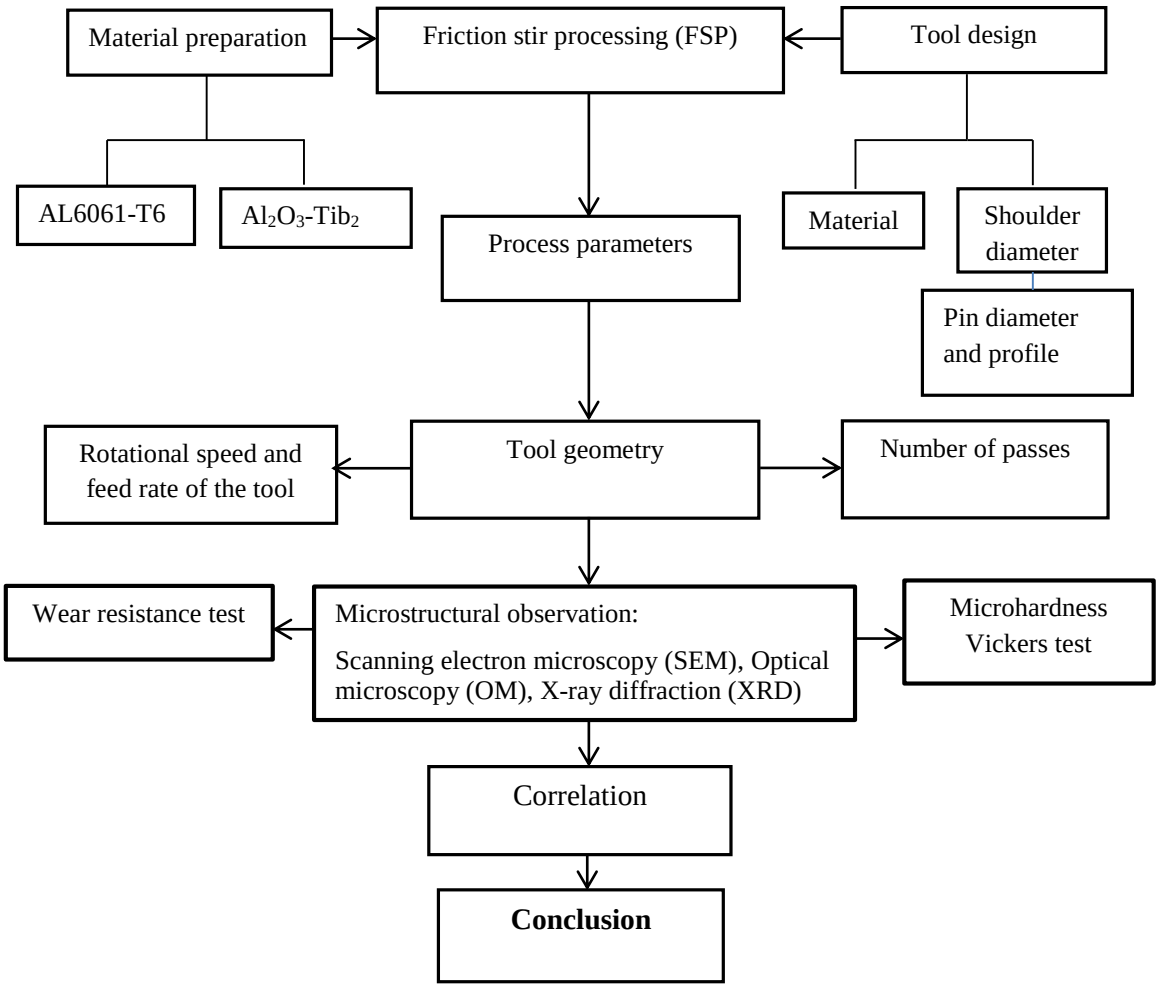

Figure 15. friction stir processing steps

3.2 Experimental setup (number of passes)

The hotpressed commercial Al6061 alloy with 5mm thickness is the alloy examined in the current study. The chemical components of the used aluminum is shown in Table 3.

Table 3: Chemical compositions of 6061-T6 aluminum alloy (wt. %)

Elements	**Mn**	**Fe**	**Mg**	**Si**	**Cu**	**Zn**	**Ti**	**Cr**	**Al**
6061-T6 Aluminum alloy	**0.0 - 0.15**	**0.0 - 0.70**	**0.80 - 1.20**	**0.40 - 0.80**	**0.15 - 0.40**	**0.0 - 0.25**	**0.0 - 0.15**	**0.04 - 0.35**	**Balance**

Al_2O_3-Tib_2 nanocomposite with a mean diameter of 500nm was made use of as reinforcement particles. This powder was prepared under a project at School of Metallurgy and Materials Engineering, University of Tehran, and the outcomes of the mentioned project are made available in the published papers [139.140].

The FSP was coordinated using vertical milling machine Figure 16. The tilt angle between the tool and normal direction of the plate surfaces was adjusted to 3º Fig 17. Also, the penetration depth of the tool into the plates was kept constant in all the experiments. A groove 2mm wide and 3mm deep was on the BM made to contain the powder during friction stirring. Approximately 1 g/ cm length of the sample of Al_2O_3-Tib_2 powder was included to the groove made on the substrate and then compacted as shown in Figure 18.

Figure 16. The vertical milling machine

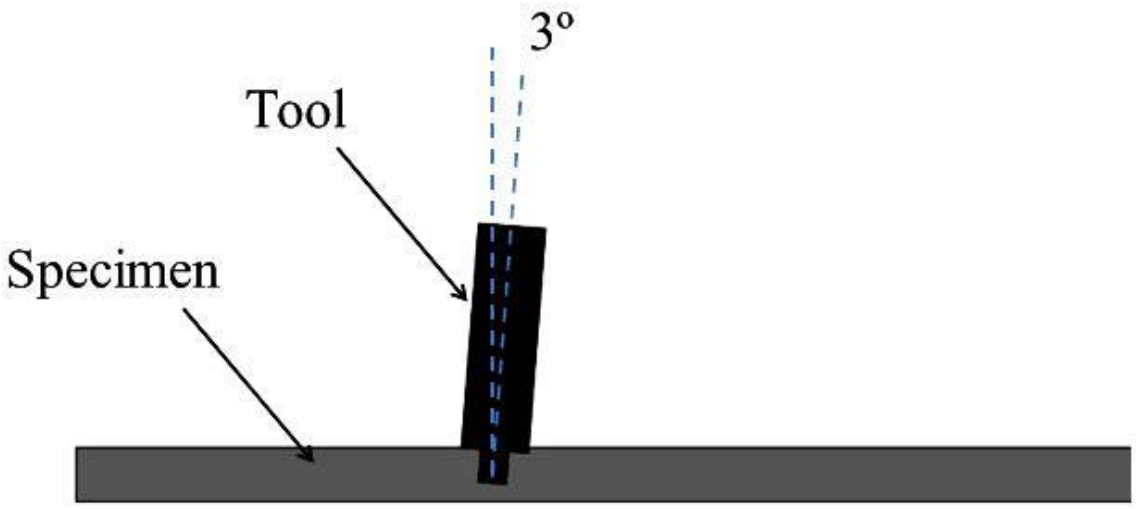

Figure 17. The angle between tool and normal direction of the plate surfaces

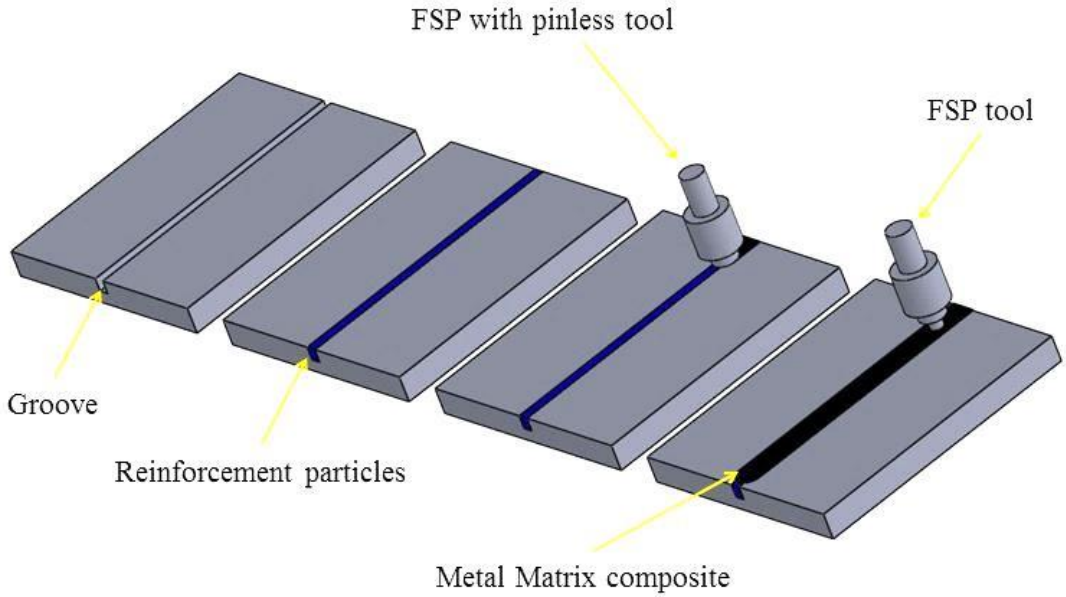

Figure 18. Schematic diagram of friction stir processing.

An earlier steel tool (hardened H-13 steel bar with 20mm diameter) was used for closing the upper surface of the groove to hinder outpouring of the powders during FSP. Al_2O_3-Tib_2 powder was then introduced into the matrix using another tool made from hardened H-13 tool steel with a shoulder diameter of 16 mm, a pin diameter of 5 mm, and a pin length of 4.5 mm Figure 19. The samples were under numerous numbers of passes from one to four using 1250 (r/min) spindle speed at 16 (mm/min) feed rate and given in Table4.

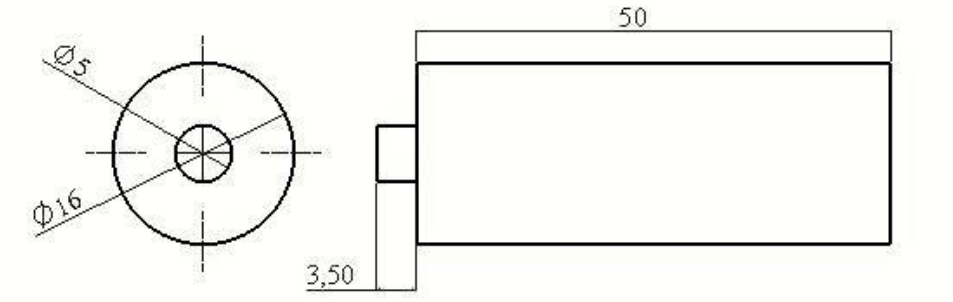

Figure 19. Friction stir processing tool

Table 4: FSP process parameters

Number of Passes	Spindle speed (r/min)	Feed rate (mm/min)
1 pass	1250	16
2 passes	✓	✓
3 passes	✓	✓
4 passes	✓	✓

Making use of optical microscopy and scanning electron microscopy (SEM) to carry out microstructural observations on the cross sections perpendicular to the tool traverse direction. Moreover, the Vickers hardness test was carried out along the centreline on the traverse cross section of the stirred zone using a 500 g load for 15 s for reaching the hardness profiles. The wear test was done with a pin-on-disk tribometer in accordance with the ASTM G99-04 standard. Materials under research were used to create round prismatic pins with a 5mm diameter. The duplicate discs were created using GCr15 steel with 55 HRC hardness and a surface roughness of Ra= 0.2 μm. The diameter of the sliding track on the disk surface was 11 mm. Before the wear test, each pin specimen was meshed down using 1000- grit abrasive paper. The wear tests were executed under dry sliding conditions for 2000 s with a constant load of 50N and a sliding speed of 0.5 m/s. All wear experimental specimens were cleaned in acetone and the weight measured to an accuracy of ±1mg before the testing and at different sliding length during the test.

3.3 Experimental setup tool geometry

The primary material and reinforcement particles used included Al6061 and Al_2O_3-Tib_2 nano powder respectively. Varying tool pin profiles were extracted using H13 steel to form the composite layer. Figure 20 elaborates the different tool geometries, including straight cylindrical (SC), threaded cylindrical (TH), taper cylindrical (TC),

square (SQ), and triangular (TR) pin profiles along with their dimensions. As can be seen from Figure 20, the length of the pin profiles was 4 mm, and all pin profiles were designed inside of a circle with a diameter of 5 mm. The diameter of the shoulders was 16 mm.

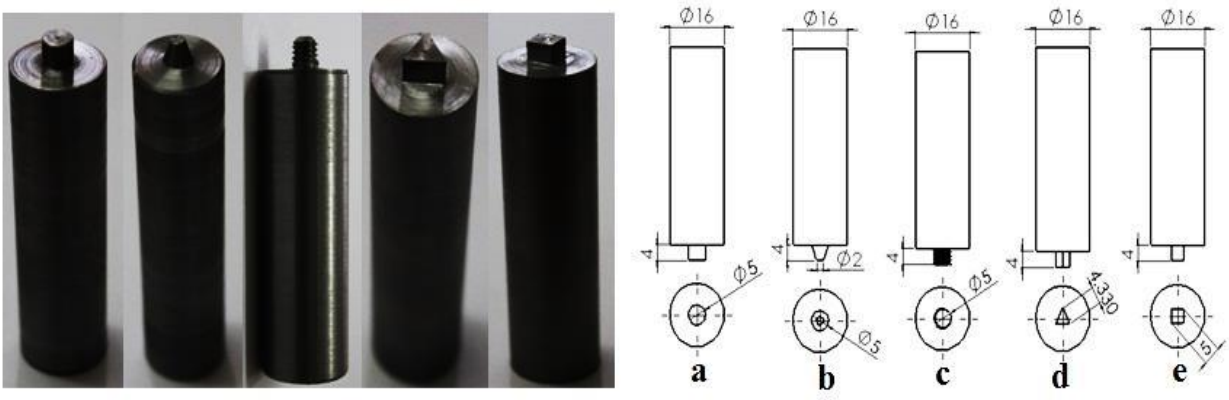

Figure 20. FSP tool pin profiles: (a) straight cylindrical, (b) taper cylindrical, (c) threaded cylindrical, (d) triangular, and (e) square

At a rotational speed of 1500 r/min, and at a traverse speed (feed rate) of 25 mm/min, one pass FSP of the different samples was executed. The procedures and tool parameters used for FSP are summarized in Table 5.

Table 5: FSP parameters and tool specification used in this study

Process parameters	Values
Tool rotational speed (rpm)	1500
Welding speed (mm/min)	25
Tool tilt angle	3°
Tool shoulder diameter (mm)	16
Tool material	H13
Tool hardness (HRC)	55
Pin length (mm)	4
Pin diameter of the tools (mm)	5

There exist two major factors that determine the parameters to be selected. Firstly, high heat input condition, i.e. low feed rate in connection with high rotational speed was chosen to procedural constraint for the material for creating more heat and plastic deformation, which can lead to a better distribution of the second phases. Secondly, the process and material parameters influences the final microstructure and mechanical properties of the FSPed materials. Thus, in order to stream line the effect of tool pin profile on the properties of the processed base metals, the other process parameters should be set in constant situations. Figure 3 shows the FSP process and a sample generated after FSP. The top surface of the sample shows us that there were no defects (such as voids and cracks) on the surface of the specimen, and a very smooth surface was gotten. For microstructural observations, the samples were extracted from the cross sections of the FSPed samples perpendicular to the processing direction. The samples were etched with Keller's reagent to show the macro and microstructure. Microstructural observation was done using an optical microscope (OM) and a scanning electron microscope (SEM) after preparing samples using different grit abrasive papers and mechanical polishing, . X-ray

diffraction (XRD) analysis was conducted using Cu Ka radiation at 40 kV and 30 mA to examine the powder composition. In order to ascertain that the used powder was nano sized, transmission electron microscope (TEM) was used. The Vickers hardness test was used to get the hardness outline using a 500 g load for 15 s.

3.4 Experimental setup (rotational speed, feed rate, number of passes)

AL6061-T6 alloy was used as a material in this study. Thickness of the AL plate is 5mm. conventional vertical milling machine was utilized to perform FSP. A groove was generated in middle of the plate with 1mm width and 4mm depth of cut to pour reinforcement particles and pin less tool was used to close the groove. The rectangular pin tool was used in this paper. The material of the tool was H13 steel. Fig. 44 shows schematic of the used tool. Al6061/ Al_2O_3-Tib_2 nano composite was generated using different process parameters of FSP. Rotational speed, feed rate of the tool and number of passes were used as a various process parameters and each of them include different levels which are shown in table 5. Several hardness measurements were done in process zone in each specimen to gain the precise hardness value of the sample. Artificial neural networks (ANN) and response surface methodology (RSM) were employed to predict the hardness performance of the friction stir processed Al6061/ Al_2O_3-Tib_2 nano composite. Matlab and Minitab were utilized as statistical software to design the metamodels for predicting of mechanical properties of composite layer.

3.4.1 Mechanical properties (hardness)

Vickers microhardness was utilized to obtain hardness behavior of the composite layer. Test load was 500 g for 15 second. Several hardness measurements were done

in process zone in each specimen to gain the precise hardness value of the sample. Table 6 shows parameters.

Table 6: Various process parameters

Rotational speed (rpm)	1500-1800 (2 level)
Feed rate (mm/min)	25-50-100 (3 level)
Number of passes (n)	1-2-3-4 (4 level)

Chapter 4

RESULT AND DISCUSSION

4.1 INTRODUCTION

The experimental outcomes and the resultant analysis of the mechanical tests and SEM analysis on the Al 6061 / Al_2O_3-Tib_2 surface hybrid composite (SHC) samples will be presented in this chapter.

4.2 Microstructural observations

Shown in Figure 21 is the XRD phase analysis of the used Al_2O_3-Tib_2 nanocomposite powder. Also, the ideal SEM photo of the used Al_2O_3-Tib_2 nanocomposite is illustrated in Figure 22. XRD phase analysis showed that the composition of the powder consists of Al_2O_3– 35wt% TiB_2 (by ignoring the other impurities, it was assumed that the remainder is Al_2O_3 of 65% by wt. %), and the SEM micrograph shows the presence of ultrafine Al_2O_3-Tib_2 composite particles.

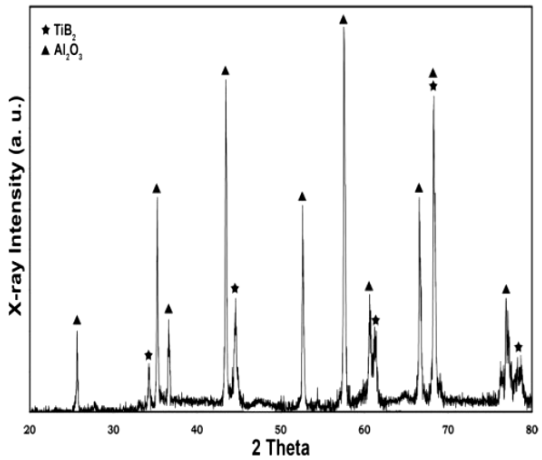

Figure 21. XRD phase analysis of the Al_2O_3-Tib_2.

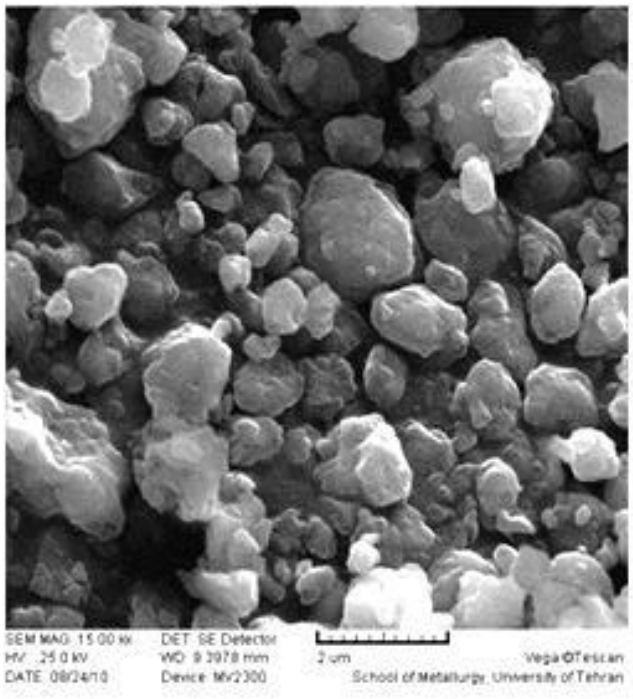

Figure 22. The SEM micrograph of Al_2O_3-Tib_2 composite particles

The conventional cross-sectional macrostructure of the processed material is illustrated in Figure 23. Going by the Figure 23, the macrostructure was made up of three different sectors including BM, thermomechanically affected zone, and stir zone (SZ). Also, the SZ with approximately 6–7mm width showed a characteristic onion-ring structure, as shown in Figure 23. The Al_2O_3-Tib_2 particles were mostly dispersed throughout this period by the vigorous stirring during FSP.

Figure 23. The typical cross-sectional macrostructure of the processed

The particle dispersion within the central cross-sectional area was macroscopically uniform, as illustrated in Figure 24(a), after one-pass FSP, However, the observed clustering particle size was ideally 10–20 mm, which is slightly bigger than the size of individual Al_2O_3-Tib_2 particles (500 nm).The clustering size of Al_2O_3-Tib_2 was further reduced, as shown in Figure 24(b) and (c) after two to four passes,. The size of clustered particles reduced with an increase in the amount of FSP passes, as illustrated in Figure 25.

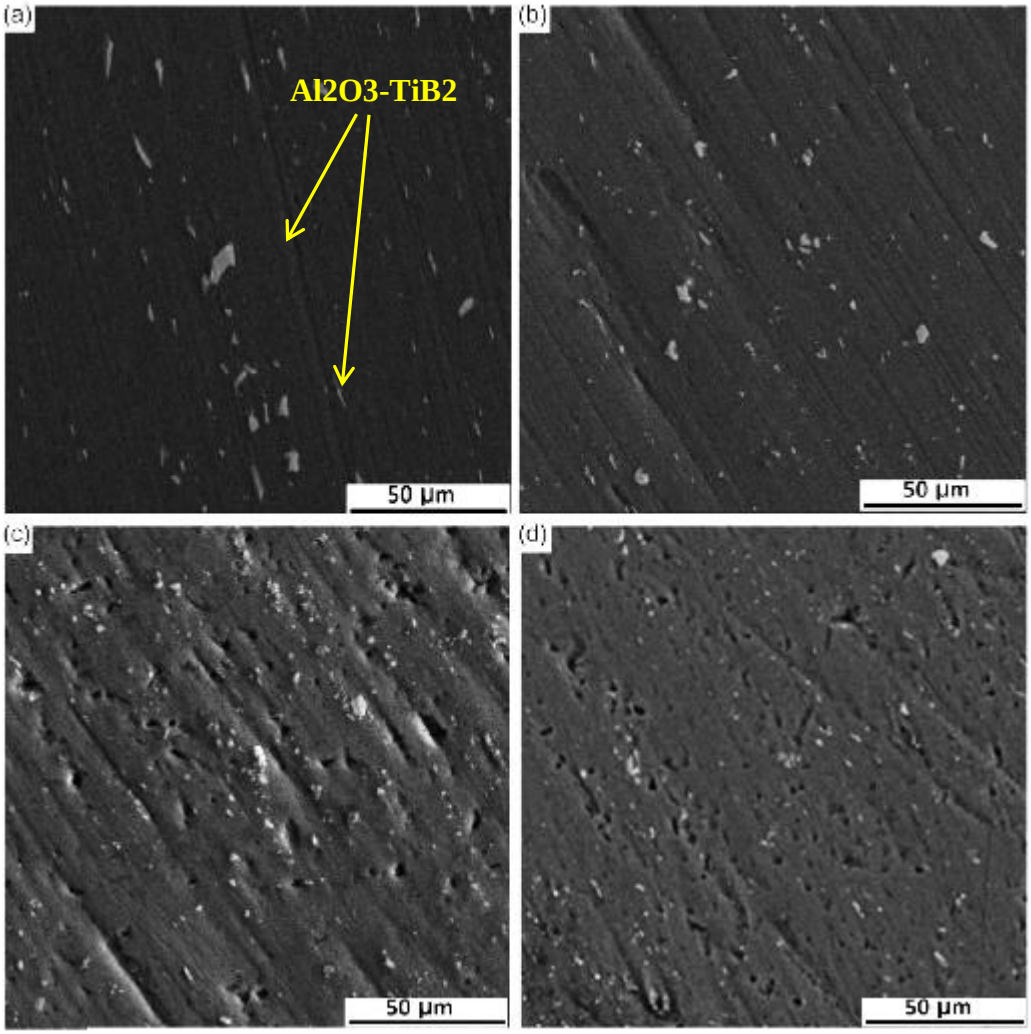

Figure 24. SEM micrographs showing the particle dispersion: (a) one pass, (b) two pass, (c) three pass, and (d) four pass.

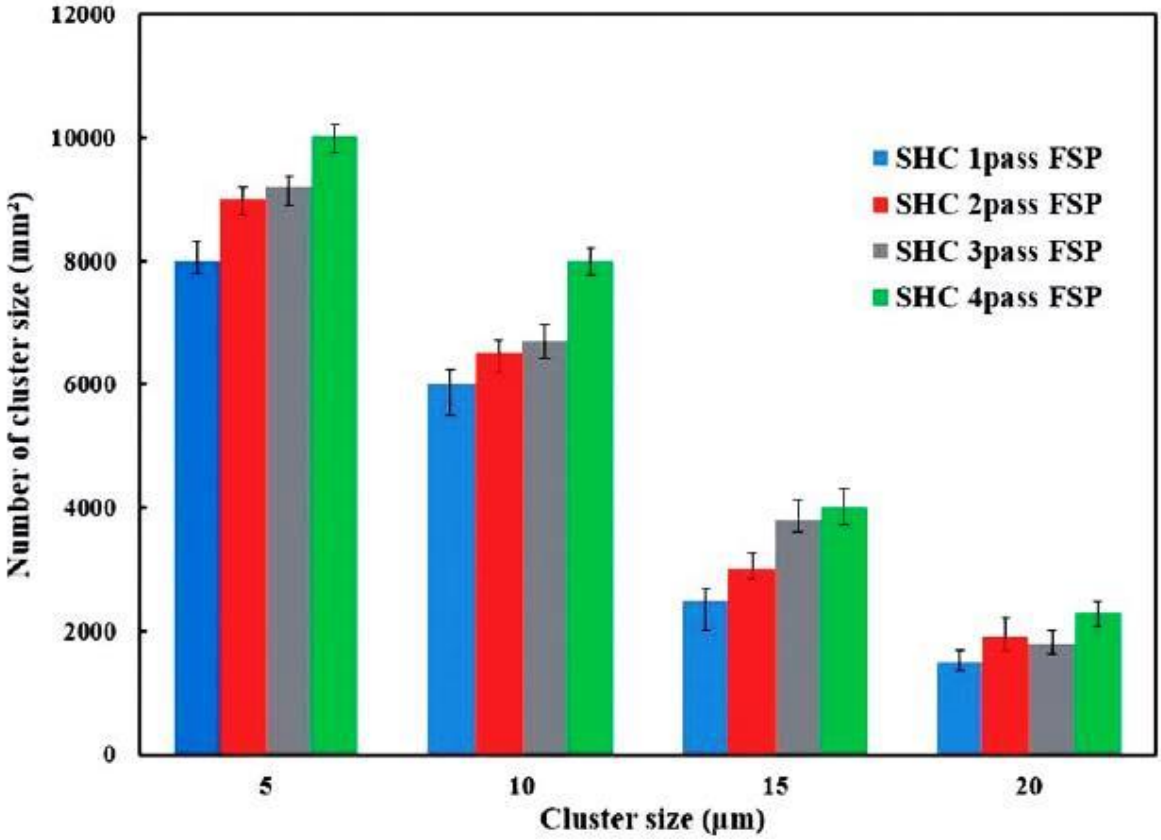

Figure 25. Statistical results for the clustered Al_2O_3-Tib_2 in the central regime after one to four FSP passes

The microstructures of the BM and processed materials at varying conditions are illustrated in Figure 26. According to Figure 26, the grain size of the SZ was reduced with an increase in the amount of the FSP passes. In all the processed materials, the stretched grains of the BM were substituted with the fine-equiaxed grains, gotten from dynamic recrystallization during FSP. The conventional grain size of the Al6061 alloy (without Al_2O_3-Tib_2 particles) after the same four-pass FSP was measured to be approximately 6 mm. Thus, the microstructures in the processed specimens with Al_2O_3-Tib_2 can be reduced to a much smaller size than is possible in the parent alloy.

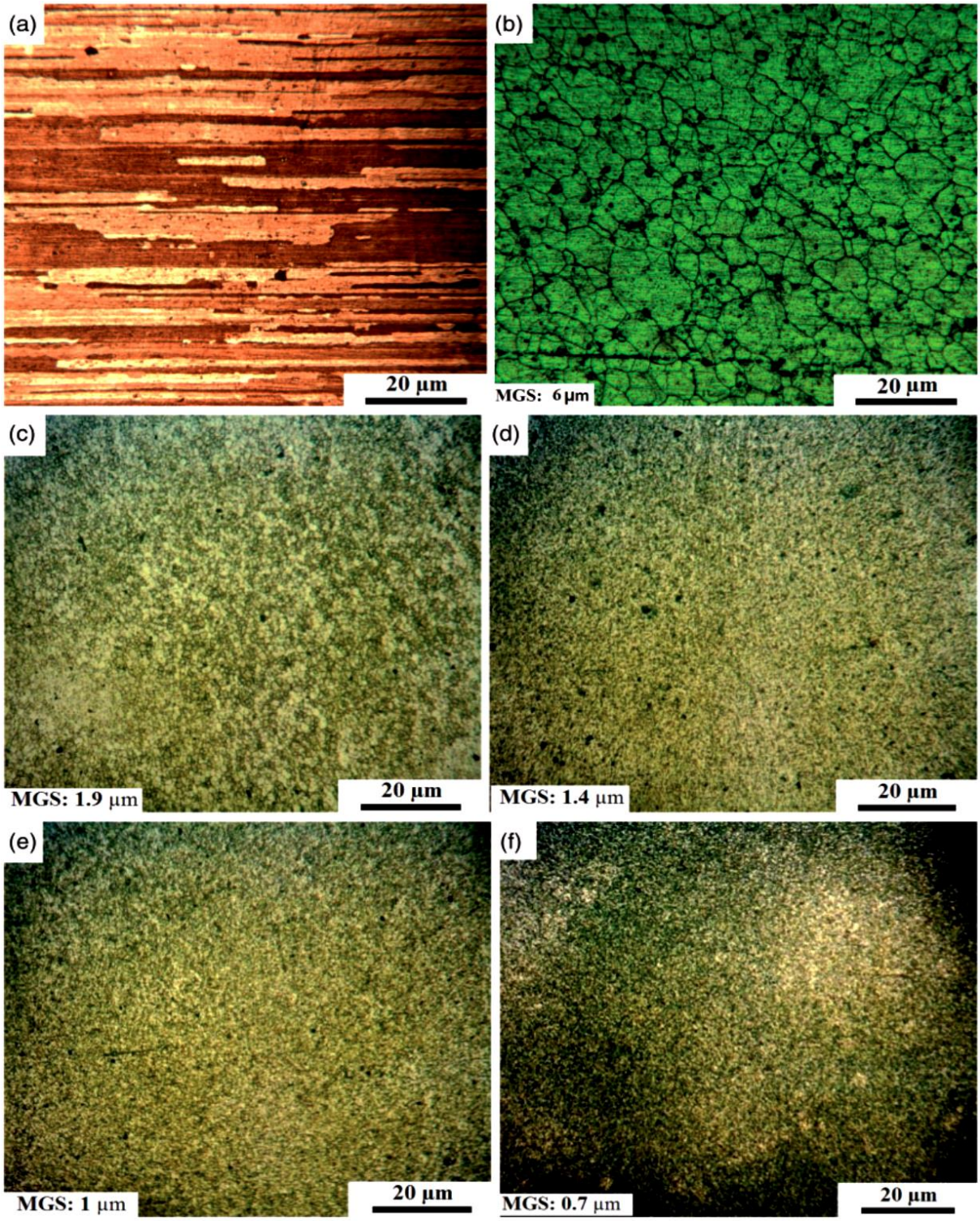

Figure 26. The microstructure of the: (a) BM, (b) four-passed sample without Al_2O_3-TiB_2, (c) one-passed sample with Al_2O_3-TiB_2, (d) two-passed sample with Al_2O_3-TiB_2, (e) three-passed sample with Al_2O_3-TiB_2, and (f) four-passed sample with Al_2O_3-TiB_2.

4.3 Effect of pass number on hardness

The hardness of the Al6061– Al_2O_3-Tib_2 SHC made by one-, two-, and four-pass FSP and also the hardness of the four-pass FSP Al6061 are shown in Figure 27. For SHC, the hardness relied basically on the existence and uniform distribution of Al_2O_3-Tib_2 particles. It was discovered that as the pass number increased, the hardness also increased. After FSP, the random spread of hardness within the FSP stirred zone is taken to be minor, meaning that the pin stirring dispersed the Al_2O_3-Tib_2 powders efficiently in a reasonably uniform way, particularly after more than two passes. In fact, with the increase in the FSP passes, the tool shoulder produced enough heat input and shears force to easily enclose the softening metal around the reinforcement particles. Thus, increasing the number of passes which led to a good demarcation and distribution in the nugget zone. [77,18] For the Al alloy with no Al_2O_3-Tib_2 powder, after four FSP passes, the microhardness profile exhibits a general softening and reduction of hardness in the SZ with a reduction from 110HV (for the BM) to 101HV (average amount for the SZ). Therefore, it can be observed that the SZ exhibited a lower hardness than the Al6061, in spite of the smaller grain size. These results imply that the hardness distribution of the stirred zone was independent of the grain size considering the Hall– Petch relation. [141] Therefore; other factors may control the mechanical properties of the stirred zone, such as precipitations and dislocation density [142-144].

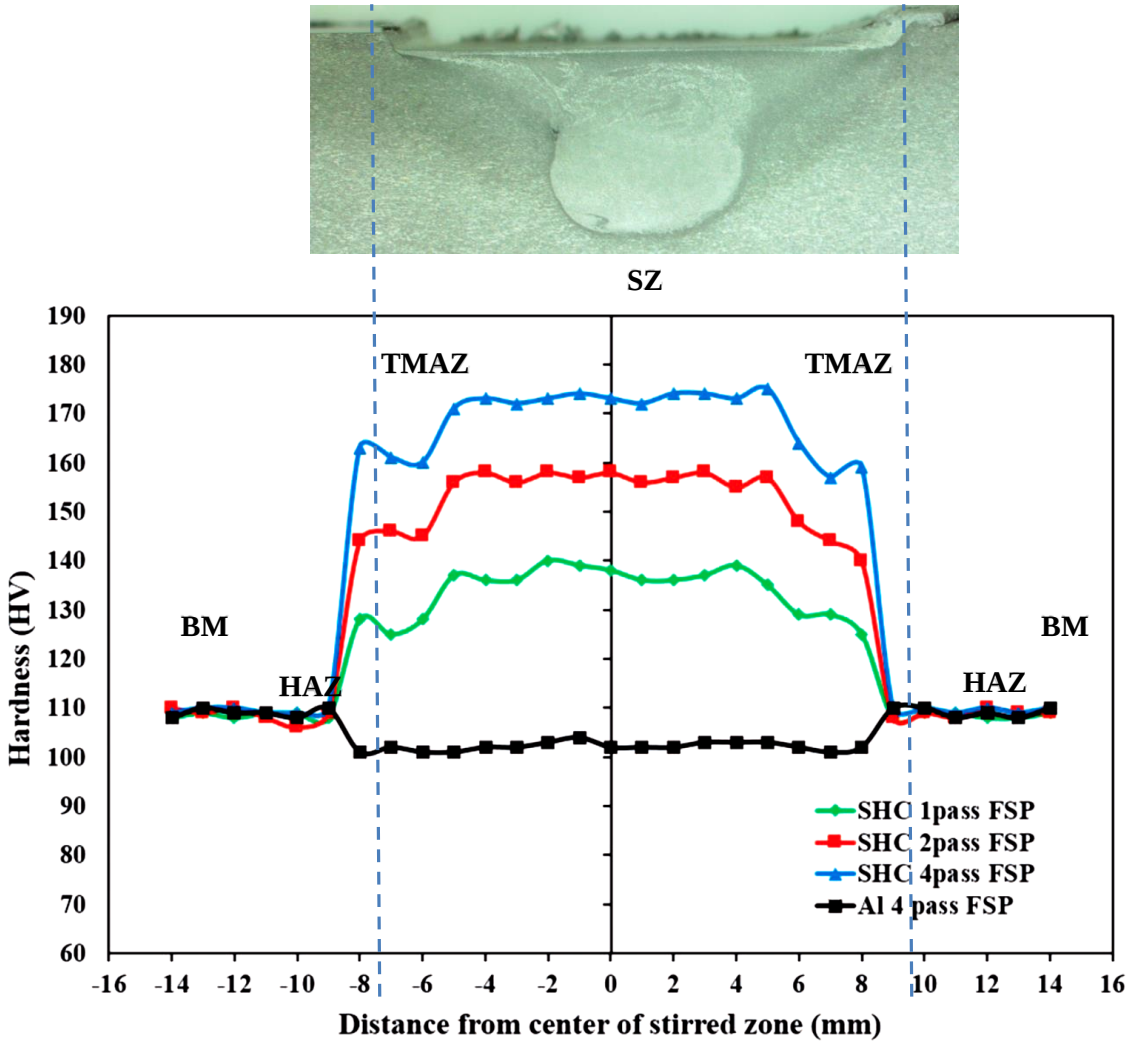

Figure 27. Variations of the microhardness distributions of the friction stir-processed 6061 Al alloy (without Al_2O_3-Tib_2) and surface hybrid composite layers.

4.4 Effect of pass number on wear rate

Figure 28 shows the variation of friction coefficient as a function of sliding distance for the Al6061 and SHCs. The mean friction coefficient of the Al6061 was found to be 0.68. The mean friction coefficient of the processed samples was 0.41 and 0.29 for two and four passes, respectively, which is much smaller than that of the Al6061. The initial increase in the friction coefficient of the Al6061 sample might be as a result of the increase in the frictional force required to overcome the high adhesive contact between the cylinder and the tested surface. [145,146] Variations to the length of localized plastic deformation at real contact areas might cause difference in

the friction coefficient, since the SHCs are harder, less plastic deformation and hence lower friction is expected.[147]

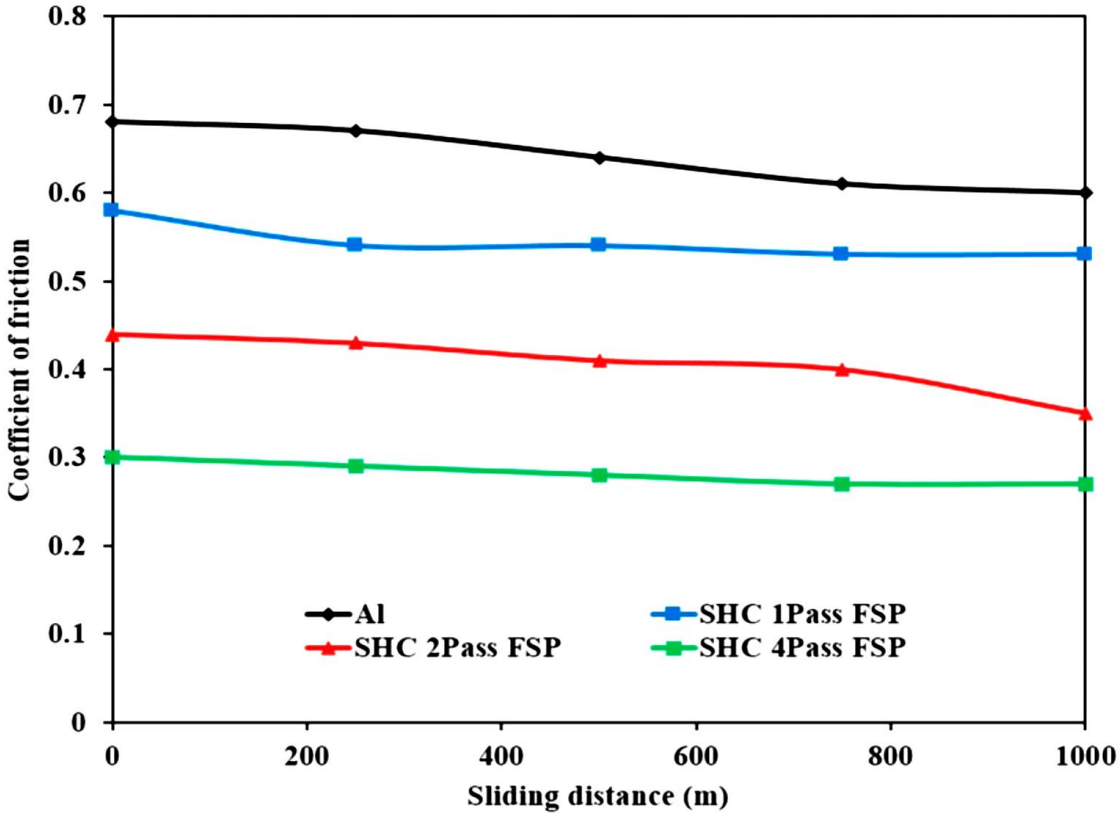

Figure 28. Change in the coefficient of friction with sliding distance for as-received Al and surface hybrid composite layer produced by one, two, and four FSP passes.

The relation between weight loss and the sliding distance of the Al6061 and SHC sample is further illustrated in Figure 29. The wear weight loss increased with increasing sliding distance. Furthermore, FSP was found to be useful in enhancing wear resistance under an input load of 10 N. The amount of weight loss of the Al6061 sample is higher than in the FSP samples. Although the weight loss curve of the FSP samples nearly reached a balanced state at long distances, the curve of the Al6061 appeared to increase at a constant rate. For the Al6061, the wear rate (weight loss/sliding distance) was high during the initial length of time of wear, after which it belittled. However, for the SHC produced by two-pass and four-pass FSP, the wear

rate was partly constant during sliding (Figure 30). A concise comparison of the graphs in Figures 29 and 30 also shows that both the extent of wear and the rate of wear are significantly lower in the SHCs in comparison to the Al6061 substrate. The major reasons for the increased wear resistance of the SHCs as compared with the Al6061 are the existence of the hard TiB_2 ceramic particles at the surface layer, the presence of the fine primary Al_2O_3 particulates, and the depreciation of surface defects such as pores and cavities due to FSP. Cavities reduce the contact area during the wear test, which increases the actual pressure on the outer surface of the specimen and thus increases the wear rate. The reduction of the wear rate of the SHCs with increasing tool rotational speed is is seen as a result of the increase of the hardness of the SHCs with increasing the tool rotational speed. [148-150]

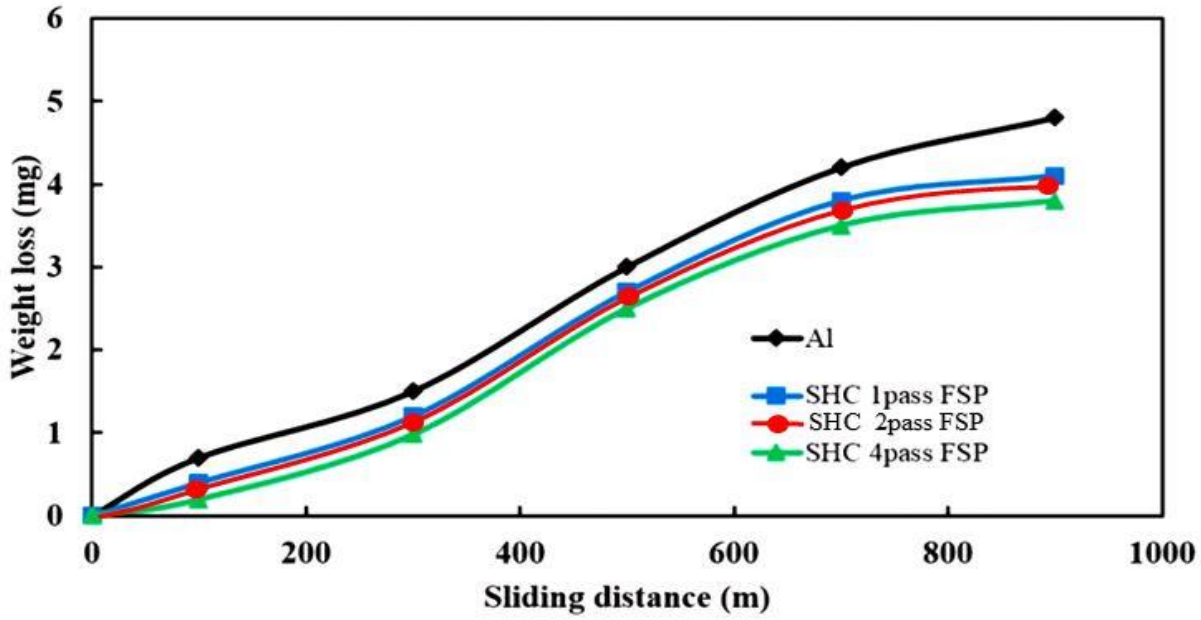

Figure 29. Change in the reduction in pin weight with sliding distance for as-received Al and surface hybrid composite layer produced by one, two and four FSP passes.

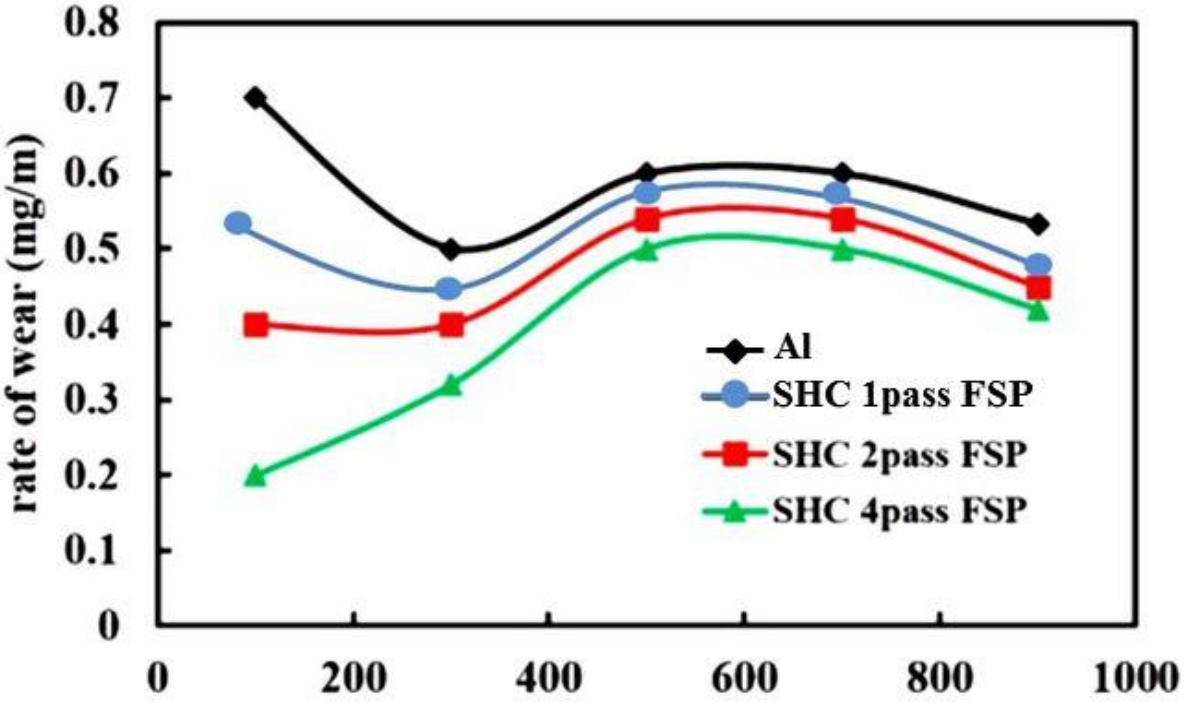

Figure 30. Change in the rate of wear with sliding distance for as-received Al and surface hybrid composite layer produced by one, two and four FSP passes.

Outcomes show that fabricated SHCs, decreases wear rate and friction coefficient of the base material, and therefore improves wear resistance. Reinforcing Al_2O_3-Tib_2 particles in SHC sustains wearing loads and hampers the direct load contact of the aluminum matrix and disk. The production of SHC positively affects wear behavior with the hardness enhancement. The best result (i.e., microstructure, hardness, and wear properties) was shown in the four-pass FSP specimens, so it is better to reveal it as the conclusive result. A comprehensive study of the scanning electron micrograph of the worn surfaces and the variation of the coefficient of friction for the SHC layer produced by four FSP passes and the Al6061 alloy was undertaken to comprehend the mechanism of wear. Figure 31 shows the micrographs of the worn surfaces of the Al6061 and the four-pass SHC, sample produced through testing at a normal load of 10 N.

It looks as if both adhesive and abrasive mechanisms contribute to wear of the four-pass SHC, sample according to Figure 31(b). The adhesive component of the wear mechanism can be inferred from the evidence of metal flow. In addition, the abrasive wear component is obvious from the ploughed grooves inside the wear tracks and the formation of wear debris. Comparatively, there was more wear debris for the Al6061 sample than for the four-passed SHC sample, in consensus with the results of the weight loss curve. It is known that with the abrasive wear mechanism, the wear of the material depreciates with increasing hardness. The high wear resistance of the four-passed SHC sample is attributed to a lower coefficient of friction and the improved hardness in this region [151].

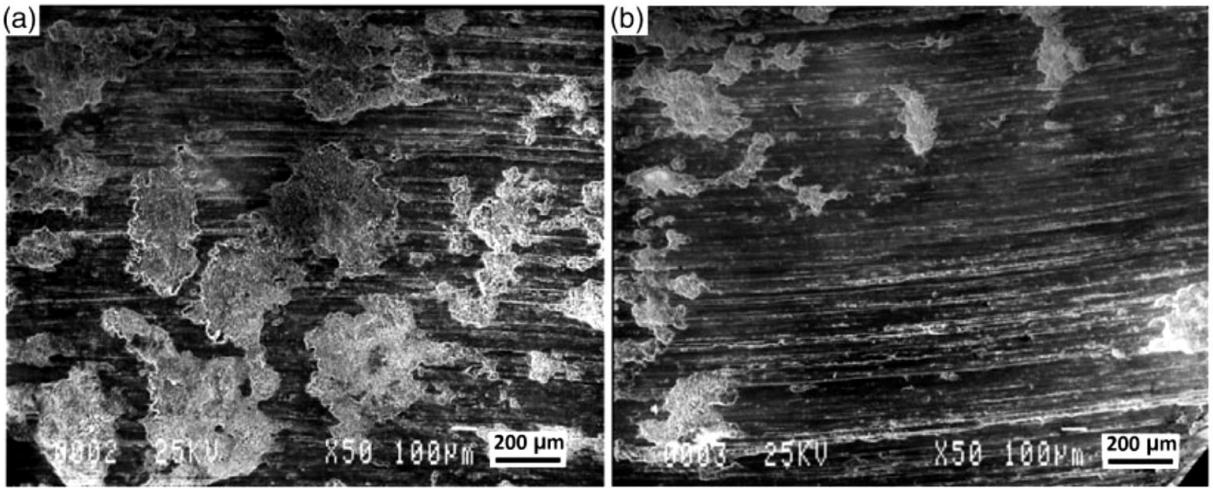

Figure 31. SEM micrograph of the worn out track of: (a) Al and (b) surface hybrid composite layer produced by four FSP passes.

4.5 Microstructural observation

Figure 32 shows the XRD phase analysis of the used powder. The composition of the powder was Al_2O_3–35wt% TiB_2. Figure 33 illustrates the TEM images of the Al_2O_3-Tib_2 nanoparticles. The XRD and TEM results validate the fact that the used powder for the FSP was nano-sized Al_2O_3-Tib_2 powder.

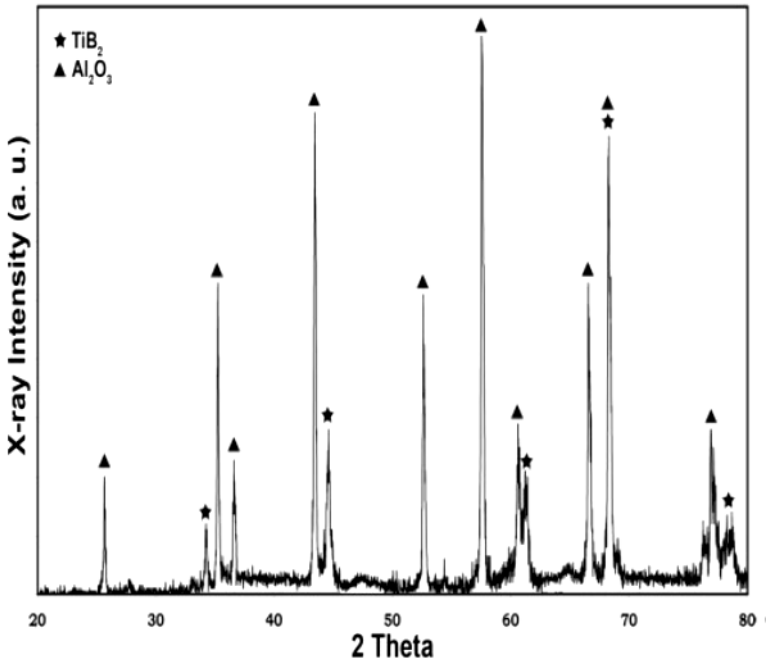

Figure 32. XRD phase analysis of the Al_2O_3-Tib_2 nanoparticles.

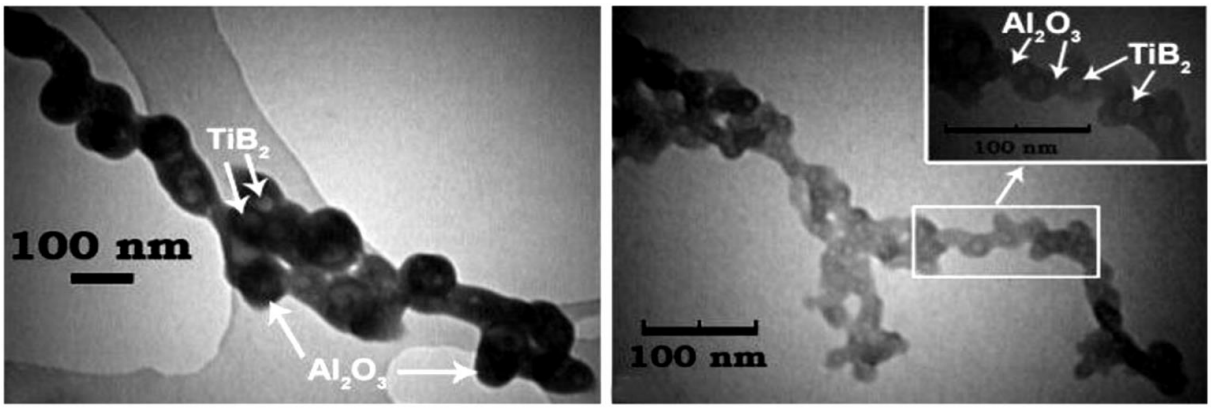

Figure 33. TEM micrograph of the Al_2O_3-Tib_2 nanoparticles.

The macrostructures of the different samples are demonstrated in Figure 34. Intense plastic deformation at high temperature during FSP results in production of a recrystallized fine-grained microstructure within the stirred zone (SZ). In addition, as a result of severe slope of strain, strain rate, and temperature from the middle of the stirred zone to base metal (BM) the macrostructure usually has four different zones. These various zones are BM, thermomechanically affected zone (TMAZ), heat-affected zone (HAZ), and SZ. [152-154] The shape and size of the SZ is dependent on the process parameters, such as the tool geometry, rotating speed of the tool, the temperature of the process and the thermal conductivity of the material.The SZ of the samples processed by TR and SQ pins is wider and deeper than those of the other pins as can be seen from macrostructures. In addition, going by the SEM micrographs (Figure 7), in the aspect of TR and SQ pins, the SZ shows an onion ring pattern in which the reinforcements (Al_2O_3-Tib_2) are mainly distributed. This is as a result of enough heat input produced via these tools, so the material flow required to form the onion ring pattern is attained. The main outcome of the macrostructure results is that a uniform distribution of the second particles (Al_2O_3-Tib_2) can be achieved in the larger SZ when the TR and SQ pins are used.

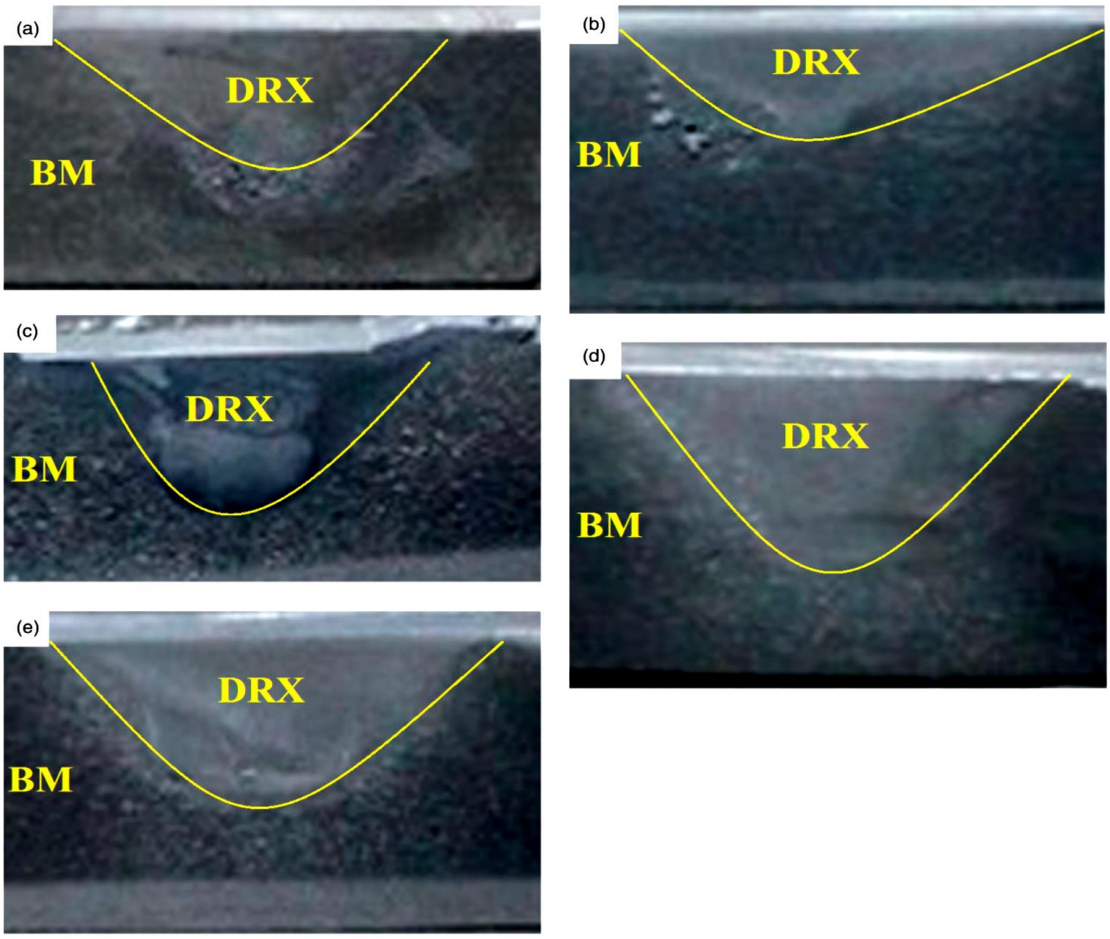

Figure 34. Macrostructure of the samples processed by different pin profile tools: (a) straight cylindrical, (b) taper cylindrical, (c) threaded cylindrical, (d) triangular, and (e) square.

Dynamic recrystallization during FSP leads to the formation of fine and equiaxed grains in the SZ. [155,156] Figure 35 shows the microstructure of the area between SZ and TMAZ of the samples processed with TR and SQ pin profiles. As can be observed from Figure 8, the grain size refinement in the SZ is visible in comparison to TMAZ, which is as a result of the dynamic recrystallization in the stir zone. As highlighted before, because of strain and temperature difference between SZ and TMAZ, the dynamic recrystallization cannot accomplished in TMAZ due to insufficient heat and material deformation [92.155].

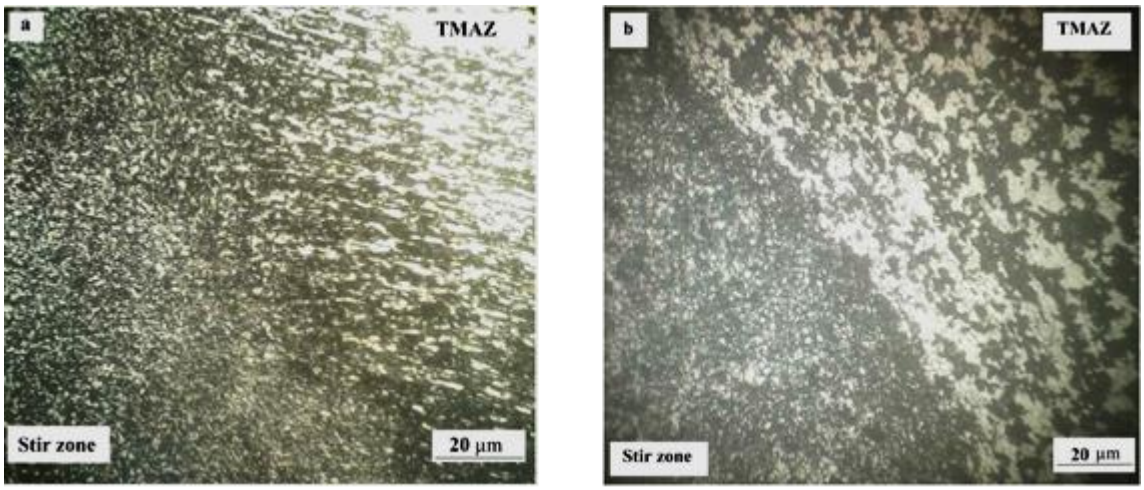

Figure 35. Microstructure of the stir zone and TMAZ in samples generated by: (a) square, and (b) TR pin profile tools.

Figure 36 illustrates the BM and SZ microstructures of the samples created by different tool pin profiles. The outcome of Figure 36 is that a grain size refinement in SZ happens to be in comparison to the BM, which is due to the dynamic recrystallization during FSP. Tool geometry is one of the most important process parameters that affect the grain size of the nugget zone. Samples produced via rectangular and TR tool pin profiles experience pulsating actions in their nugget zone due to tool geometry. A 1500 r/min rotational speed is used to generate the samples, so the number of tool rotations per second is 25. The TR tool pin profile has three flat faces; therefore, this tool can produce 75 pulses/s (25×3= 75). The SQ tool pin profile has 4 flat edges, so it creates 100 pulses/s (25×4=100). Other tools cannot generate pulsating actions due to their geometry[157]. Therefore, higher grain refinement is noticed in samples generated using TR and SQ tool pin profiles in comparison to other samples as a result of the higher pulsating action in the SZ. These pulses results in the formation of finer grains, which can result in the improvement of the mechanical properties. [157] it is known that pulsating effect can lead to both larger deformation and higher temperature. The larger deformation

results in finer grains, but on the other hand the higher temperature may lead to grain growth. In this study it can be it can be inferred that the deformation is the dominant factor controlling the grain refinement process during the FSP. The reason for his result is the fact that the other process parameters such as rotational speed, feed rate, pin and shoulder sizes, etc. were constant during the all processes, which are known as effective parameters that influences the produced heat. Therefore, the heat amount during processing by using different tool pin profiles can be assumed constant. In this condition, the dominant factor will be just the amount of the plastic deformation.

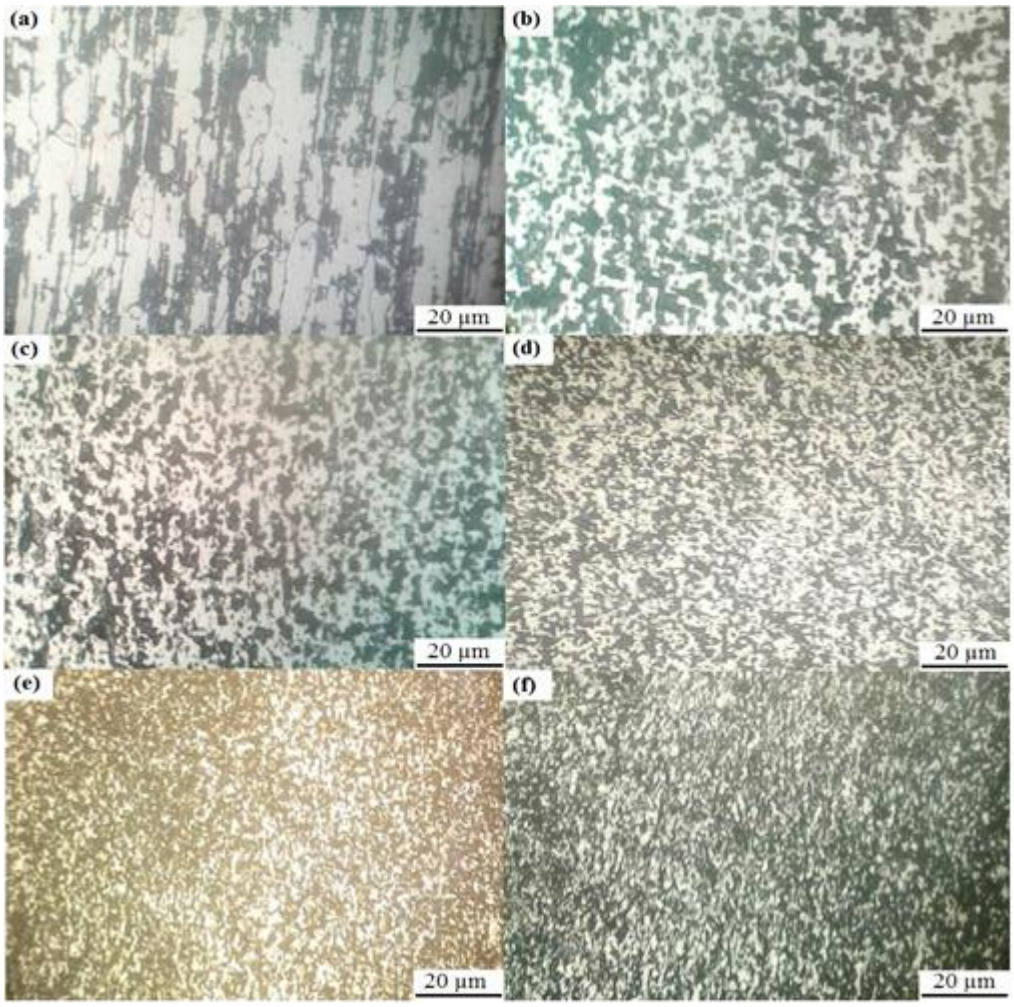

Figure 36. The microstructure of the: (a) base metal, and samples generated by: (b) SC pin profile (average grain size of 2.4 µm), (c) TC pin profile (average grain size of 2.3 µm), (d) TH pin profile (average grain size of 1.8 µm), (e) TR pin profile (average grain size of 1.2 µm), and (f) SQ pin profile (average grain size of 1.1 µm).

The SEM micrographs of the cross-sectional area of the samples generated using different tool pin profiles is illustrated in Figure 37. The results points towards the fact that the distribution of the second phase particles is more uniform in samples generated by the SQ and triangle tools. The sharp edges and corners of these tools causes better stirring of the material and good material flow, and hence results in a better distribution of the second particles. [90.91] Moreover, after processing utilizing different tool geometries, the clustering size of Al_2O_3-Tib_2 depreciate as shown in Figure 38. The minimization of the clustering size of the particles in samples processed via TR and SQ tool pins is higher than the other samples due to the tool geometry, which outputs a more uniform distribution of reinforcement particles.

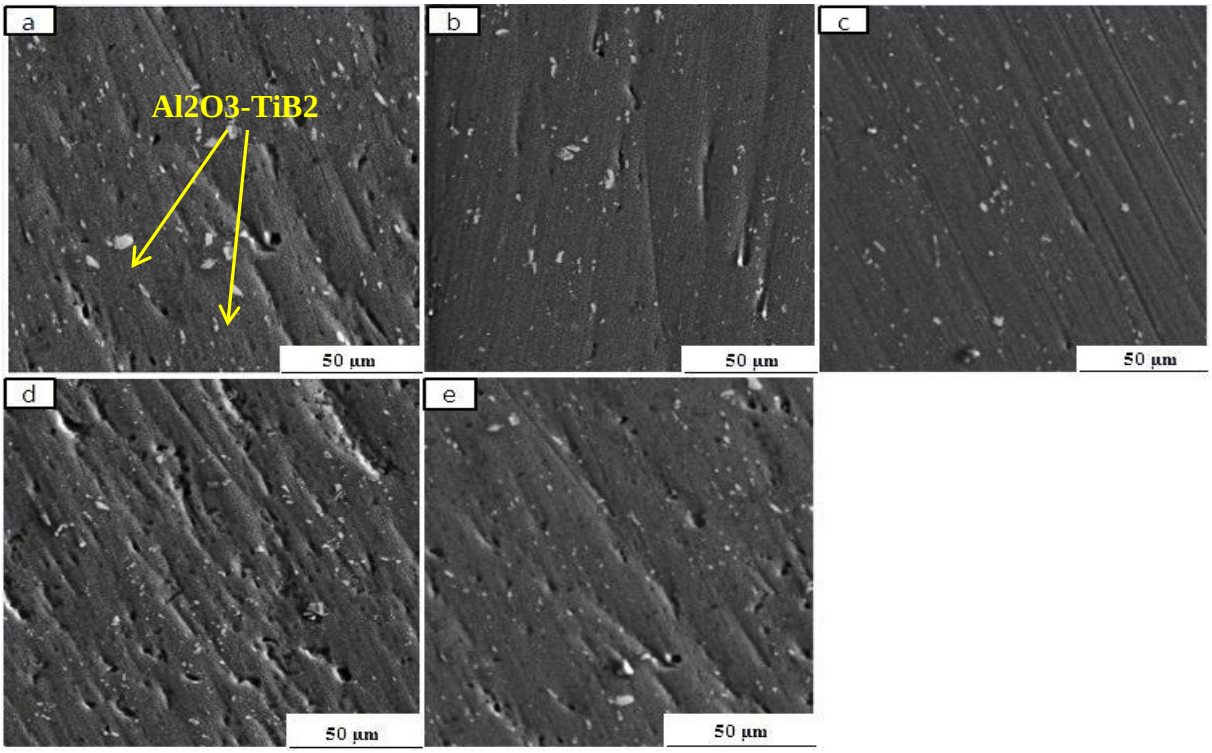

Figure 37. SEM images displaying the distribution of Al_2O_3-Tib_2 nanoparticles in samples fabricated by: (a) SC pin profile, (b) TC pin profile, (c) TH pin profile, (d) TR pin profile, and (e) SQ pin profile.

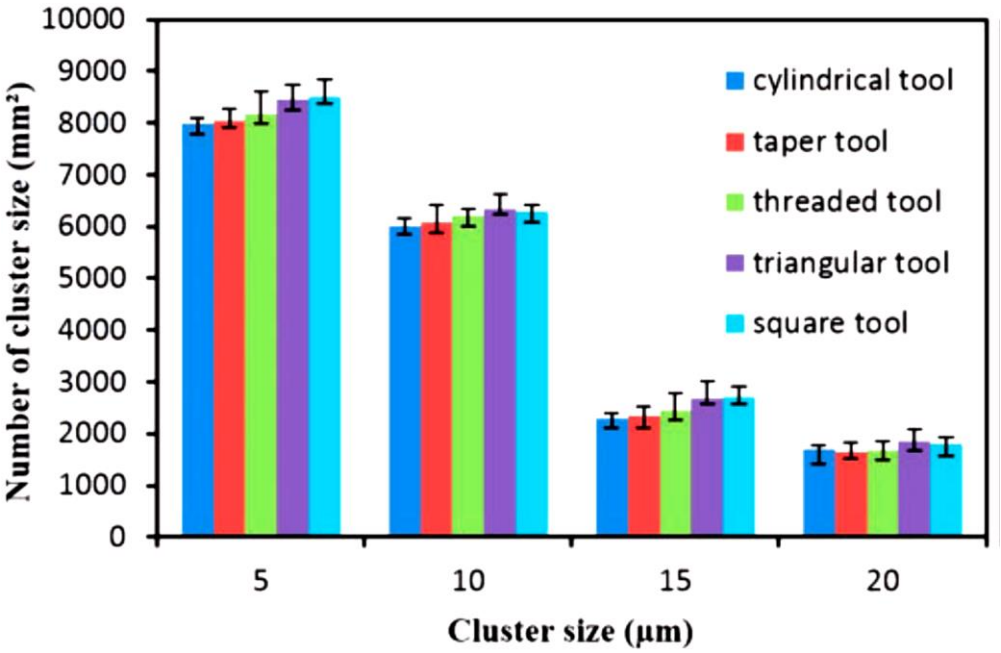

Figure 38. Results for the clustered Al_2O_3-Tib_2 in the stir zone of samples generated via different tools.

4.6 Effect of the tool pin profile on hardness

Figure 39 shows the hardness profiles for the different samples processed by various tool pin profiles. The mean hardness of the BM was 110 HV, and the mean hardness of the SZ for the processed samples were higher than 138 HV, because of the presence of finer grains and pinning effect of the hard Al_2O_3-Tib_2 particles. From Figure 39, the results show that the samples generated using SQ and TR pin tools have increased hardness in comparison to the other samples. Based on the microstructural observation, the best uniform distribution of reinforcement particles took place in the samples generated by the SQ and TR pin tools, which resulted in a better stirring of the material in the SZ and good material flow. Hence, the result of the uniform distribution of reinforcement particles into the matrix causes mechanical property enhancement in the fabricated composites. Besides, the occurrence of dynamic recrystallization in SZ resulted in the formation of very fine recrystallized

grains in this area, which could be another reason for the hardness increment [77, 98, 158-160].

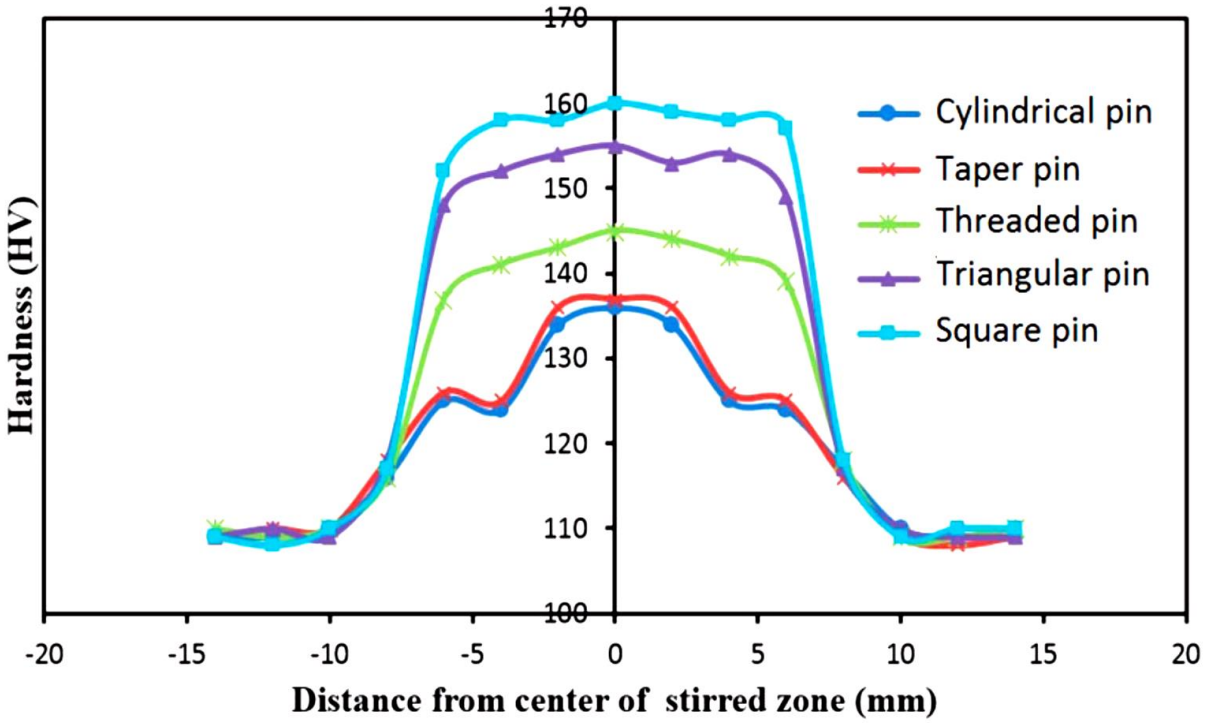

Figure 39. Alteration of the microhardness allocation of samples generated via different tool pin profiles.

4.7 Influence of the tool pin profile on the wear

Before the wear test was carried out property abrasive paper (1000 grit) was used to create a smooth surface for the samples. A 50N force was applied to the specimen, and the speed of the sliding was 0.5 m/s. The wear test went on for 2000 s. All wear test specimens were cleansed with acetone, and the weight of samples was made with at an accuracy of 1mg prior to testing and at different sliding distances during the test. Conclusively, SEM was used to characterize the worn out surface of the different samples. The wear test was carried out via pin on- disk tribometer according to the ASTM G99-04 standard. Cylindrical pins with a 5mm diameter were cut out from the nugget zone of samples and base material. The discs were

made of GCr15 steel, which has a 55 HRC hardness and surface roughness of 0.2 mm.

Figure 40 illustrates the variation of the friction coefficient with respect to the sliding distance for the received Al6061 and the processed samples. The friction coefficient of the received Al6061 was 0.68. The friction coefficients of the samples generated by triangle and SQ pin profiles were 0.41 and 0.39, respectively, which were less than those of the other generated samples and BM. Figure 41 illustrates the weight loss of BM and the processed samples subjected to the wear test. The weight loss of samples is considered with respect to the sliding distance of the wear test, and increasing sliding distance causes increased wear weight loss. The result shows that the weight loss of the received aluminum 6061 samples is larger than the samples processed via FSP.

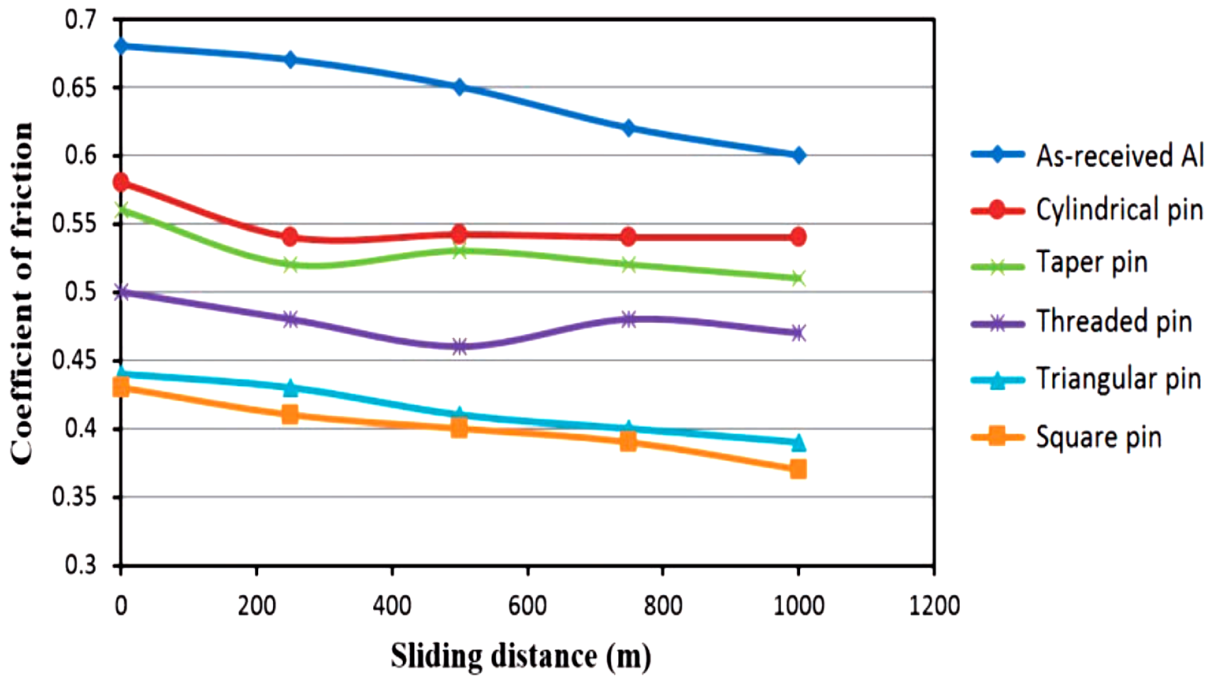

Figure 40. Alteration in the friction coefficient with sliding distance for the received Al and the specimens generated via different tool profiles.

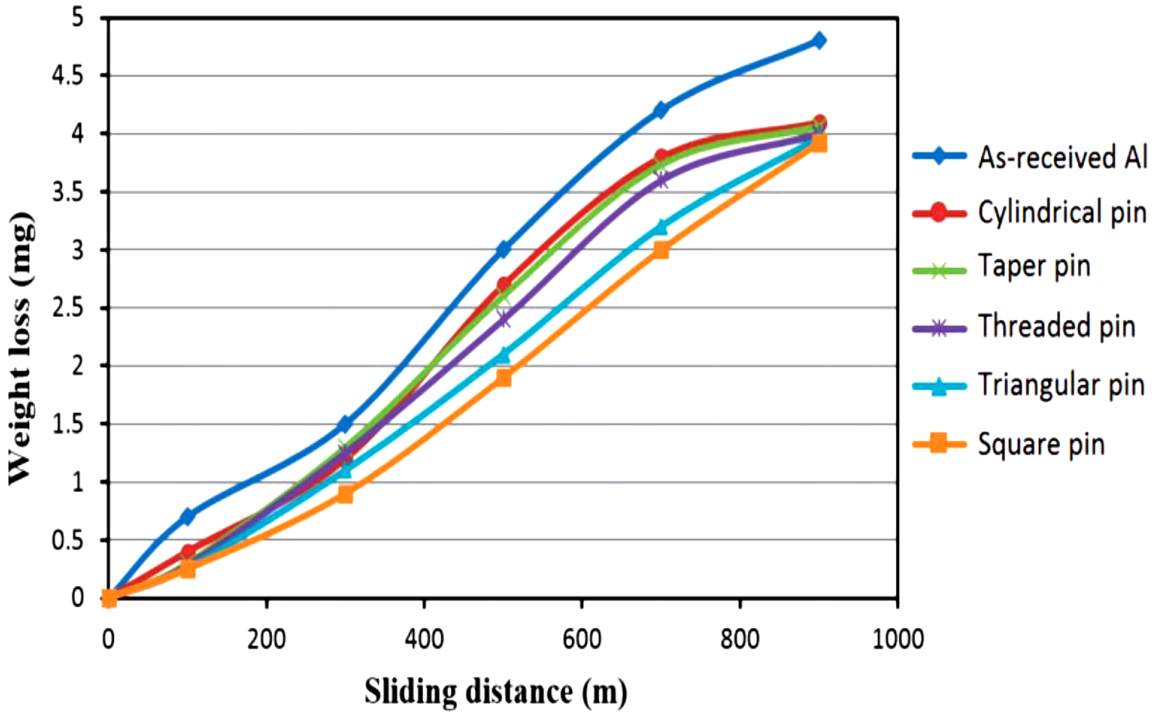

Figure 41. Alteration in the weight loss of the pin with sliding distance for received Al and samples fabricated with different tool pin profiles.

In addition, the weight loss of the processed samples using the SQ and TR tool pin profiles is less than the other samples due to better wear resistance. In fact, the presence of hard Al_2O_3-Tib_2 particles in the processed samples is the main reason for the higher wear resistance than aluminum 6061. FSP causes a decrease in surface defects, such as cavities and pores, which increases the wear rate of specimens [161]. The greater homogeneity of the distributed hard Al_2O_3-Tib_2 particles provides higher wear resistance in the samples generated using SQ and TR pin tools [162].

The wear rates of the generated composites and the BM are shown in Figure 42. The incorporation of the Al_2O_3-Tib_2 as reinforcement particles into a composite diminished the rate of wear considerably. The existence of the Al_2O_3-Tib_2 particles accompanied by the metallurgical alterations related to the stirring process reinforced the aluminum alloy. The wear resistance increment can be associated with

strengthening mechanisms such as substructure strengthening, Orowan strengthening, obstruction and work hardening mechanisms. Based on the microstructural observation, the main purpose for the improvement of wear resistance can be expatiated as follows. The existence of extreme grain refinement in the generated composite resulted in substructure strengthening. The fine dispersion of Al_2O_3-Tib_2 reinforcement particles in the Al matrix led to the enhancement of dislocation density and Orowan strengthening. Therefore, the wear resistance of the samples produced using SQ and TR tool pin profiles is greater than the other samples due to more grain refinement and uniform distribution of the reinforcement particles.

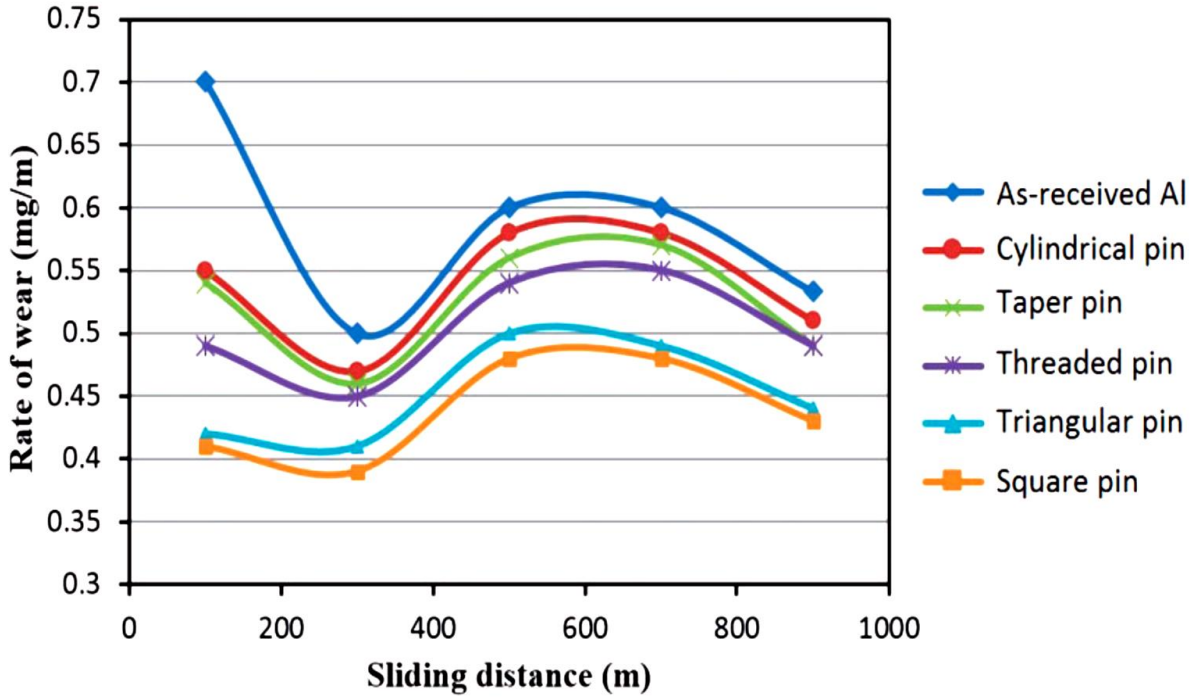

Figure 42. Alteration in the wear rate with sliding distance for received Al and specimens generated via different tool pin profiles.

Figure 43 indicates the SEM diagram of the worn surfaces of the composites and Al BM. The worn surface of the Al matrix elaborates on the maximum amount of plastic deformation or metal flow. Frictional action between sliding pin and rotating disc produces heat, which plasticizes the Al BM. Therefore, the proof of plastic

deformation or metal flow demonstrates an adhesive wear mechanism. As seen from Figure 43, the worn surfaces of the composites are vividly distinct from the Al BM, in which the metal flow is obviously reduced. The formation of wear debris and plunged grooves inside the wear tracks verifies abrasive wear mechanism. The plastic deformation or metal flow of the Al matrix was limited owing to the existence of the hard Al_2O_3-Tib_2 particles which minimizes the contact area between the sliding pin and rotating disc. The Al_2O_3-Tib_2 particles bear the wearing load.

From Figure 43(e) and (f), a smooth wear surface having grooves for specimens generated by TR and SQ pin is obvious [161, 163, and 57]. Based on the microstructural observations, it is determined that tool pin profile could strongly affect the wear characteristics of the generated composite.

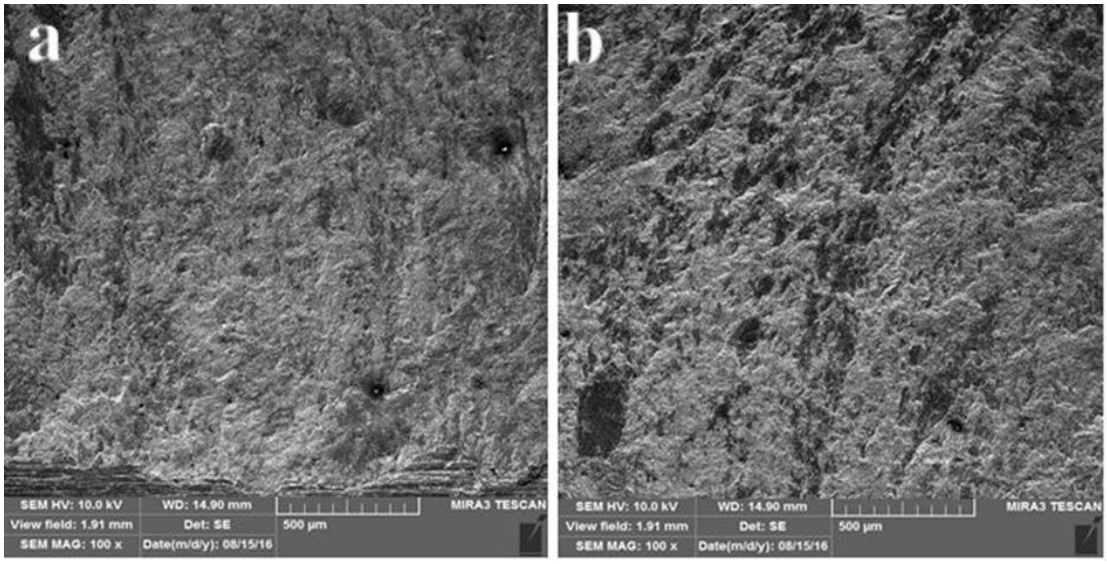

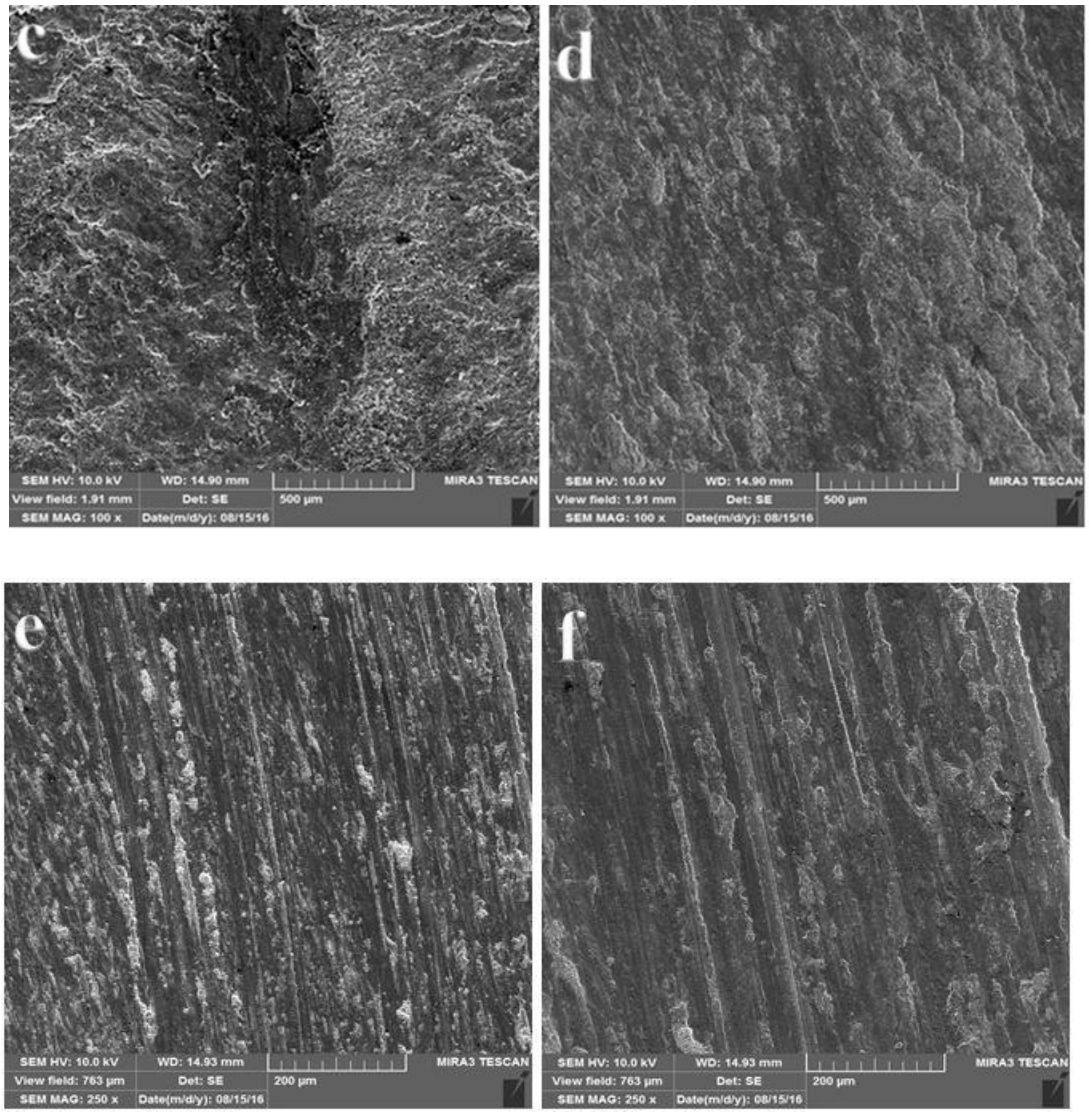

Figure 43. SEM micrograph of the worn out track of: (a) received Al, and processed samples of: (b) SC pin profile, (c) TC pin profile, (d) TH pin profile, (e) TR pin profile, and (f) SQ pin profile.

Chapter 5

METAMODELING

5.1 Estimation of Hardness behavior of Al6061/ Al_2O_3-Tib_2 nano composite

In this chapter, the artificial neural networks and response surface methodology were utilized to estimate the hardness behavior of the friction stir processed Al6061/ Al_2O_3-Tib_2 nano composite.

In this study, Al 6061 / Al_2O_3-Tib_2 hybrid nano-composite layer was fabricated using FSP and specimen was cut from the Transvers cross section to analyze influence of process parameters on the microstructure and mechanical properties. The hardness behavior of the processed zone shows that the process parameters of FSP such as number of passes; rotational speed and feed rate of the tool can be effective on the mechanical properties of the specimen. The hardness was modeled by artificial neural network (ANN) and response surface methodology (RSM). The predicted hardness values were compared with experimental values and a performance of two models was compared to each other.

5.2 Artificial Neural Network

Neural network is utilized to perform data-processing for large number of processing elements. The processing elements are generally prepared into a classification of

layers. ANN is designed via 3 layers which named the input, output, and hidden layers. Every layer involves 1 or more nodes which are shown in Figure 45(a). The links between the nodes show the information movement between the nodes. There are no activation function and weight for input layers so, and output layers demonstrate response for assumed inputs. The process for the development of ANN model is displayed in Figure 44.

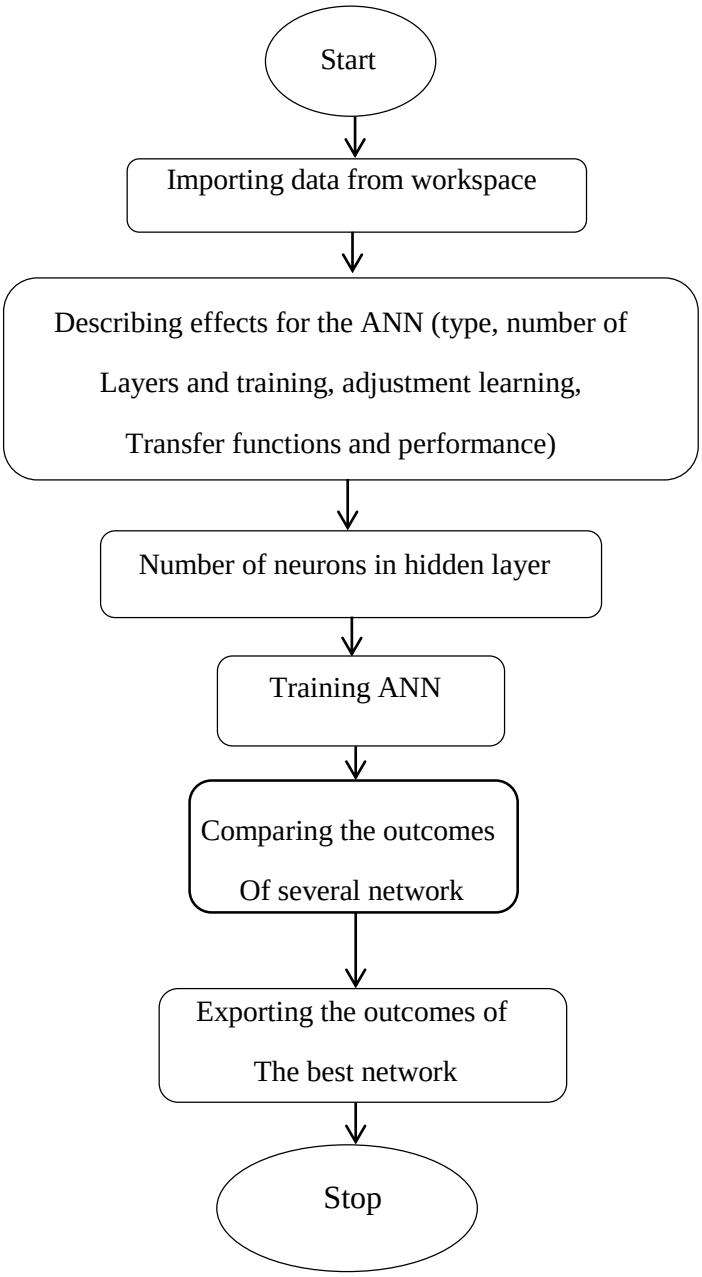

Figure 44. Steps included in the development of ANN model

5.2.1 Learning Algorithm of Back propagation:

It is a methodical technique for training multi-layer ANNs. Based on Back propagation algorithm, the networks acquires a distributed record between the input and output layers. This algorithm permits experimental achievement of the input, output recording information in multilayer networks. The difference between this algorithm and others is calculation of the weights over the learning phase of the network. In multilayer observations, computing the weights of hidden layers in a finest way is problematic to find minimum output error. The errors must be calculated to appraise the weights. The error in output layers is alteration between real and desired output. The performance of the ANN can be valued by separating the data into 3 sets: training set, validating set and testing set. Training set was used to set the ANN. The generalization of network is signified by validating set. The training will stop when generalization stops. The general performance of the ANN is demonstrated by testing set.

5.3 Results and discussion

5.3.1 Experimental results

The hardness behavior of the FSPed samples was tested by Vickers microhardness. The result of hardness test is shown in Table8. These outcomes demonstrate that process parameters of FSP such as rotational speed, feed rate of the tool and number of passes have a direct influence on the hardness behavior. Increasing rotational speed of the tool causes to higher heat input and higher plastic deformation in processed zone which result in better distribution of reinforcement particles and reduction of clustering. Furthermore decreasing feed rate of the tool generates higher heat input, more grain refinement which causes to more hardness. The outcomes showed that raise in the number of passes causes a more uniform dispersion of

reinforcement particles and consequently, reduction of particles clustering which is main reason for hardness increase.

5.3.2 Implementing of ANN

In this investigation, the fully established feed forward error back propagation algorithm is utilized to implement training for ANN, that is the most known and effective algorithm for training. Rotational speed of the tool, welding speed and number of passes represents as inputs nodes of ANN. The hardness behavior of the processed specimen regarded output nodes. 1 hidden layer included 8 neurons for the layer. Transferring function among all layers was tan-sigmoid function which is described as follows [114]:

$$\emptyset(x) = \frac{2}{1+e^{-2x}} - 1 \qquad \text{Eq. (8)}$$

Mean squared error (MSE) has been defined by the following equations:

$$MSE = \frac{\sum_{i=1}^{N}(e_i - o_i)^2}{N} \qquad \text{Eq. (9)}$$

Mean squared error processes the average of the squares of the errors among the observed value or experimental value (ei) and the estimated value (oi). N is total number of data.

Traingdx function was utilized as network training function. This function assesses bias and weight values consistent with gradient descent momentum and an adaptive learning rate. The function traingdx syndicate adaptive learning rate with momentum training. Backpropagation was utilized to compute results of performance regarding the bias and weight variables X. Each variable was attuned consistent with gradient descent with momentum. The algorithm of traingdx was indicated by the following equations:

$$dx = mc * dx(prev) + lr * mc * dperf/dx \quad \text{Eq. (10)}$$

Where dx (prev) is the prior alteration to the weight or bias, Lr is the factor of learning rate. For every repetition, if performance reduces to the goal, then the learning rate is improved by the factor lr_inc. If performance rises by more than the factor max_perf_inc, the learning rate is attuned by the factor lr_dec and the change, which improved the performance, is not complete. Figure 45(a), 45(b) demonstrates the model and architecture of this ANN respectively: 3 layers with full linkage and 3 input nodes are recorded into input layer to define 1 output. In this training, the total data sets were 24 which are acquired from FSP process. 16 data sets between 24 data sets are utilized in training process and 4 of them were used for validating process. The hidden layer includes 8 nodes. 12 sequences were performed for training process. To evaluate the overall performance of the trained ANN, the experimental results were compared to estimated results which are reported in Table 8, as the outcomes show liability of ANN. Figure 46 demonstrates the experimental results compared with estimated results of training dataset. Generalization ability of trained network was obtained via validating datasets which is presented in Figure 47. Mean squared error (MSE) was utilized to assess the performance of the trained ANN in estimation procedure. Capability of the trained ANN to estimate hardness of composite layer was indicated in Figure 48(a). Figure 48(b) indicates Plot of data regressions for all data sets. Maximum error for hardness behavior was 1.21 which is acceptable.

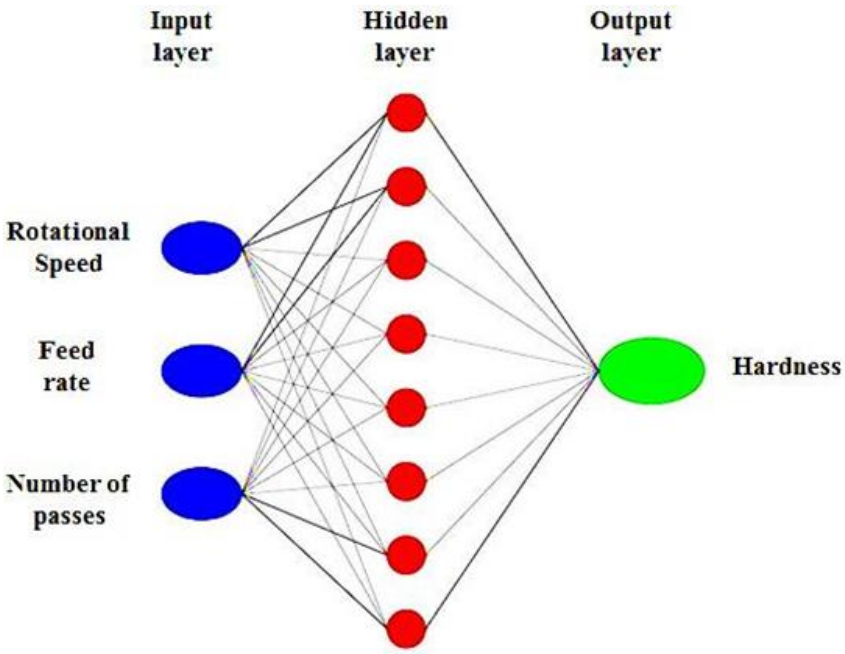

Figure 45.(a) The ANN model.

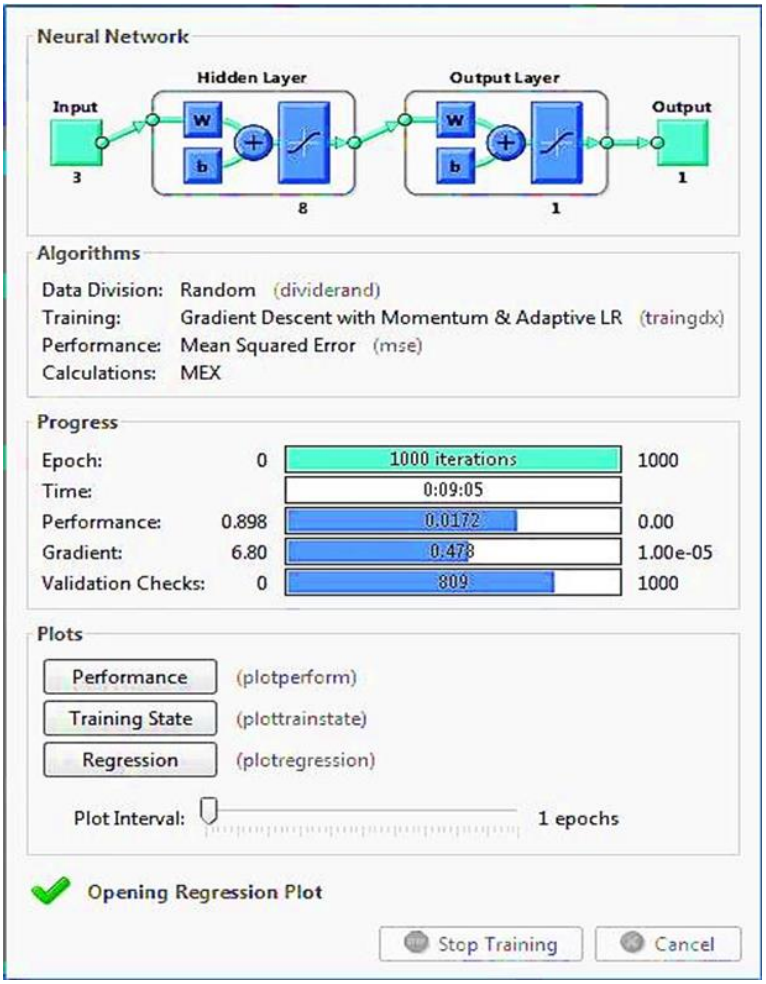

Figure 45.(b) The Neural Network Architecture.

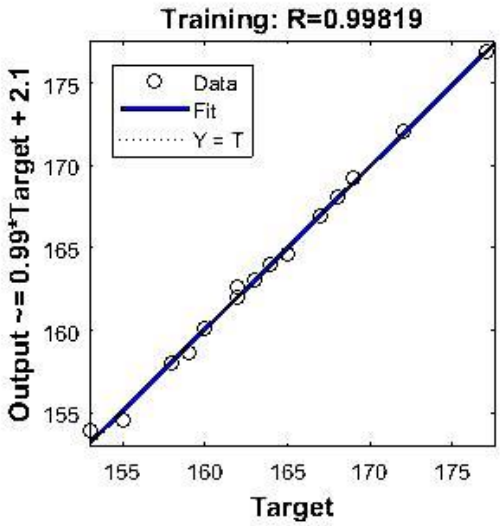

Figure 46. Training set

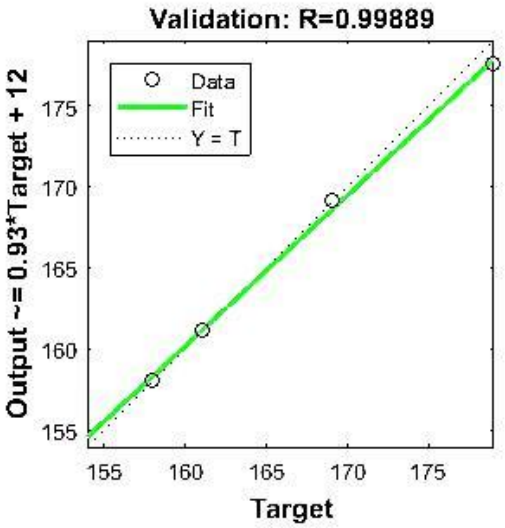

Figure 47. Validating set

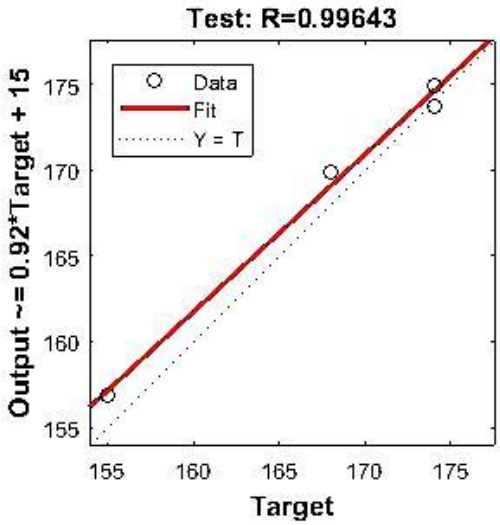

Figure 48. (a) Testing set

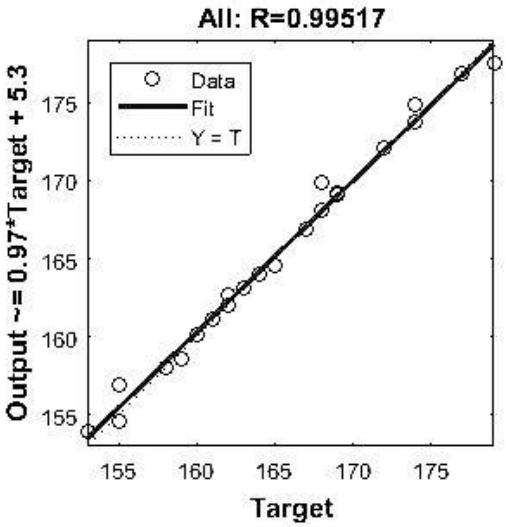

Figure 48. (b) Plot of data regressions (all)

5.4 Response Surface Methodology (RSM)

RSM is a mathematical model which has been utilized for optimizing and modeling the process parameters. The RSM has been used to optimize the responses which are a function of several input parameters and mathematical correlation between measured responses and the process parameters can be predicted by this model. The RSM contain following steps for FSP process: Recognizing the FSP effective factors; Deliberating a realistic limits of the recognized parameters; generating a desired

experimental design; implementing the examinations according to the generated experimental design; evaluating the responses; Launching the mathematical model; discovering the effect of the parameters on responses: predicting and optimizing the responses.

In this research, full factorial design with 24 runs, three FSP parameters containing rotational speed of the tool with 2 level, feed rate(welding speed) with 3 level , and number of passes with 4 level was engaged to design of experiments. Table 6 illustrates actual values and levels of FSP parameters. Furthermore, the measured response was the hardness.

5.4.1 Choosing the experimental design and modeling

The simple mathematical model which can be developed in RSM is based on a linear function. For its usage, it is vital that the responses attained be well fixed to the following relationship [164]:

$$Y = \beta_0 + \sum_{i=1}^{K} \beta_i X_i + \varepsilon \quad \text{Eq. (11)}$$

K= number of parameters, β_0 = constant term, β_i = coefficients of the linear parameters, X_i = represents the parameters, ε= residual related to the experiments

According to equation 11, the response would not extant any curvature. Thus second order model must be applied. This model should have both the first-order effects and the relations between the different experimental parameters. By the way, the following equation will be utilized [164]:

$$Y = \beta_0 + \sum_{i=1}^{K} \beta_i X_i + \sum_{1 \le i \le j}^{k} B_{ij} X_i X_j + \varepsilon \quad \text{Eq. (12)}$$

B_{ij}= coefficients of the interaction parameters. Moreover, to cover quadratic terms, the polynomial equation is needed which is shown in equation 13.

$$Y = \beta_0 + \sum_{i=1}^{K} \beta_i X_i + \sum_{i=1}^{k} B_{ii} X_i^2 + \sum_{1 \le i \le j}^{k} B_{ij} X_i X_j + \varepsilon \quad \text{Eq. (13)}$$

B_{ii}= coefficients of the quadratic parameter

5.4.2 Launching mathematical model

Demonstrating the hardness value by H, the response function can be identified in the form specified in Equation (14):

H= f(R, F, N) Eq. (14)

As the utilized regression equation in this chapter (Eq. (13)), the designated polynomials for the three FSP parameters (R, F and N) will be obtained as Eq. (15).

$$H= b0 + b1(R) + b2 (F) +b3 (N) + b11 (R2) + b22 (F2) + b33 (N2) + b12 (RF) + b13 (RN) + b23 (FN)$$ Eq. (15)

The mathematical relationships among the FSP parameters and the response hardness have been achieved as follows:

$$H= 128.58 + 0.01764 R – 0.2432 F + 9.85 N + 0.000567 F×F + 0.208 N×N + 0.000088 R×F - 0.00256 R×N – 0.03586 F×N$$ Eq. (16)

The important factors (main and interaction) were recognized by analysis of variance technique via DOE which is shown in Table7. P-values <0.05 expose that the coefficients are important and P-values >0.1 reveal that the coefficients are not significant. Therefore, P-values shows that R, F, N, RF, RN, FN are important terms for hardness estimation. After considering just important terms for mathematical relation the following equation was obtained:

$$H= 128.58 + 0.01764 R – 0.2432 F + 9.85 N + 0.000088 R×F - 0.00256 R×N – 0.03586 F×N$$

Additionally, the F-values exhibit that the order of the more important terms in hardness model is as follows:

N>F>R>FN>RN>RF

Table 7: Analysis of Variance

Source	DF	Adj SS	Adj MS	F-Value	P-Value
Model	8	1131,52	141,441	140,50	0,000
Linear	3	1034,65	344,882	342,60	0,000
R	1	148,95	148,952	147,97	0,000
F	1	306,25	306,250	304,22	0,000
N	1	579,44	579,444	575,61	0,000
Square	2	3,62	1,811	1,80	0,199
F*F	1	2,58	2,580	2,56	0,130
N*N	1	1,04	1,042	1,03	0,325
2-Way Interaction	3	45,98	15,328	15,23	0,000
R*F	1	4,07	4,074	4,05	0,063
R*N	1	4,41	4,408	4,38	0,054
F*N	1	37,50	37,501	37,25	0,000
Error	15	15,10	1,007		
Total	23	1146,62			

5.5 Results and discussions

Figure 49-51 demonstrate contour and 3D graph of hardness values with different process parameters. According to the graphs, by increasing rotational speed, the hardness of composite is increased and reduction of advancing speed causes hardness increment. Additionally, it can be realized that the hardness values of the composite layer is vastly influenced by the number of passes. Increase in number of passes lead to improved hardness values. Table 8 shows the experimental and RSM predicted values for the hardness behavior. Maximum error for RSM predicted values is 1.10 which is satisfactory.

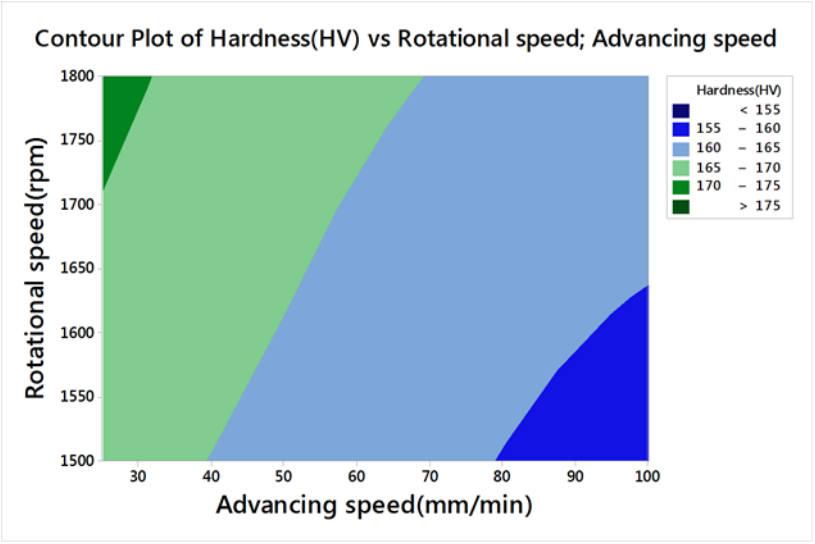

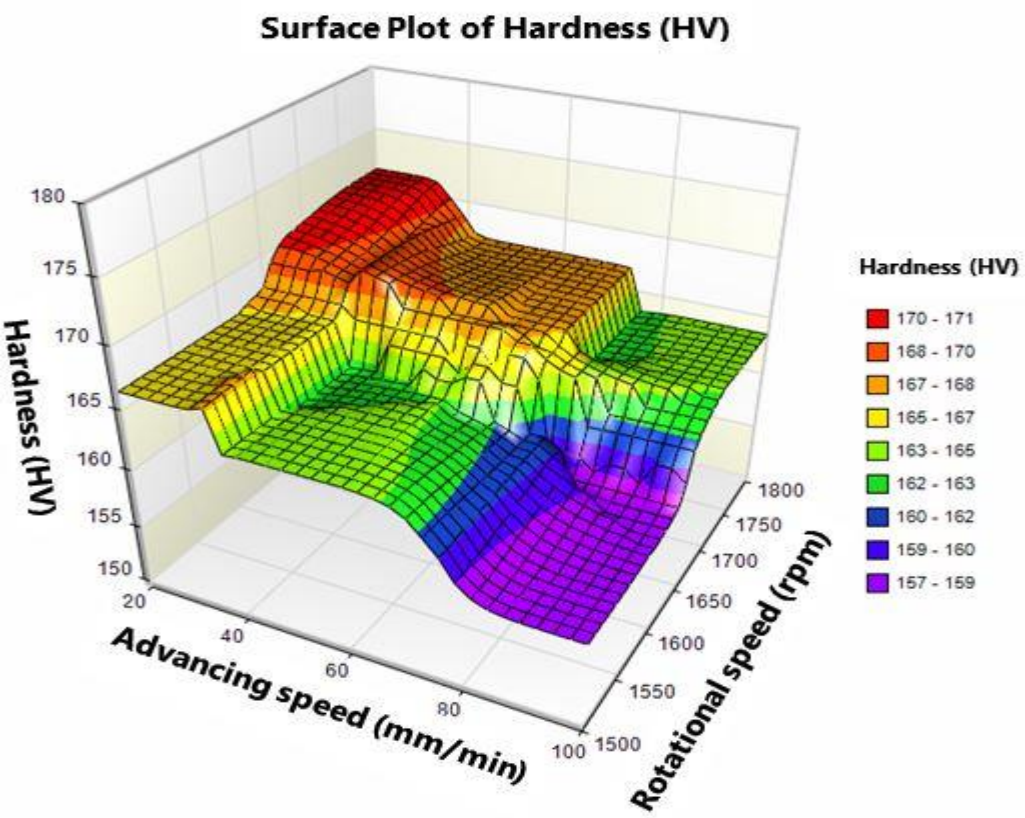

Figure 49. Contour and 3D graph of hardness values with rotational speed and advancing speed.

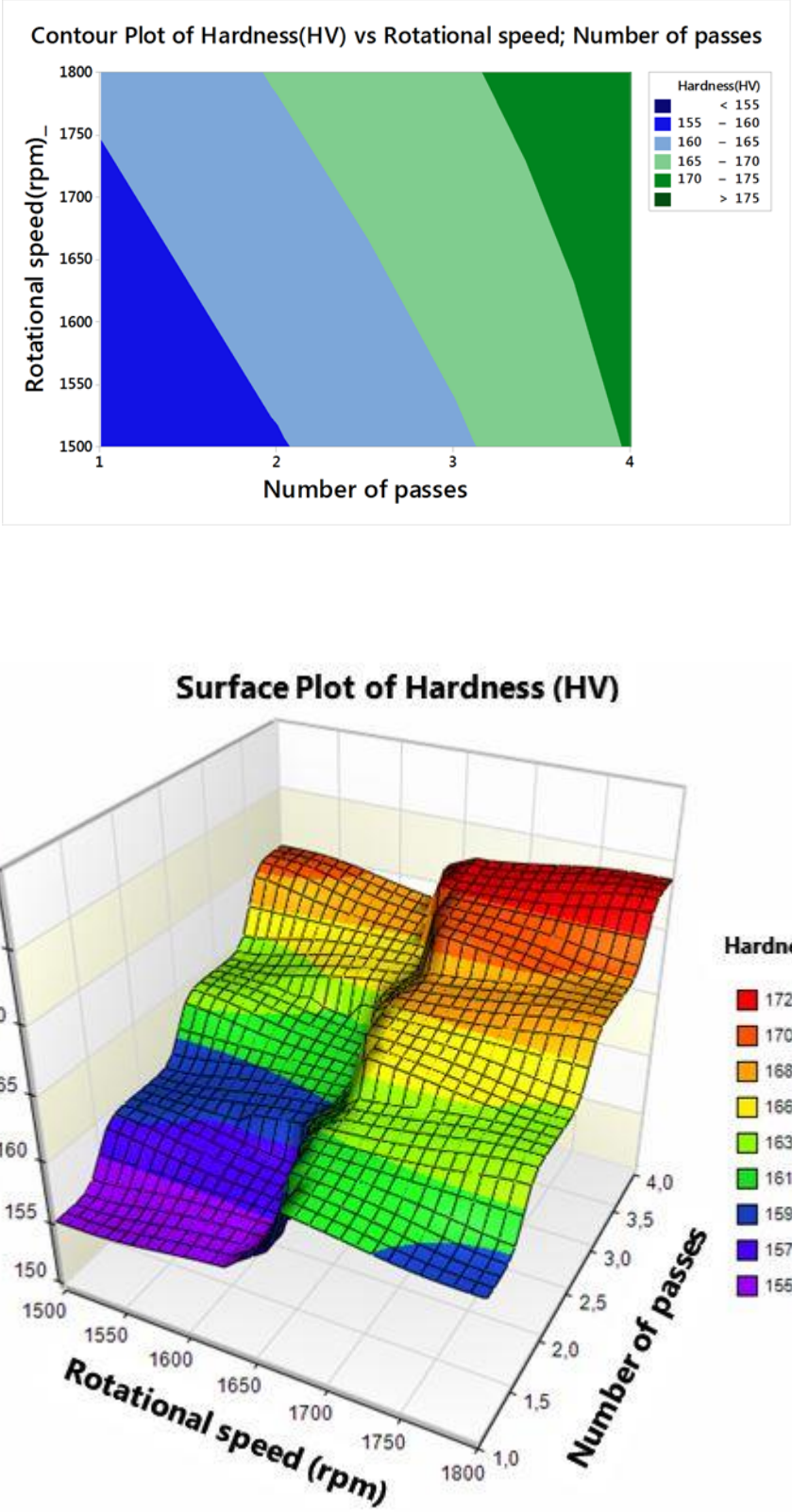

Figure 50. Contour and 3D graph of hardness values with rotational speed and number of passes.

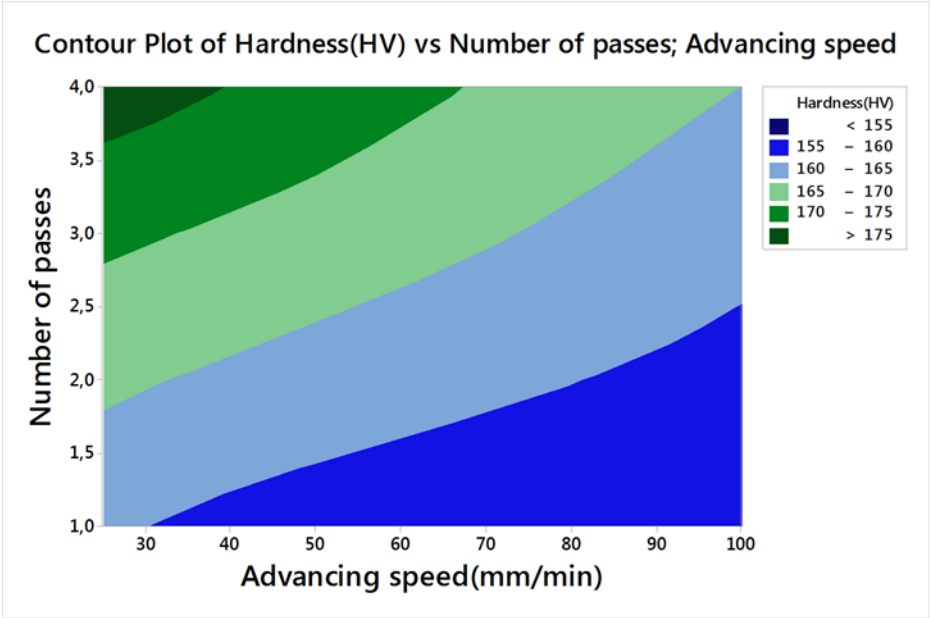

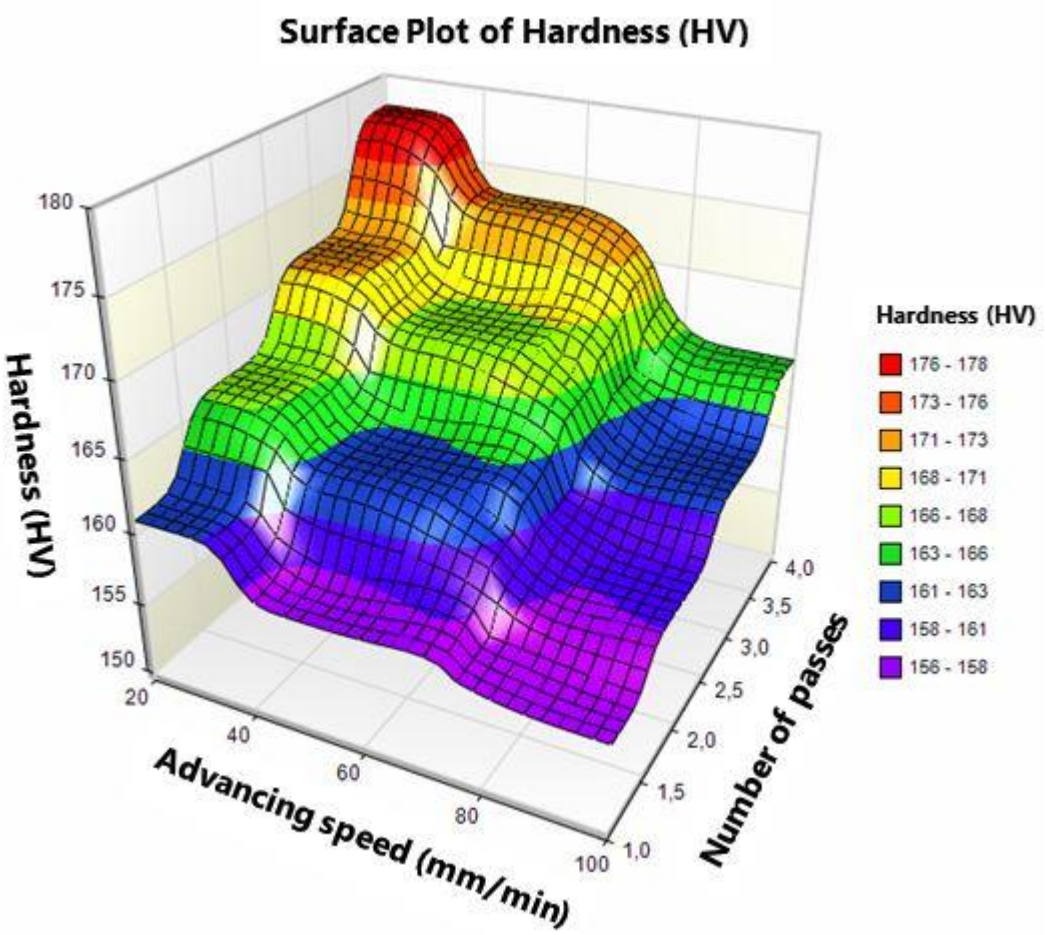

Figure 51. Contour and 3D graph of hardness values with advancing speed and number of passes.

Table 8: Experimental and ANN, RSM estimated outcomes of hardness

Rotational speed (rpm)	Advancing speed (mm/min)	Number of passes (n)	Hardness (HV) (experimental)	Hardness(HV) (ANN, estimation)	Error (%)	Hardness(HV) (RSM, estimation)	Error (%)
1500	100	1	153	153.95	0.62	152.240	-0.496
1500	100	2	155	154.57	-0.27	155.296	0.191
1500	100	3	158	158.01	0.006	158.769	0.487
1500	100	4	162	161.97	-0.01	162.658	0.406
1500	50	1	155	156.89	1.21	155.337	0.217
1500	50	2	161	161.15	0.09	160.186	-0.506
1500	50	3	167	166.89	-0.06	165.451	-0.927
1500	50	4	172	172.09	0.05	171.133	-0.504
1500	25	1	158	157.98	-0.01	157.948	-0.033
1500	25	2	163	163.07	0.04	163.693	0.425
1500	25	3	168	169.82	1.08	169.855	1.104
1500	25	4	177	176.84	-0.09	176.433	-0.320
1800	100	1	159	158.62	-0.23	159.408	0.257
1800	100	2	162	162.67	0.41	161.698	-0.187
1800	100	3	165	164.6	-0.24	164.404	-0.361
1800	100	4	168	168.08	0.04	167.526	-0.282
1800	50	1	160	160.11	0.06	161.183	0.740
1800	50	2	165	164.6	-0.24	165.265	0.161
1800	50	3	169	169.23	0.13	169.764	0.452
1800	50	4	174	174.88	0.5	174.680	0.391
1800	25	1	164	164.02	0.01	163.133	-0.528
1800	25	2	169	169.1	0.05	168.112	-0.526
1800	25	3	174	173.72	-0.16	173.507	-0.283
1800	25	4	179	177.52	-0.82	179.319	0.178

Figure. 52 and Table 8 display the estimated hardness values from ANN and RSM models and the actual values in variable experimental conditions. Results indicate that the experimental values are in close agreement with the estimated values. The estimation errors of ANN and RSM models are less than 1.5% which illustrates that the equation of the models is a very trustworthy tool for estimating the hardness values with high accuracy. Furthermore, the outcomes demonstrate that ANN modeled the hardness behavior better than RSM.

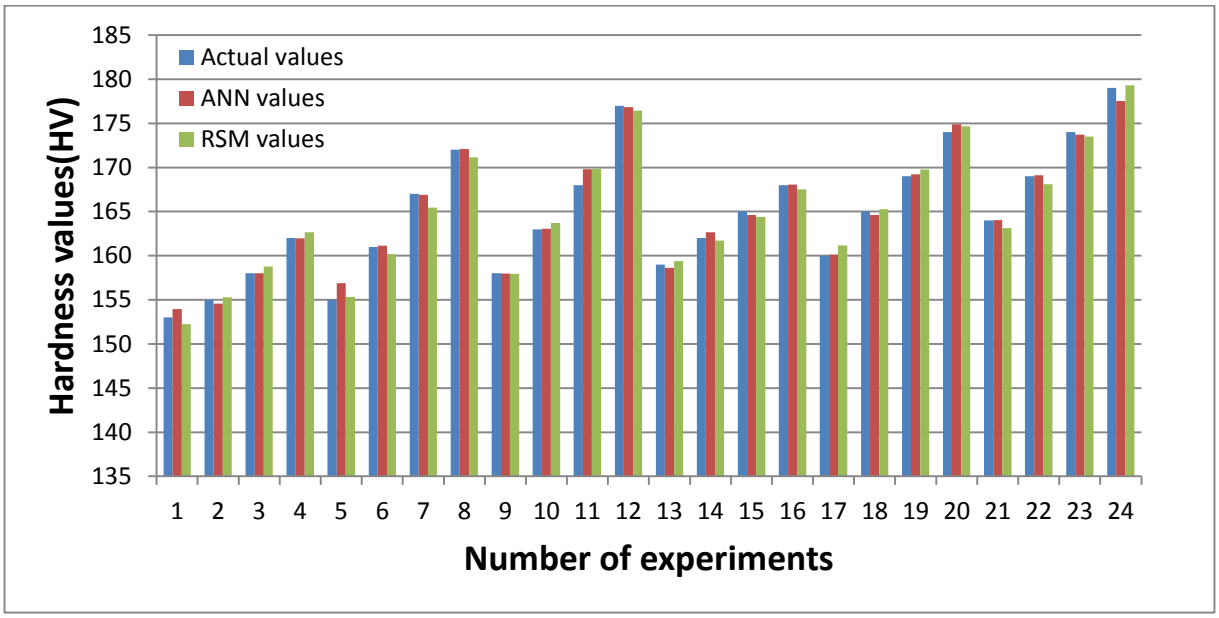

Figure 52. Variation of the hardness values with experimental numbers.

Chapter 6

CONCLUSION

In the present investigation, the A16061/Al_2O_3-Tib_2 Surface hybrid composite (SHC) is produced by the FSP. The microstructure, hardness, and wear behavior were evaluated with a view of observing the dispersion of the Al_2O_3-Tib_2 particles. The obtained results can be summarized as follow:

6.1 Effect of number of passes

Increasing the number of FSP passes leads to a more uniform dispersion of Al_2O_3-Tib_2 particles. A good dispersion of Al_2O_3-Tib_2 particles is gotten for the SHC produced by four FSP passes.

The FSP with Al_2O_3-Tib_2 particles more effectively decrease the grain size of the Al6061 matrix, the finest grain size is obtained as 0.7 μm by four FSP passes. With an increasing number of FSP passes the hardness of the SHC increases significantly. The peak hardness for the SHC is 175 HV, while that of the samples treated by the FSP without Al_2O_3-Tib_2 particles and the Al6061 are 100HV and 110 HV, respectively.

Wear resistance against a steel disk is significantly improved in SHC produced by four FSP passes in comparison to Al6061. The mechanism of wear is a mixture of abrasive and adhesive.

6.2 Effect of tool pin geometry

Fabrication of Al6061/ Al_2O_3-Tib_2 nanocomposite layers can be successfully carried out by FSP method using different tool pin profiles of straight cylindrical, threaded cylindrical, taper, triangle, and square.

Grain refinement takes place in the processed samples, and more grain refinement is gotten for samples produced using SQ and TR pin tool profile as a result of the pulsating action in the SZ of these samples.

The spread of the reinforcement particles (Al_2O_3-Tib_2) in specimens generated by the SQ and TR tool pin profiles is more uniform than those of the other pin profiles. It is due to the tool geometry, such as sharp edges and corners, which produce better stirring of the material and good material flow. Therefore, greater reduction of particle clustering is observed in these samples.

The hardness of the samples produced by the SQ and TR tool pin profiles is higher than those of other pin profiles due to the more uniform distribution of Al_2O_3-Tib_2 hard particles and finer grain sizes. The maximum hardness is 160 HV, which is observed in the specimen produced using SQ pin profile, whereas the hardness of the specimen generated with a SC tool and the received Al6061is 138 HV and 110 HV, respectively.

In comparison with the other samples the wear resistance has been enhanced in the samples produced via SQ and TR tool pin profiles due to the higher hardness of the specimen surfaces.

6.3 Estimation of mechanical properties of Al6061/ Al_2O_3-Tib_2 nano composite

The artificial neural networks and response surface method have been successfully applied to predict the hardness behavior of the friction stir processed Al6061/ Al_2O_3-Tib_2 nano composite.

ANN is reliable tool for modeling the hardness behavior of the FSPed composite layer. The trained ANN demonstrates acceptable outcomes while comparing the experimental values. Likewise Response surface methodology could be utilized to model the hardness of the processed composite layer.

The results of both models show that the estimated values for hardness of processed zone has the error less than 1.5% which is reliable and evaluation of the estimated values of both models and the experimental values approves that the ANN is better methodology than RSM.

6.4 Future Works

In addition to the contributions which have been already made in this study, there are several suggestions that can be performed to further advance this research topic. The following points are a summary of recommendations for future work:

1. A similar experimental test study could be designed to evaluate the effect of other process parameters such as tilt angle of the tool, dwell of time of the tool, down force of the tool, process conditions(under water).

2. A finite element analysis could be implemented to simulate temperature and material flow of FSPed composite layer.

3. Different morphology of reinforcement particles (Al_2O_3-Tib_2) and their altered weight ratio could be as effective parameters for the performance of the composite layer.

REFERENCES

[1] W. M. Thomas, E. D. Nicholas, J. D. Needham, M. G. Murch, P. Templesmith, and C. J. Daws, 1991.

[2] Mishra RS, Ma ZY. Friction stir welding and processing. Materials Science and Engineering R: Reports 2005;50.

[3] Cavaliere P, De Marco PP. Friction stir processing of AM60B magnesium alloy sheets. Materials Science and Engineering A 2007;462:393-7.

[4] Fuller CB, Mahoney MW. The effect of friction stir processing on 5083-H321/5356 Al arc welds: Microstructural and mechanical analysis. Metallurgical and Materials Transactions A: Physical Metallurgy and Materials Science 2006;37:3605-15.

[5] Oh-Ishi K, McNelley TR. Microstructural modification of as-cast NiAl bronze by friction stir processing. Metallurgical and Materials Transactions A: Physical Metallurgy and Materials Science 2004;35 A:2951-61.

[6] Arora HS, Singh H and Dhindaw BK. Composite fabrication using friction stir processing—a review. Int J Adv Manuf Technol 2012; 61: 1043–1055.

[7] Shafiei-Zarghani A, Kashani-Bozorg SF and Hanzaki AZ. Wear assessment of Al/Al2O3 nano-composite surface layer produced using friction stir processing. Wear 2011; 270: 403–412.

[8] Dolatkhah A, Golbabaei P, Besharati Givi MK, et al. Investigating effects of process parameters on microstructural and mechanical properties of Al5052/SiC metal matrix composite fabricated via friction stir processing. J Mater Des 2012; 37: 458–464.

[9] Misak HE, Widener CA, Burford DA, et al. Fabrication and characterization of carbon nanotube nanocomposites into 2024-T3 Al substrates via friction stir welding process. J Eng Mater Technol 2014; 136: 024501.

[10] Keshavamurthy R. Microstructure and hardness distribution in friction stir welded Al6061-TiB2 in-situ metal matrix composite. Int J Mech Prod Eng 2014; 2: 73–76.

[11] MISHRA, Rajiv S.; MA, Z. Y.; CHARIT, Indrajit. Friction stir processing: a novel technique for fabrication of surface composite. Materials Science and Engineering: A, 2003, 341.1: 307-310.

[12] Shafiei-Zarghani A, Kashani-Bozorg SF, Zarei-Hanzaki A. Microstructures and mechanical properties of Al/Al2O3 surface nano-composite layer produced by friction stir processing. Mater Sci Eng A 2009;500:84–91.

[13] Chu, Q., Yang, X. W., Li, W. Y., Zhang, Y., Lu, T., Vairis, A., & Wang, W. B. (2018). On visualizing material flow and precipitate evolution during probeless friction stir spot welding of an Al-Li alloy. Materials Characterization, 144, 336-344.

[14] Huang, Y., Huang, T., Wan, L., Meng, X., & Zhou, L. (2019). Material flow and mechanical properties of aluminum-to-steel self-riveting friction stir lap joints. Journal of Materials Processing Technology, 263, 129-137.

[15] Rahimzadeh Ilkhichi A, Soufi R, Hussain G, et al. Establishing mathematical models to predict grain siz and hardness of the friction stir-welded AA 7020 aluminum alloy joints. Metall Mater Trans B 2015; 46: 357–365.

[16] Heidarzadeh A, Vatankhah Barenji R, Esmaily M, et al. Tensile properties of friction stir welds of AA 7020 aluminum alloy. T Indian I Metals, Epub ahead of print, 1 March 2015. DOI: 10.1007/s12666-014-0508-2. [17]. MISHRA, Rajiv S.; MA, Z. Y.; CHARIT, Indrajit. Friction stir processing: a novel technique for fabrication of surface composite. Materials Science and Engineering: A, 2003, 341.1: 307-310.

[17] Gopan, V., Sreekumar, P. S., Chandran, J. P., Vijay, W., & Kumar, M. S. (2018). Experimental Investigation on the Effect of Process Parameters on Friction Stir Processing Of Aluminium. Materials Today: Proceedings, 5(5), 13674-13681.

[18] Vijayavel, P., & Balasubramanian, V. (2018). Effect of pin volume ratio on wear behaviour of friction stir processed LM25AA-5% SiCp metal matrix composites. Alexandria engineering journal.

[19] Heidarpour, A., Mazaheri, Y., Roknian, M., & Ghasemi, S. (2019). Development of Cu-TiO2 surface nanocomposite: Effect of pass number on

microstructure, mechanical properties, tribological and corrosion behavior. Journal of Alloys and Compounds.

[20] Sathiskumar, R., Dinaharan, I., Murugan, N., & Vijay, S. J. (2015). Influence of tool rotational speed on microstructure and sliding wear behavior of Cu/B4C surface composite synthesized by friction stir processing. Transactions of Nonferrous Metals Society of China, 25(1), 95-102.

[21] Kumar S, Sarma VS and Murty BS. Effect of temperature on the wear behavior of Al-7Si-TiB2 in-situ composites. Met Mat Trans A 2009; 40: 223–231.

[22] Singh, H., Raina, A., & Haq, M. I. U. (2018). Effect of TiB2 on Mechanical and Tribological Properties of Aluminium Alloys–A Review. Materials Today: Proceedings, 5(9), 17982-17988.

[23] Duddukuri R, Koc R, Mawdsley J, et al. Synthesis of nano-size TiB2 powders using carbon coated precursors. In: 22 (ed.) Nanostructured materials and nanotechnology. New York: John Wiley, 2011, p.165 [AQ2].

[24] James SJ, Venkatesan K, Kuppan P, et al. Comparative study of composites reinforced with SiC and TiB2. Procedia Eng 2014; 97: 1012–1017.

[25] Michael Rajan HB, Ramabalan S, Dinaharan I, et al. Effect of TiB2 content and temperature on sliding wear behavior of AA7075/TiB2 in situ aluminum cast composites. Arch Civil Mech Eng 2014; 14: 72–79.

[26] S.G. Epstein, J.G. Kaufman, P. Pollak," Aluminum and Its Alloys", 1994, The Aluminum Association, Inc. Washington,D.C.

[27] W. D. Callister, Materials Science and Engineering, An Introduction. York, PA: John Wiley & Sons, Inc., 2007.

[28] R. H. Krock, in ASTM Proceeding Philadelphia, PA, 1963.

[29] K. U. Kainer, Metal Matrix Composites. Custom-made Materials for Automotive and Aerospace Engineering. Weinheim: WILEY-VCH Verlag GmbH & Co. KGaA, , 2006

[30] CHAWLA, Krishan K. Metal matrix composites. Wiley-VCH Verlag GmbH & Co. KGaA, 2006.

[31] MORTENSEN, Andreas; LLORCA, Javier. Metal matrix composites. Annual review of materials research, 2010, 40: 243-270.

[32] HUNT, Warren; HERLING, Darrell R. Aluminum metal matrix composites. Advanced Materials & Processes, *162 (2): 39-44*, 2004, 162.PNNL-SA-39568.

[33] PRASAD, S. V.; ASTHANA, R. Aluminum metal-matrix composites for automotive applications: tribological considerations. Tribology letters, 2004, 17.3: 445-453.

[34] RAWAL, Suraj P. Metal-matrix composites for space applications. JOM Journal of the Minerals, Metals and Materials Society, 2001, 53.4: 14-17.

[35] RAJAN, T. P. D.; PILLAI, R. M.; PAI, B. C. Reinforcement coatings and interfaces in aluminium metal matrix composites. Journal of Materials Science, 1998, 33.14: 3491-3503.

[36] NAIR, S. V.; TIEN, J. K.; BATES, R. C. SiC-reinforced aluminium metal matrix composites. International Metals Reviews, 1985, 30.1: 275-290.

[37] REJIL, C. Maxwell, et al. Microstructure and sliding wear behavior of AA6360/(TiC+ B 4 C) hybrid surface composite layer synthesized by friction stir processing on aluminum substrate. Materials Science and Engineering*: A*, 2012, 552: 336-344.

[38] ARURI, Devaraju, et al. Wear and mechanical properties of 6061-T6 aluminum alloy surface hybrid composites [(SiC+ Gr) and (SiC+ Al 2 O 3)] fabricated by friction stir processing. journal of materials research and technology, 2013, 2.4: 362-369.

[39] SURESHA, S.; SRIDHARA, B. K. Wear characteristics of hybrid aluminium matrix composites reinforced with graphite and silicon carbide particulates. Composites Science and Technology, 2010, 70.11: 1652-1659.

[40] MILLER, W. S.; HUMPHREYS, F. J. Strengthening mechanisms in particulate metal matrix composites. Scripta metallurgica et materialia, 1991, 25.1: 33-38.

[41] Nardone, V.C.; Prewo, K.M. On the strength of discontinuous silicon carbide reinforced aluminum composites. Scripta Metal. **1986**, 20, 43–48. [Google Scholar] [CrossRef]

[42] Zhang, Z.; Chen, D.L. Contribution of Orowan strengthening effect in particulate-reinforced metal matrix nanocomposites. Mat. Sci. Eng. A **2008**, 483–484, 148–152. [Google Scholar] [CrossRef]

[43] Sanaty-Zadeh, A. Comparison between current models for the strength of particulate-reinforced metal matrix nanocomposites with emphasis on consideration of Hall–Petch effect. Mat. Sci. Eng. A **2012**, 531, 112–118. [Google Scholar] [CrossRef]

[44] Hull, D.; Bacon, D.J. Introduction to Dislocations, 4th ed.; Butterworth Einemann: Oxford, UK, 2001. [Google Scholar]

[45] C. R. Kennedy, "Proceedings of the 7th CIMTEC-World Ceramics Congress," in Elsevier, New york, 1991, p. 691.

[46] COOK, A. J.; WERNER, P. S. Pressure infiltration casting of metal matrix composites. Materials Science and Engineering*: A*, 1991, 144.1-2: 189-206.

[47] GHOMASHCHI, M. R.; VIKHROV, A. Squeeze casting: an overview. Journal of Materials Processing Technology, 2000, 101.1: 1-9.

[48] Bhaskar, Chandra & Kandpal, Bhaskar Chandra & Kumar, Jatinder & Singh, Hari. (2014). Production technologies of metal matrix composite -A Review.

[49] K. U. Kainer, Metal Matrix Composites. Custom-made Materials for Automotive and Aerospace Engineering. Weinheim: WILEY-VCH Verlag GmbH & Co. KGaA, , 2006.

[50] K. k. Chawla and L. B. Godfroid, "Faracture behavior of Al 1100/Al 2024 laminate Composites " in Proceedings of the 6th International Conference on Fracture (ICF6), New Delhi, India, 1984.

[51] ALIZADEH, M.; PAYDAR, M. H. Fabrication of nanostructure Al/SiC P composite by accumulative roll-bonding (ARB) process. Journal of Alloys and Compounds, 2010, 492.1: 231-235.

[52] Bujari, Suresh & Kurahatti, Rajashekar. (2016). A REVIEW ON PROCESSING AND TRIBOLOGICAL PROPERTIES OF METAL MATRIX COMPOSITES. International Journal of Advancement in Engineering Technology, Management & Applied Science. 3. 302-310.

[53] N. Chawla, J. J. Williams, and R. Saha, J. Light Metals, vol. 2, pp. 215-227, 2002.

[54] MISHRA, Rajiv Sharan; DE, Partha Sarathi; KUMAR, Nilesh. Friction stir processing. In: Friction Stir Welding and Processing. Springer International Publishing, 2014. p. 259-296.

[55] MAHONEY, M. W.; LYNCH, S. P. Friction-Stir Processing. ROCKWELL SCIENTIFIC CO THOUSAND OAKS CA, 2006.

[56] MISHRA, Rajiv S.; MA, Z. Y.; CHARIT, Indrajit. Friction stir processing: a novel technique for fabrication of surface composite. Materials Science and Engineering*: A*, 2003, 341.1: 307-310.

[57] MA, Z. Y. Friction stir processing technology: a review. Metallurgical and materials Transactions A, 2008, 39.3: 642-658.

[58] ARORA, H. S.; SINGH, H.; DHINDAW, B. K. Composite fabrication using friction stir processing—a review. The International Journal of Advanced Manufacturing Technology, 2012, 61.9: 1043-1055.

[59] HSU, C. J., et al. Al–Al 3 Ti nanocomposites produced in situ by friction stir processing. Acta Materialia, 2006, 54.19: 5241-5249.

[60] WANG, Wei, et al. A novel way to produce bulk SiCp reinforced aluminum metal matrix composites by friction stir processing. Journal of materials processing technology, 2009, 209.4: 2099-2103.

[61] MORISADA, Y., et al. MWCNTs/AZ31 surface composites fabricated by friction stir processing. Materials science and engineering*: A*, 2006, 419.1: 344-348.

[62] BARMOUZ, M., et al. Investigation of mechanical properties of Cu/SiC composite fabricated by FSP: effect of SiC particles' size and volume fraction. Materials Science and Engineering: A, 2011, 528.3: 1740-1749.

[63] SU, Jian-Qing; NELSON, Tracy W.; STERLING, Colin J. Friction stir processing of large-area bulk UFG aluminum alloys. Scripta materialia, 2005, 52.2: 135-140.

[64] CHANG, C. I.; DU, X. H.; HUANG, J. C. Achieving ultrafine grain size in Mg–Al–Zn alloy by friction stir processing. Scripta Materialia, 2007, 57.3: 209-212.

[65] ELANGOVAN, K.; BALASUBRAMANIAN, V. Influences of pin profile and rotational speed of the tool on the formation of friction stir processing zone in AA2219 aluminium alloy. Materials Science and Engineering*: A*, 2007, 459.1: 7-18.

[66] MA, Z. Y.; SHARMA, S. R.; MISHRA, R. S. Effect of friction stir processing on the microstructure of cast A356 aluminum. Materials Science and Engineering*: A*, 2006, 433.1: 269-278.

[67] SANTELLA, M. L., et al. Effects of friction stir processing on mechanical properties of the cast aluminum alloys A319 and A356. Scripta Materialia, 2005, 53.2: 201-206.

[68] DARRAS, B. M., et al. Friction stir processing of commercial AZ31 magnesium alloy. Journal of materials processing technology, 2007, 191.1: 77-81.

[69] PARK, Seung Hwan C.; SATO, Yutaka S.; KOKAWA, Hiroyuki. Microstructural evolution and its effect on Hall-Petch relationship in friction stir welding of thixomolded Mg alloy AZ91D. Journal of materials science, 2003, 38.21: 4379-4383.

[70] CHARIT, Indrajit; MISHRA, Rajiv S. Low temperature superplasticity in a friction-stir-processed ultrafine grained Al–Zn–Mg–Sc alloy. *Acta Materialia*, 2005, 53.15: 4211-4223.

[71] MA, Z. Y.; MISHRA, Rajiv S.; MAHONEY, Murray W. Superplastic deformation behaviour of friction stir processed 7075Al alloy. *Acta materialia*, 2002, 50.17: 4419-4430.

[72] AZIZIEH, M.; KOKABI, A. H.; ABACHI, P. Effect of rotational speed and probe profile on microstructure and hardness of AZ31/Al 2 O 3 nanocomposites fabricated by friction stir processing. Materials & Design, 2011, 32.4: 2034-2041.

[73] CAVALIERE, P. Mechanical properties of friction stir processed 2618/Al 2 O 3/20p metal matrix composite. Composites Part A: Applied Science and Manufacturing, 2005, 36.12: 1657-1665.

[74] MAZAHERI, Y.; KARIMZADEH, F.; ENAYATI, M. H. A novel technique for development of A356/Al 2 O 3 surface nanocomposite by friction stir processing. Journal of Materials Processing Technology, 2011, 211.10: 1614-1619.

[75] HSU, C. J., et al. Al–Al 3 Ti nanocomposites produced in situ by friction stir processing. Acta Materialia, 2006, 54.19: 5241-5249.

[76] HSU, C. J.; KAO, P. W.; HO, N. J. Ultrafine-grained Al–Al 2 Cu composite produced in situ by friction stir processing. Scripta Materialia, 2005, 53.3: 341-345.

[77] DOLATKHAH, A., et al. Investigating effects of process parameters on microstructural and mechanical properties of Al5052/SiC metal matrix composite fabricated via friction stir processing. Materials & Design, 2012, 37: 458-464.

[78] BAURI, Ranjit; YADAV, Devinder; SUHAS, G. Effect of friction stir processing (FSP) on microstructure and properties of Al–TiC in situ composite. Materials Science and Engineering: A, 2011, 528.13: 4732-4739.

[79] LIU, Z. Y., et al. Singly dispersed carbon nanotube/aluminum composites fabricated by powder metallurgy combined with friction stir processing. Carbon, 2012, 50.5: 1843-1852.

[80] Hsu C.J., Kao P.W., Ho N.J. Intermetallic-reinforced aluminum matrix composites produced in situ by friction stir processing. Mater. Lett. 2007;61:1315–1318.

[81] Dixit M., Newkirk J.W., Mishra R.S. Properties of friction stir-processed Al 1100NiTi composite. Scr. Mater. 2007;56:541–544.

[82] Lee I.S., Kao P.W., Ho N.J. Microstructure and mechanical properties of AlFe in situ nanocomposite produced by friction stir processing. Intermetallics. 2008;16:1104–1108. doi: 10.1016/j.intermet.2008.06.017. [Cross Ref]

[83] BARMOUZ, Mohsen; GIVI, Mohammad Kazem Besharati; SEYFI, Javad. On the role of processing parameters in producing Cu/SiC metal matrix composites via friction stir processing: Investigating microstructure, microhardness, wear and tensile behavior. Materials characterization, 2011, 62.1: 108-117.

[84] VATANKHAH BARENJI, Reza, et al. Wear properties of Al–Al2O3/TiB2 surface hybrid composite layer prepared by friction stir process. Journal of Composite Materials, 2016, 50.11: 1457-1466.

[85] SHARIFITABAR, M., et al. Fabrication of 5052Al/Al 2 O 3 nanoceramic particle reinforced composite via friction stir processing route. Materials & Design, 2011, 32.8: 4164-4172.

[86] ZOHOOR, Mehdi; GIVI, MK Besharati; SALAMI, P. Effect of processing parameters on fabrication of Al–Mg/Cu composites via friction stir processing. Materials & Design, 2012, 39: 358-365.

[87] AZIZIEH, M.; KOKABI, A. H.; ABACHI, P. Effect of rotational speed and probe profile on microstructure and hardness of AZ31/Al 2 O 3 nanocomposites fabricated by friction stir processing. Materials & Design, 2011, 32.4: 2034-2041.

[88] CHARIT, Indrajit; MISHRA, Rajiv S. Abnormal grain growth in friction stir processed alloys. Scripta materialia, 2008, 58.5: 367-371.

[89] Garcı´a-Bernal MA, Mishra RS, Verma R, et al. Influence of friction stir processing tool design on microstructure and superplastic behavior of Al-Mg alloys. Mater Sci Eng A 2016; 670: 9–16.

[90] Faraji G, Dastani O and Mousavi SAAA. Effect of process parameters on microstructure and micro-hardness of AZ91/Al2O3 surface composite produced by FSP. J Mater Eng Perform 2011; 20: 1583–1590.

[91] Mahmoud ERI, Takahashi M, Shibayanagi T, et al. Effect of friction stir processing tool probe on fabrication of SiC particle reinforced composite on aluminum surface. Sci Tech Weld Join 2009; 14: 413–425.

[92] Azizieh M, Kokabi AH and Abachi P. Effect of rotational speed and probe profile on microstructure and hardness of AZ31/Al2O3 nanocomposites fabricated by friction stir processing. Mater Design 2011; 32: 2034–2041.

[93] Yu Z, Zhang W, Choo H, et al. Transient heat and material flow modeling of friction stir processing of magnesium alloy using threaded tool. Metall MaterTrans A 2011; 43: 724–737.

[94] Arora HS, Singh H and Dhindaw BK. Composite fabrication using friction stir processing—a review. Int J Adv Manuf Technol 2012; 61: 1043–1055.

[95] Mishra RS, Ma ZY and Charit I. Friction stir processing: a novel technique for fabrication of surface composite. Mater Sci Eng A 2003; 341: 307–310.

[96] Mahmoud ERI, Ikeuchi K and Takahashi M. Fabrication of SiC particle reinforced composite on aluminium surface by friction stir processing. Sci Tech Weld Join 2008; 13: 607–618.

[97] Lee IS, Kao PW and Ho NJ. Microstructure and mechanical properties of Al-Fe in situ nanocomposite produced by friction stir processing. Intermetallics 2008; 16: 1104–1108.

[98] Qian J, Li J, Xiong J, et al. In situ synthesizing Al3Ni for fabrication of intermetallic-reinforced aluminum alloy composites by friction stir processing. Mater Sci Eng A 2012; 550: 279–285.

[99] EL-RAYES, Magdy M.; EL-DANAF, Ehab A. The influence of multi-pass friction stir processing on the microstructural and mechanical properties of Aluminum Alloy 6082. Journal of Materials Processing Technology, 2012, 212.5: 1157-1168.

[100] CUI, G. R., et al. Effects of friction stir processing parameters and in situ passes on microstructure and tensile properties of Al-Si-Mg Casting. Metallurgical and Materials Transactions A, 2014, 45.12: 5318-5331.

[101] Khorrami, M.S.; Kazeminezhad, M.; Kokabi, A.H. The effect of SiC nanoparticles on the friction stir processing of severely deformed aluminum. Mater. Sci. Eng. A 2014, 602, 110–118.

[102] Wakchaure, K. N., Thakur, A. G., Gadakh, V., & Kumar, A. (2018). Multi-Objective Optimization of Friction Stir Welding of Aluminium Alloy 6082-T6 Using hybrid Taguchi-Grey Relation Analysis-ANN Method. Materials Today: Proceedings, 5(2), 7150-7159.

[103] Chu, Q., Li, W. Y., Yang, X. W., Shen, J. J., Vairis, A., Feng, W. Y., & Wang, W. B. (2018). Microstructure and mechanical optimization of probeless friction stir spot welded joint of an Al-Li alloy. Journal of Materials Science & Technology.

[104] Rudi, H., Ghorbannazhad, P., & Hubbe, M. A. (2018). Optimizing the mechanical properties of papers reinforced with refining and layer-by-layer treated recycled fibers using response surface methodology. Carbohydrate polymers, 200, 391-399.

[105] Fakhri, L. A., Ghanbarzadeh, B., Dehghannya, J., Abbasi, F., & Ranjbar, H. (2018). Optimization of mechanical and color properties of polystyrene/nanoclay/nano ZnO based nanocomposite packaging sheet using response surface methodology. Food Packaging and Shelf Life, 17, 11-24.

[106] Naik, A. B., & Reddy, A. C. (2018). Optimization of tensile strength in TIG welding using the Taguchi method and analysis of variance (ANOVA). Thermal Science and Engineering Progress, 8, 327-339.

[107] Kumari, S., Tiyyagura, H. R., Douglas, T. E., Mohammed, E. A., Adriaens, A., Fuchs-Godec, R., ... & Skirtach, A. G. (2018). ANN prediction of corrosion behaviour of uncoated and biopolymers coated cp-Titanium substrates. Materials & Design, 157, 35-51.

[108] Vignesh, R. V., & Padmanaban, R. (2018). Artificial neural network model for predicting the tensile strength of friction stir welded aluminium alloy AA1100. Materials Today: Proceedings, 5(8), 16716-16723.

[109] Britto, A. S. F., Raj, R. E., & Mabel, M. C. (2018). Prediction and optimization of mechanical strength of diffusion bonds using integrated ANN-GA approach with process variables and metallographic characteristics. Journal of Manufacturing Processes, 32, 828-838.

[110] Satyanarayana, G., Naidu, G. S., & Babu, N. H. (2017). Artificial neural network and regression modelling to study the effect of reinforcement and deformation on volumetric wear of red mud nano particle reinforced aluminium matrix composites synthesized by stir casting. Boletín de la Sociedad Española de Cerámica y Vidrio.

[111] Britto, A. S. F., Raj, R. E., & Mabel, M. C. (2017). Prediction of shear and tensile strength of the diffusion bonded AA5083 and AA7075 aluminium alloy using ANN. Materials Science and Engineering: A, 692, 1-8.

[112] Asante-Okyere, S., Xu, Q., Mensah, R. A., Jin, C., & Ziggah, Y. Y. (2018). Generalized regression and feed forward back propagation neural networks in modelling flammability characteristics of polymethyl methacrylate (PMMA). Thermochimica Acta, 667, 79-92.

[113] Rekha, C. R., Nayar, V. U., & Gopchandran, K. G. (2018). Prediction of plasmons in silver nanorods using artificial neural networks with back propagation algorithm. Optik, 172, 721-729.

[114] Esfe, M. H., Rostamian, H., Esfandeh, S., & Afrand, M. (2018). Modeling and prediction of rheological behavior of Al2O3-MWCNT/5W50 hybrid nano-lubricant by artificial neural network using experimental data. Physica A: Statistical Mechanics and its Applications.

[115] Y. Rostamiyan, A. Fereidoon, A.H. Mashhadzadeh, M.R. Ashtiyani, A. Salmankhani Using response surface methodology for modeling and optimizing tensile and impact strength properties of fiber orientated quaternary hybrid nano composite Compos B Eng, 69 (2015), pp. 304-316.

[116] Sktani, Z. D. I., Rejab, N. A., Ratnam, M. M., & Ahmad, Z. A. (2018). Fabrication of tougher ZTA ceramics with sustainable high hardness through

(RSM) optimisation. International Journal of Refractory Metals and Hard Materials, 74, 78-86.

[117] Punugupati, G., Kandi, K. K., Bose, P. S. C., & Rao, C. S. P. (2018). Modeling and optimization of wear characteristics of gelcast fused silica ceramic composites using RSM. Materials Today: Proceedings, 5(2), 6946-6953.

[118] Vijayavel, P., and V. Balasubramanian. "Effect of pin volume ratio on wear behaviour of friction stir processed LM25AA-5% SiCp metal matrix composites." Alexandria Engineering Journal (2018).

[119] Zhang, Z. Y., et al. "Microstructural evolution and mechanical properties of friction stir processed ZrB2/6061Al nanocomposites." Journal of Alloys and Compounds 762 (2018): 312-318.

[120] Hosseinzadeh, Ali, and Guney Guven Yapici. "High Temperature Characteristics of Al2024/SiC Metal Matrix Composite fabricated by Friction Stir Processing." Materials Science and Engineering: A (2018).

[121] Arokiasamy, S., and B. Anand Ronald. "Enhanced properties of Magnesium based metal matrix composites via Friction Stir Processing." Materials Today: Proceedings 5.2 (2018): 6934-6939.

[122] Salih, Omar S., et al. "Microstructure and Mechanical Properties of Friction Stir Welded AA6092/SiC Metal Matrix Composite." Materials Science and Engineering: A (2018).

[123] Rahsepar, Mansour, and Hamed Jarahimoghadam. "The influence of multipass friction stir processing on the corrosion behavior and mechanical properties of zircon-reinforced Al metal matrix composites." Materials Science and Engineering: A 671 (2016): 214-220.

[124] Huang, Guoqiang, et al. "Microstructure, mechanical properties and strengthening mechanism of titanium particle reinforced aluminum matrix composites produced by submerged friction stir processing." Materials Science and Engineering: A 734 (2018): 353-363.

[125] Sharifitabar, M., M. Kashefi, and S. Khorshahian. "Effect of friction stir processing pass sequence on properties of Mg–ZrSiO4–Al2O3 surface hybrid micro/nano-composites." Materials & Design 108 (2016): 1-7.

[126] John, Jacob, S. P. Shanmughanatan, and M. B. Kiran. "Effect of tool geometry on microstructure and mechanical Properties of friction stir processed AA2024-T351 aluminium alloy." Materials Today: Proceedings 5.1 (2018): 2965-2979.

[127] Bauri, Ranjit, et al. "Effect of process parameters and tool geometry on fabrication of Ni particles reinforced 5083 Al composite by friction stir processing." Materials Today: Proceedings 2.4-5 (2015): 3203-3211.

[128] Mirjavadi, Seyed Sajad, et al. "Effect of multi-pass friction stir processing on the microstructure, mechanical and wear properties of AA5083/ZrO2 nanocomposites." Journal of Alloys and Compounds 726 (2017): 1262-1273.

[129] Kishan, V., Aruri Devaraju, and K. Prasanna Lakshmi. "Tribological Properties of Nano TiB 2 particle Reinforced 6061-T6 Aluminum Alloy Surface Composites via Friction stir processing." Materials Today: Proceedings 5.1 (2018): 1615-1619.

[130] Huang, Guoqiang, and Yifu Shen. "The effects of processing environments on the microstructure and mechanical properties of the Ti/5083Al composites produced by friction stir processing." Journal of Manufacturing Processes 30 (2017): 361-373.

[131] Khodabakhshi, F., et al. "Microstructure and texture development during friction stir processing of Al–Mg alloy sheets with TiO2 nanoparticles." Materials Science and Engineering: A 605 (2014): 108-118.

[132] Vatankhah Barenji, Reza, et al. "Wear properties of Al–Al2O3/TiB2 surface hybrid composite layer prepared by friction stir process." Journal of Composite Materials 50.11 (2016): 1457-1466.

[133] Khojastehnezhad, Vahid M., Hamed H. Pourasl, and Reza Vatankhah Barenji. "Effect of tool pin profile on the microstructure and mechanical properties of friction stir processed Al6061/Al2O3—TiB2 surface hybrid composite layer." Proceedings of the Institution of Mechanical Engineers, Part L: Journal of Materials: Design and Applications (2017): 1464420717715048.

[134] Louly, M. A., O. M. Lemine, and A. Gharbi. "Modeling of the microstructural properties of (x) ZnO (1− x) Fe2O3 nanocrystallines by artificial neural network and response surface methodology." Measurement 95 (2017): 70-76.

[135] Shandilya, Pragya, P. K. Jain, and N. K. Jain. "RSM and ANN modeling approaches for predicting average cutting speed during WEDM of SiCp/6061 Al MMC." Procedia Engineering 64 (2013): 767-774.

[136] Kumar, Ravinder, and Santram Chauhan. "Study on surface roughness measurement for turning of Al 7075/10/SiCp and Al 7075 hybrid composites by using response surface methodology (RSM) and artificial neural networking (ANN)." Measurement 65 (2015): 166-180.

[137] Ohale, P. E., Chigozie F. Uzoh, and Okechukwu Dominic Onukwuli. "Optimal factor evaluation for the dissolution of alumina from Azaraegbelu clay in acid solution using RSM and ANN comparative analysis." south african journal of chemical engineering 24 (2017): 43-54.

[138] Kartic, D. Navamani, B. CH Aditya Narayana, and M. Arivazhagan. "Removal of high concentration of sulfate from pigment industry effluent by chemical precipitation using barium chloride: RSM and ANN modeling approach." Journal of environmental management 206 (2018): 69-76.

[139] Rabiezadeh A, Hadian AM and Ataie A. Preparation of alumina/titanium diboride nano-composite powder by milling assisted sol-gel method. Int J Refrac Met H 2012; 31: 121–124.

[140] Rabiezadeh A, Ataie A and Hadian AM. Sintering of Al2O3-TiB2 nano-composite derived from milling assisted sol-gel method. Int J Refrac Met 2012; 33: 58–64.

[141] Morisada Y, Fujii H, Nagaoka T, et al. MWCNTs/AZ31 surface composites fabricated by friction stir processing. Mater Sci Eng A 2006; 419: 344–348.

[142] Heidarzadeh A, Khodaverdizadeh H, Mahmoudi A, et al. Tensile behavior of friction stir welded AA 6061-T4 aluminum alloy joints. J Mater Des 2012; 37: 166–173.

[143] Heidarzadeh A and Saeid T. Prediction of mechanical properties in friction stir welds of pure copper. J Mater Des 2013; 52: 1077–1087.

[144] Heidarzadeh A, Saeid T, Khodaverdizadeh H, et al. Establishing a mathematical model to predict the tensile strength of friction stir welded pure copper joints. Metall Mater Trans B 2013; 44: 175–183.

[145] Mahmoud ERI, Takahashi M, Shibayanagi T, et al. Wear characteristics of surface-hybrid-MMCs layer fabricated on aluminum plate by friction stir processing. Wear 2010; 268: 1111–1121.

[146] Zahmatkesh B, Enayati MH and Karimzadeh F. Tribological and microstructural evaluation of friction stir processed Al2024 alloy. J Mater Des 2010; 31: 4891–4896.

[147] Aldajah SH, Ajayi OO, Fenske GR, et al. Effect of friction stir processing on the tribological performance of high carbon steel. Wear 2009; 267: 350–355.

[148] Raaft M, Mahmoud TS, Zakaria HM, et al. Microstructural, mechanical and wear behavior of A390/graphite and A390/Al2O3 surface composites fabricated using FSP. Mater Sci Eng A 2011; 528: 5741–5746.

[149] Chen YC and Nakata K. Evaluation of microstructure and mechanical properties in friction stir processed SKD61 tool steel. Mater Charac 2009; 60: 1471–1475.

[150] Ma ZY. Friction stir processing technology: a review. Metall Mater Trans A 2008; 39: 642–658.

[151] Raaft, M., Mahmoud, T. S., Zakaria, H. M., & Khalifa, T. A. (2011). Microstructural, mechanical and wear behavior of A390/graphite and A390/Al2O3 surface composites fabricated using FSP. Materials Science and Engineering: A, 528(18), 5741-5746.

[152] Hosseini SA, Ranjbar K, Dehmolaei R, et al. Fabrication of Al5083 surface composites reinforced by CNTs and cerium oxide nano particles via friction stir processing. J Alloy Comp 2015; 622: 725–733.

[153] Elangovan K and Balasubramanian V. Influences of tool pin profile and welding speed on the formation of friction stir processing zone in AA2219 aluminium alloy. J Mater Process Technol 2008; 200: 163–175.

[154] Chen Y, Liu H and Feng J. Friction stir welding characteristics of different heat- treated-state 2219 aluminum alloy plates. Mater Sci Eng A 2016; 420: 21–27.

[155] Yang R, Zhang Z, Zhao Y, et al. Effect of multi-pass friction stir processing on microstructure and mechanical properties of Al3Ti/A356 composites. Mater Charact 2015; 106: 62–69.

[156] Khodabakhshi F, Simchi A, Kokabi AH, et al. Effects of nanometric inclusions on the microstructural characteristics and strengthening of a friction-stir processed aluminum–magnesium alloy. Mater Sci Eng A 2015; 642: 215–229.

[157] Elangovan K, Balasubramanian V and Valliappan M. Influences of tool pin profile and axial force on the formation of friction stir processing zone in AA6061 aluminium alloy. Int J Adv Manuf Technol 2008; 38: 285–295.

[158] Yadav D and Bauri R. Processing, microstructure and mechanical properties of nickel particles embedded aluminium matrix composite. Mater Sci Eng A 2012; 528: 1326–1333.

[159] Lee IS, Kao PW and Ho NJ. Microstructure and mechanical properties of Al–Fe in situ nanocomposite produced by friction stir processing. Intermetallics 2008; 16: 1104–1108.

[160] Hamdollahzadeh A, Bahrami M, Nikoo MF, et al. Microstructure evolutions and mechanical properties of nano-SiC-fortified AA7075 friction stir weldment: The role of second pass processing. J Manuf Proc 2015; 20: 367–373.

[161] Raaft M, Mahmoud TS, Zakaria HM, et al. Microstructural, mechanical and wear behavior of A390/graphite and A390/Al_2O_3 surface composites fabricated using FSP. Mater Sci Eng A 2011; 528: 5741–5746.

[162] Yu Z, Zhang W, Choo H, et al. Transient heat and material flow modeling of friction stir processing of magnesium alloy using threaded tool. Metall MaterTrans A 2011; 43: 724–737.

[163] Chen YC and Nakata K. Evaluation of microstructure and mechanical properties in friction stir processed SKD61 tool steel. Mater Charact 2009; 60: 1471–1475.

[164] Barenji, Reza Vatankhah, Hamed H. Pourasl, and Vahid M. Khojastehnezhad. "Electrical discharge machining of the AISI D6 tool steel: Prediction and modeling of the material removal rate and tool wear ratio." Precision Engineering 45 (2016): 435-444.